

# NAVAL POSTGRADUATE SCHOOL

## Monterey, California



19980527 058

### THESIS

**A COMPARISON OF THE NOGAPS AND GFDN  
DYNAMICAL TRACK PREDICTION MODELS  
DURING THE 1997 WESTERN NORTH PACIFIC  
TYPHOON SEASON**

by

Robert G. Schnabel

March, 1998

Thesis Co-Advisors:

R. L. Elsberry  
L. E. Carr, III

Approved for public release; distribution is unlimited.

DTIC QUALITY INSPECTED 2

REPORT DOCUMENTATION PAGE			Form Approved OMB No. 0704-0188	
Public reporting burden for this collection of information is estimated to average 1 hour per response, including the time for reviewing instruction, searching existing data sources, gathering and maintaining the data needed, and completing and reviewing the collection of information. Send comments regarding this burden estimate or any other aspect of this collection of information, including suggestions for reducing this burden, to Washington Headquarters Services, Directorate for Information Operations and Reports, 1215 Jefferson Davis Highway, Suite 1204, Arlington, VA 22202-4302, and to the Office of Management and Budget, Paperwork Reduction Project (0704-0188) Washington DC 20503.				
1. AGENCY USE ONLY (Leave blank)	2. REPORT DATE March 1998	3. REPORT TYPE AND DATES COVERED Master's Thesis		
4. TITLE AND SUBTITLE A Comparison of the NOGAPS and GFDN Dynamical Track Prediction Models During the 1997 Western North Pacific Typhoon Season		5. FUNDING NUMBERS		
6. AUTHOR(S) Robert G. Schnabel				
7. PERFORMING ORGANIZATION NAME(S) AND ADDRESS(ES) Naval Postgraduate School Monterey CA 93943-5000		8. PERFORMING ORGANIZATION REPORT NUMBER		
9. SPONSORING/MONITORING AGENCY NAME(S) AND ADDRESS(ES)		10. SPONSORING/MONITORING AGENCY REPORT NUMBER		
11. SUPPLEMENTARY NOTES The views expressed in this thesis are those of the author and do not reflect the official policy or position of the Department of Defense or the U.S. Government.				
12a. DISTRIBUTION/AVAILABILITY STATEMENT Approved for public release; distribution is unlimited.		12b. DISTRIBUTION CODE		
13. ABSTRACT (maximum 200 words) The performance of both the U.S. Navy (NOGAPS) and regional (GFDN) dynamical track prediction models during the 1997 western North Pacific typhoon season is documented. In the context of the Systematic Approach of Carr and Elsberry, a knowledge base of six conceptual models (summary in Table 8.1) is proposed that associates recurring tropical cyclone (TC) forecast track errors with various types of TC and environmental structures. Twenty-one storms of the 27 analyzed have periods in which at least one significant track error source was identified (summary in Table 8.3). More situations (23) were identified in the NOGAPS forecasts than in the GFDN forecasts (14). Individual case studies are presented to illustrate recurring scenarios with poor performance in either the NOGAPS model, GFDN model, or both. Use of these conceptual models and their supporting case studies may allow the JTWC forecaster to better understand how the NOGAPS model and GFDN model may perform in specified synoptic environments. It is hoped that the JTWC forecaster can use the information in this study to provide more accurate TC tracks by rejecting inappropriate model guidance during future typhoon seasons in the western North Pacific. In addition, this study may provide feedback to dynamical model producers as to situations in which large track errors have occurred, in hopes that the model might be improved in the future.				
14. SUBJECT TERMS Tropical cyclone track forecasting.			15. NUMBER OF PAGES 137	
			16. PRICE CODE	
17. SECURITY CLASSIFICATION OF REPORT Unclassified	18. SECURITY CLASSIFICATION OF THIS PAGE Unclassified	19. SECURITY CLASSIFICATION OF ABSTRACT Unclassified	20. LIMITATION OF ABSTRACT UL	



Approved for public release; distribution is unlimited.

**A COMPARISON OF THE NOGAPS AND GFDN DYNAMICAL TRACK  
PREDICTION MODELS DURING THE 1997 WESTERN NORTH  
PACIFIC TYPHOON SEASON**

Robert G. Schnabel

Lieutenant, United States Navy

B.S., University of South Carolina, 1992

Submitted in partial fulfillment  
of the requirements for the degree of

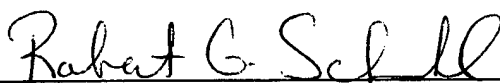
**MASTER OF SCIENCE IN METEOROLOGY AND PHYSICAL  
OCEANOGRAPHY**

from the

**NAVAL POSTGRADUATE SCHOOL**

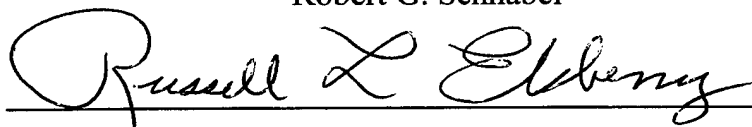
**March 1998**

Author:

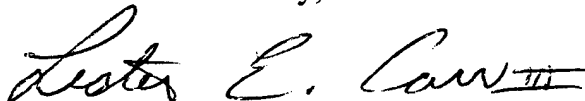


Robert G. Schnabel

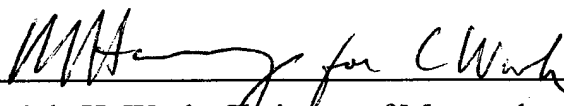
Approved by:



Russell L. Elsberry, Thesis Co-Advisor



Lester E. Carr III, Thesis Co-Advisor



Carlyle H. Wash, Chairman of Meteorology



## **ABSTRACT**

The performance of both the U.S. Navy global (NOGAPS) and regional (GFDN) dynamical track prediction models during the 1997 western North Pacific typhoon season is documented. In the context of the Systematic Approach of Carr and Elsberry, a knowledge base of six conceptual models (summary in Table 8.1) is proposed that associates recurring tropical cyclone (TC) forecast track errors with various types of TC and environment structures. Twenty-one storms of the 27 analyzed have periods in which at least one significant track error source is identified (summary in Table 8.3). More situations (23) are identified in the NOGAPS forecasts than in the GFDN forecasts (14). Individual case studies are presented to illustrate recurring scenarios with poor performance in either the NOGAPS model, GFDN model, or both. Use of these conceptual models and their supporting case studies may allow the JTWC forecaster to better understand how the NOGAPS model and GFDN model may perform in specified synoptic environments. It is hoped that the JTWC forecaster can use the information in this study to provide more accurate TC track forecasts by rejecting inappropriate model guidance during future typhoon seasons in the western North Pacific. In addition, this study may provide feedback to dynamical model producers as to situations in which large track errors have occurred, in hopes that the model might be improved in the future.



## TABLE OF CONTENTS

I. INTRODUCTION .....	1
A. TROPICAL CYCLONE TRACK FORECASTING .....	1
1. NOGAPS Synthetic Observations .....	2
2. GFDN Vortex Specification .....	3
B. BACKGROUND .....	6
C. SYSTEMATIC AND INTEGRATED APPROACH TO TC TRACK FORECASTING .....	6
D. PURPOSE OF THESIS .....	16
II. METHODOLOGY .....	17
III. FALSE DIRECT TROPICAL CYCLONE INTERACTION .....	19
A. IDEALIZED FALSE DIRECT TROPICAL CYCLONE INTERACTION CONCEPTUAL MODEL .....	19
1. Position-Induced False Direct TC Interaction .....	19
2. Horizontal Structure-Related False Direct TC Interaction ...	19
3. False TC/Second Cyclonic Circulation Direct Interaction .....	21
B. CASE STUDIES .....	21
1. Super Typhoon Fred (19W) .....	22
2. Tropical Storm Scott (11W) .....	26

3.	Super Typhoon Nestor (7W)	38
IV.	TRANSITION INTO THE MIDLATITUDE WESTERLIES	45
A.	CONCEPTUAL MODEL OF RETARDED TRANSITION INTO MIDLATITUDE WESTERLIES	45
B.	CONCEPTUAL MODEL FOR MOTION-INDUCED SHIFTING OF TC WIND FIELD CENTER	45
C.	1997 CASE STUDIES	48
1.	Super Typhoon Keith (29W)	48
2.	Typhoon Marie (6W)	55
D.	STATISTICS/VARIATIONS	62
V.	ERRONEOUS INDIRECT TROPICAL CYCLONE INTERACTION	67
A.	BACKGROUND	67
B.	ERRONEOUS INDIRECT TROPICAL CYCLONE INTERACTION CONCEPTUAL MODEL	67
C.	CASE STUDIES	69
1.	TY Zita (17W) and TY Amber (18W)	69
2.	ST Bing (19W) and TY Amber (18W) Remnants	76
D.	1997 STATISTICS/VARIATIONS	83
VI.	TOO RAPID S/DR TO P/PO TRANSITION	93

A.	TOO RAPID S/DR TO P/PO TRANSITION CONCEPTUAL MODEL	
	.....	93
B.	CASE STUDY .....	93
C.	STATISTICS .....	97
VII.	ERRONEOUS TC RECURVATURE THROUGH A THIN SUBTROPICAL	
	RIDGE .....	99
A.	ERRONEOUS RECURVATURE CONCEPTUAL MODEL .....	99
B.	CASE STUDY .....	99
C.	STATISTICS .....	107
VIII.	1997 STATISTICAL SUMMARY .....	109
IX.	CONCLUSIONS AND RECOMMENDATIONS .....	115
A.	CONCLUSIONS .....	115
B.	RECOMMENDATIONS AND FUTURE WORK .....	118
	LIST OF REFERENCES .....	121
	INITIAL DISTRIBUTION LIST .....	123



## ACKNOWLEDGMENTS

Several people have been a great help throughout this endeavor. I would like to thank Mr. Russ Schwanz and Mr. Bob Creasey for their help and guidance during the data manipulation phase of this project. I would also like to thank Mr. Mark Boothe for providing insight and NOGAPS data. I would also like to thank the Naval Research Laboratory of Monterey for providing GFDN data.

This project could not have been accomplished without my thesis advisors Professors Russ Elsberry and Les Carr. I especially would like to thank both of them for their ideas, expert guidance, and patience.

Foremost, I wish to thank my family; Ellen, Brendan, Samantha, and Kathryn for their love and support throughout this endeavor.

## **I. INTRODUCTION**

### **A. TROPICAL CYCLONE TRACK FORECASTING**

Tropical Cyclones (TCs) negatively impact the lives and businesses of many people throughout the world. The timely and accurate forecasting of TC movement is essential to help reduce the destruction that often accompanies these storms. Sophisticated dynamical track prediction models that contain an explicit representation of the TC structure are thought to potentially be the most accurate source of TC track guidance, since such models explicitly allow for motion-affecting nonlinear interactions between the model representations of the TC and the environment.

The Navy Operational Global Atmospheric Prediction System (NOGAPS) model is the dynamical model that provides primary numerical forecast guidance for Department of Defense (DOD) activities. Another dynamical model that provides TC numerical forecast guidance for the western North Pacific is the Fleet Numerical Meteorology and Oceanography Center (FNMOC) implementation of the Geophysical Fluid Dynamics Laboratory (GFDL) model, which is then referred to as GFDN.

For the large-scale flow, TC models usually rely on an operational global analysis. As horizontal resolution of the global models becomes smaller, TCs have become more clearly recognizable in the global analyses. However, the resolution of the global models remains too coarse to resolve accurately the interior structure of the TC. The NOGAPS and GFDN models attempt to resolve this structure in different ways, which is described in the following subsections.

## 1. NOGAPS Synthetic Observations

Goerss and Jeffries (1994; hereafter GJ) discuss the use of TC synthetic observations in the NOGAPS model. The purpose of the synthetic observations is to represent the TC position and horizontal structure in NOGAPS, at least to the extent possible given the horizontal resolution. The synthetic observations used to depict TC structure are composed of contributions from the large-scale environmental flow and cyclone-scale vortex. Because of the relatively coarse resolution of the global model, the model depiction of the TC interior is quite different from observed TC structure. Thus, the synthetic observations have been designed to be consistent with how the NOGAPS forecast model depicts TCs rather than how TCs actually appear in nature (Goerss *et al.* 1991).

Soundings are generated at 13 points for each storm: one is located at the position of the storm center, four are located 220 km north, south, east, and west of the center position; four are located 440 km northeast, southeast, southwest, and northwest of the center position; and four are located 660 km north, south, east, and west of the center position. The vortex component of the synthetic wind observations is derived from a symmetric Rankine profile that fits the maximum wind speed, and the radii of the 30-kt and 50-kt winds reported in the tropical cyclone warning message from the Joint Typhoon Warning Center (JTWC) or another forecast center.

The synthetic observations are analogous to rawinsonde soundings and consist of a 1000-mb height, and wind vectors at 1000, 925, 850, 700, and 400 mb. Notice that no upper-tropospheric or outflow-layer winds are included. The wind vectors are the sum of the large-scale environmental component and the symmetric vortex component. The warm-core

structure of the TC is simulated by decreasing the vortex wind speeds in the vertical by a scaling factor of 1.0 at 1000 mb and 0.65 at 400 mb.

The synthetic TC observations are assimilated into the NOGAPS model by the global multivariate optimum interpolation (MVOI) technique. The MVOI technique is described in detail by Goerss and Phoebus (1992). The synthetic observations are assumed to have the same error properties as radiosondes, which have the highest weightings of any observations in the MVOI. The resultant analysis may differ from the synthetic TC observation position and structure because the synthetic observations are blended with all other observations and with a 6-h prior NOGAPS forecast that is used as a background field.

Following the introduction of the synthetic TC observations in June 1990, notable improvements were achieved in the NOGAPS 48- and 72-h TC track forecasts in the western North Pacific. The impact of the synthetic observations and subsequent improvements in TC track forecasts have been described in several studies. Goerss and Petko (1995) and GJ conducted many NOGAPS model runs, both with and without the inclusion of synthetic observations, to assess the accuracy of the NOGAPS TC track forecasts. Inclusion of the synthetic observations substantially improved the NOGAPS track forecasts. Additional improvements were observed in NOGAPS TC track forecasts after October 1994, when the environmental wind structure averaged over the 13 synthetic observations was required to agree with the recent motion of the TC. This adjustment helps the model storm to move in the correct initial direction and speed.

## **2. GFDN Vortex Specification**

Kurihara *et al.* (1993) developed an initialization scheme for the GFDL Multipli-

nested Movable Mesh (MMM) hurricane model. The MMM hurricane model has been fully documented in a series of papers, notably Kurihara *et al.* (1993, 1995, 1997). Without initialization, the initial structure of the TC is inaccurate, and the TC motion can be erratic at the start of the model integration as the analyzed vortex adjusts to the much finer model resolution. The GFDL model is the combination of this initialization scheme with the MMM hurricane model. The GFDL model is initialized from a global analysis and an initialization message that specifies the observed structure of the TC. The FNMOC implementation of the GFDL model (GFDN) is almost identical to the one that runs operationally at the National Centers for Environmental Prediction (NCEP), except that the analysis section has been modified to use the NOGAPS analyses and forecasts as initial and boundary conditions. In addition, GFDN uses the JTWC TC bogus (TCBOGUS) as the initialization message.

Kurihara *et al.* (1993) discuss the initialization scheme that removes the poorly resolved, unrealistic vortex from the global analysis, and then uses a two-dimensional (radius-pressure) version of the MMM to generate a symmetric vortex that possesses a realistic and model-consistent structure. The two-dimensional symmetric vortex is then used to generate a beta-effect asymmetric circulation that is added to the symmetric vortex. Finally, the specified vortex is smoothly incorporated into the large-scale field. The scheme to construct a realistic initial field can be expressed as:

$$(\text{Initial field}) = (\text{global analysis}) - (\text{analyzed vortex}) + (\text{specified vortex}).$$

The initialization begins with the removal of the hurricane vortex in the global analysis, which is also expressed as a determination of the environmental field:

$$(\text{Environmental field}) = (\text{global analysis}) - (\text{analyzed vortex}).$$

The global analysis is first partitioned into a large-scale component, called the basic field, and the deviation from it is called the disturbance field, which includes the smaller-scale variability depicting the analyzed vortex as well as any other non-basic features. This is expressed as:

$$(\text{global analysis}) = (\text{basic field}) + (\text{disturbance field}).$$

The next step is to separate the analyzed storm, called the hurricane component, from the disturbance field. The remainder is called the non-hurricane component. This step is expressed as:

$$(\text{disturbance field}) = (\text{hurricane component}) + (\text{non-hurricane component}).$$

The environmental field is then obtained by combining the non-hurricane component with the basic field; that is,

$$(\text{Environmental field}) = (\text{basic field}) + (\text{non-hurricane component}).$$

The environmental field is identical to the global analysis outside of a filter domain. Within this filter domain, the hurricane component of the disturbance field is effectively removed from the global analysis through the use of the environmental field. The initialization is completed with the addition of a realistic storm vortex, which is generated and specified as a new hurricane component, onto the environmental field.

This hurricane model initialization scheme was modified (Kurihara *et al.* 1995) to improve the representation of the environmental fields in the initial condition. The generation process of the realistic and model-compatible vortex has also undergone some minor changes so that reasonable vortices are produced for various data conditions. The upgraded GFDL prediction system was tested for a number of cases and compared against

the previous version and yielded an overall improvement in the forecasts of storm tracks.

## **B. BACKGROUND**

Starting 22 May 1996, FNMOC ran GFDN on the off-time (06/18 UTC) watches whenever a TCBOGUS for a western North Pacific TC was received (Rennick 1997). The model applied the highest priority off-time TCBOGUS to the off-time NOGAPS analyses and used the forecast fields from the previous real-time (00/12 UTC) NOGAPS predictions for boundary conditions. These GFDN forecasts were available to JTWC by about 1130/2330 UTC, i.e., in time for their subsequent 12/00 UTC warnings.

In an evaluation of the performances of the NOGAPS and GFDN models in the western North Pacific during the 1996 typhoon season by Goerss (1997), the NOGAPS and GFDN models were found to have virtually identical forecast errors for the overall season. Interestingly, there were groups of cyclones for which NOGAPS performed significantly better than GFDN. There was also another group for which GFDN significantly outperformed NOGAPS, and still another group where both models performed similarly. While this result immediately suggests that an ensemble approach may produce forecasts with smaller errors, a forecaster would ideally like to know *a priori* which model will produce the best forecasts for a given TC.

## **C. SYSTEMATIC AND INTEGRATED APPROACH TO TC TRACK FORECASTING**

A Systematic and Integrated Approach to TC Track Forecasting (hereafter the Systematic Approach) has been developed by Carr and Elsberry (1994; hereafter CE94). The key objective of the Systematic Approach is to enable forecasters to improve upon TC track

forecasts generated by numerical and objective guidance (CE94). The central thesis of the Systematic Approach is that the forecaster may improve on dynamical and objective track prediction guidance when equipped with: (i) a meteorological data base of dynamically sound conceptual models that classify various TC-environment situations into a reasonably small number of recurring combinations of environmental structure and TC structure, and sequences of environmental change, called transitions; (ii) a knowledge base that associates certain types of recurring TC track forecasts with various TC structures and environment structure; and (iii) an implementing methodology or strategy for applying these two knowledge bases by taking account of expected guidance errors.

In the Systematic Approach, the environmental structure (Fig. 1.1) is defined in terms of synoptic patterns and regions derived from operationally analyzed NOGAPS maps (CE94). Synoptic patterns are classifications of the large-scale environment based on the existence and orientation of various synoptic circulations such as cyclones and anticyclones, or troughs and ridges. Synoptic regions are identified as smaller areas within the synoptic patterns where certain characteristic directions of environmental steering might be expected. Four synoptic patterns and seven synoptic regions (Table 1.1) are defined in the western North Pacific region. The synoptic patterns/regions that pertain to this thesis will be briefly described. A complete discussion of synoptic pattern/regions as well as detailed case studies with analyses, satellite imagery, and tracks are provided by CE94 and Carr *et al.* (1995). A key conclusion from a five-year (Carr *et al.* 1995) and later a seven-year sample is that characteristic tracks that are distinctly different are associated with each synoptic pattern/region combination.

# WESTERN NORTH PACIFIC METEOROLOGICAL KNOWLEDGE BASE

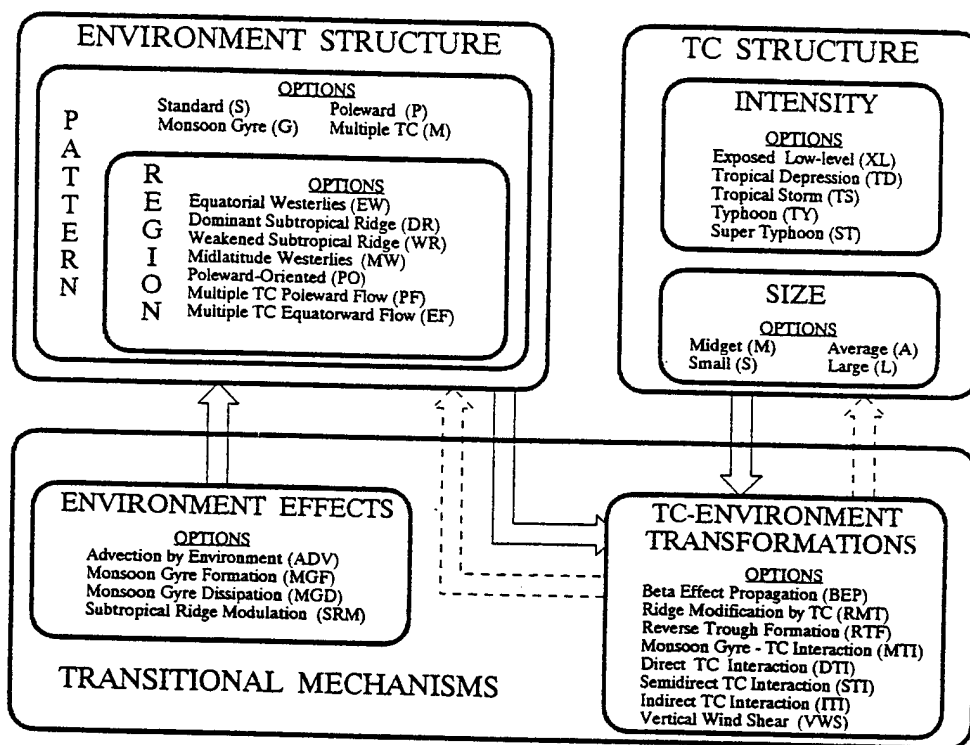


**Figure 1.1.** The meteorological knowledge base of the Systematic Approach with the environment structure synoptic patterns and regions in the upper left (Carr *et al.* 1997).

SYNOPTIC REGIONS	SYNOPTIC PATTERNS			
	Standard	Poleward-Oriented	Monsoon Gyre	Multiple Tropical Cyclone
	(S)	(P)	(G)	(M)
Dominant Subtropical Ridge (DR)	X	X	X	X
Weakened Subtropical Ridge (WR)	X			
Poleward-Oriented (PO)		X	X	
Midlatitude Westerlies (MW)	X	X	X	X
Multiple TC Poleward Flow (PF)				X
Multiple TC Equatorward Flow (EF)				X
Equatorward Westerlies (EW)	X			

**Table 1.1.** Environment structure described in terms of four Synoptic Patterns and seven Synoptic Regions that appear in various synoptic patterns (Carr *et al.* 1997).

In the Standard (S) synoptic pattern (Fig. 1.2), the axis of the subtropical anticyclone is approximately east-west, although it may be tilted longitudinally. This anticyclone may be modulated by a midlatitude trough that introduces a break, or the anticyclone may be relatively thin rather than the broad circulation shown in Fig. 1.2. Four synoptic regions are defined in the S pattern. A new Equatorial Westerlies (EW) region was recently added (Carr *et al.* 1997). The Dominant Ridge (DR) synoptic region is poleward of the equatorial trough and equatorward of the subtropical anticyclone. A separate synoptic region called the Weakened Ridge (WR) is east of, and relatively close to, the subtropical ridge break in a relatively weak (5-8 kt) southeasterly-to-southerly environmental steering flow. Finally, the Midlatitude Westerlies (MW) synoptic region is poleward of the subtropical ridge axis and east of the ridge break. A TC in the DR region usually has a predominantly westward track such as the sequence 1-2-3 in Fig. 1.2. However, a TC in the WR region may recurve (sequence 1-4-5 in Fig. 1.2) or may have "failed recurvature" and return to a position in the DR region (sequence 1-4-3 in Fig. 1.2). Of the 3435 synoptic environment characterizations in the western North Pacific during 1989-1995, approximately 60% were in the S pattern. A majority (52%) of all assignments was in the DR synoptic region of the S pattern (termed S/DR). The corresponding TC tracks for the S pattern are given in Fig. 1.3. TC tracks that are generally long and toward the west-northwest are associated with the periods when the TCs are in the S/DR combination. Short poleward tracks are associated with the S/WR combination, as TCs move through the subtropical ridge. A possible sequence is for the TC to recurve into the MW synoptic region and then accelerate, in which tracks are first northward, and then northeastward.

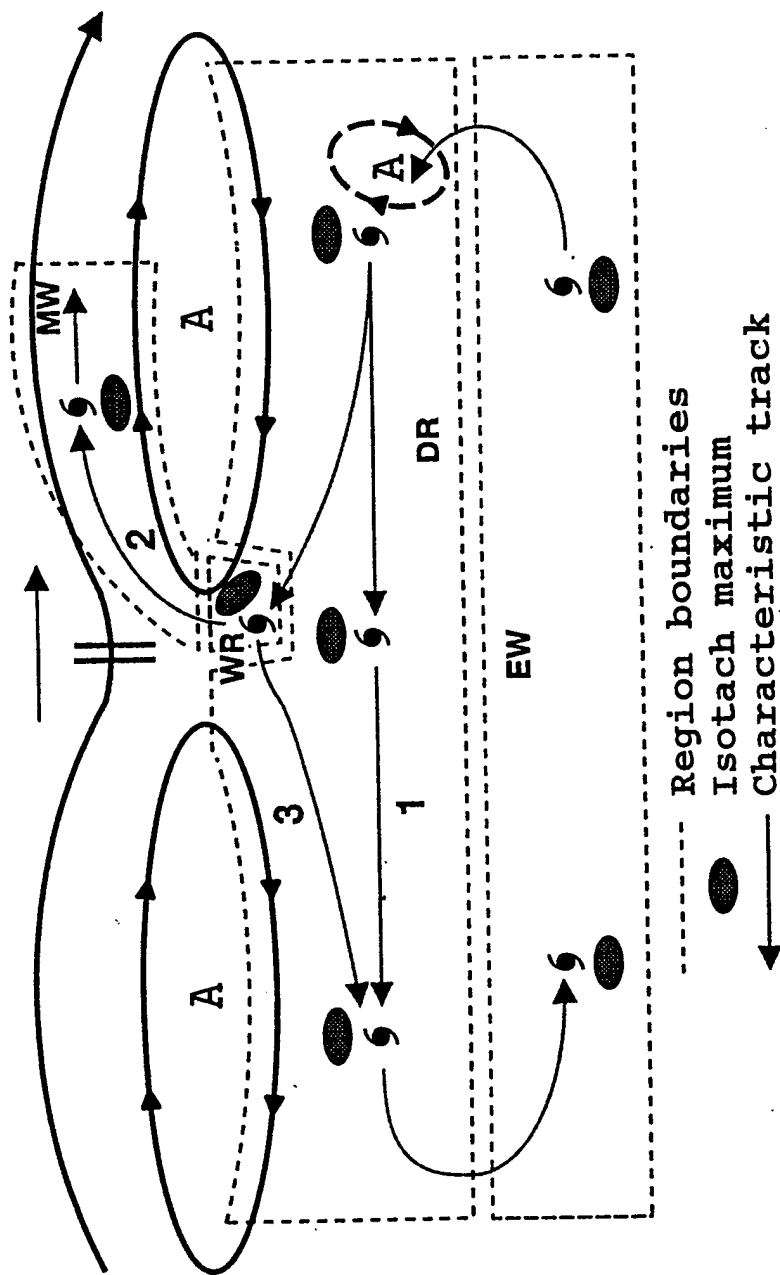


**Figure 1.2.** Schematic of the Standard (S) synoptic pattern conceptual model with the boundaries (dashed) of the associated synoptic region conceptual models added (Carr *et al.* 1997). DR denotes the Dominant Ridge region, WR the Weakened Ridge region, EW the Equatorial Westerlies, and MW the Midlatitude Westerlies region. Streamlines of an appropriate layer-mean environmental flow with the TC circulation removed are indicated by wide solid lines, with A and C indicating anticyclone and cyclone, respectively. The numbered TC symbols indicate possible sequences of tracks.

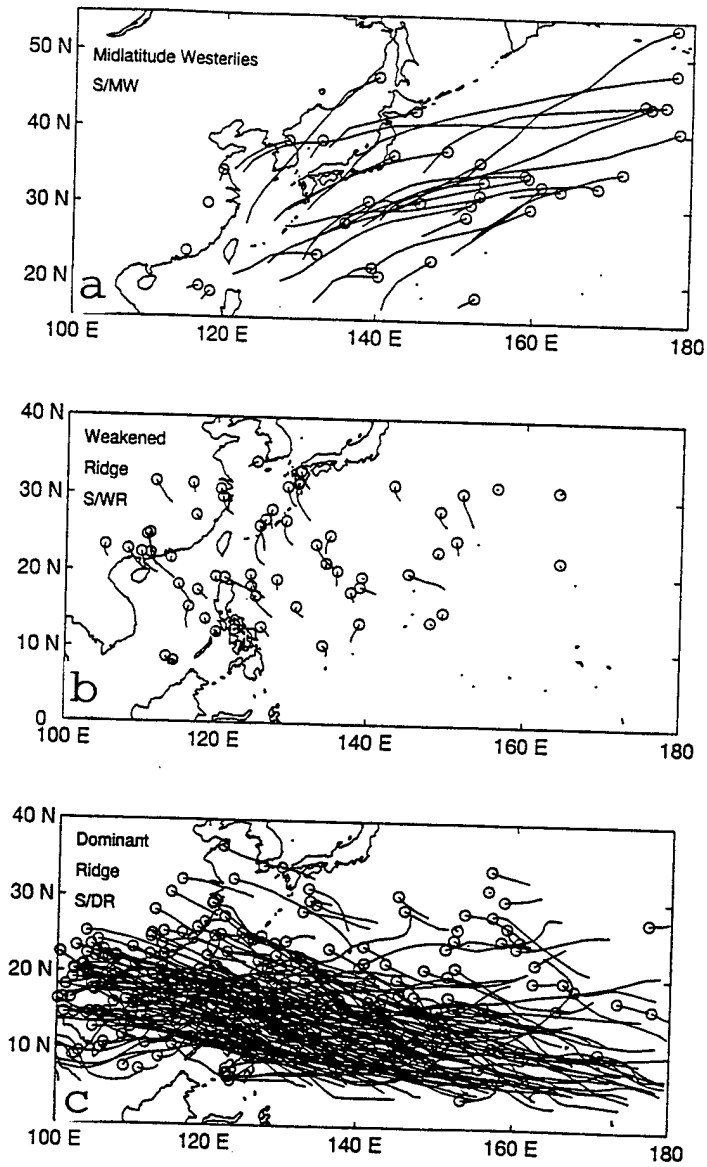


**Figure 1.3.** Storm tracks during 1989-1996 while the storm is in the Standard (S) pattern and the (a) Midlatitude Westerlies, (b) Weakened Ridge, and (c) Dominant Ridge synoptic regions (Carr *et al.* 1997). Periods of dual assignments are omitted.

In the Poleward (P) synoptic pattern (Fig. 1.4), the environment structure usually includes a significant subtropical anticyclone break poleward of the TC, and a prominent, primarily north-south oriented anticyclone to the east that extends equatorward of the TC. Two scenarios during which a P pattern can develop are discussed by CE94. The first occurs when the latitude of the monsoon trough axis increases to the east, which is called a reverse-oriented trough. The second occurs if a single TC is comparatively large relative to adjacent synoptic features. The P pattern can develop after the poleward-oriented anticyclone forms to the east and equatorward of the TC via Rossby wave dispersion in which anticyclonic vorticity advection to the east and south of the TC vortex leaves a peripheral anticyclone in its wake. Two synoptic regions are defined in the P pattern. The Poleward-Oriented (PO) synoptic region is to the east of the reverse-oriented monsoon trough and extends to a col region near the poleward end of the subtropical anticyclone. The typical TC motion in the PO region is poleward (sequence 1-2-3 in Fig. 1.4). The Midlatitude Westerlies (MW) synoptic region is analogous to the MW region of the S pattern (Fig. 1.2). The two DR regions shown in Fig. 1.4 are considered to be the DR regions of the adjacent S pattern and are not part of the P pattern.

Corresponding tracks from the P pattern are given in Fig. 1.5. The tracks in the PO region have the expected poleward tracks, but are characterized by large variations in the directions and lengths of the tracks, including some sinuous tracks. Notice that the tracks in the P pattern are different from those in the S/WR combination in Fig. 1.3. Because the meridional extent of anticyclone east of the TC in the P/PO combination (Fig. 1.4) is greater than that of the subtropical anticyclone east of the TC in the S/WR combination (Fig. 1.2),

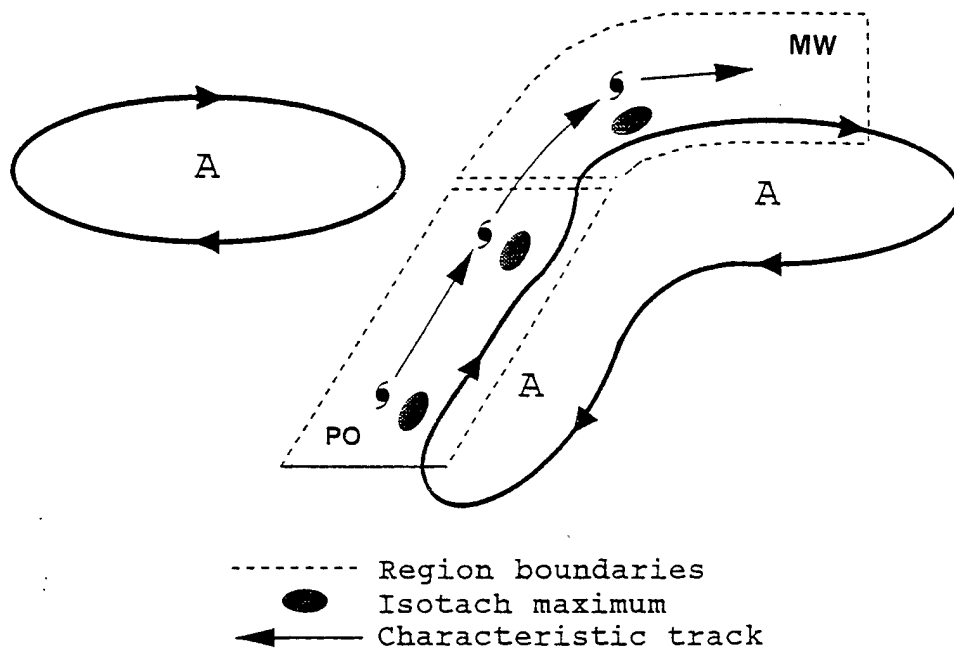


**Figure 1.4.** As in Fig. 1.2, except for the Poleward (P) synoptic pattern and associated synoptic regions (dashed lines), where PO denotes the Poleward-oriented synoptic region.

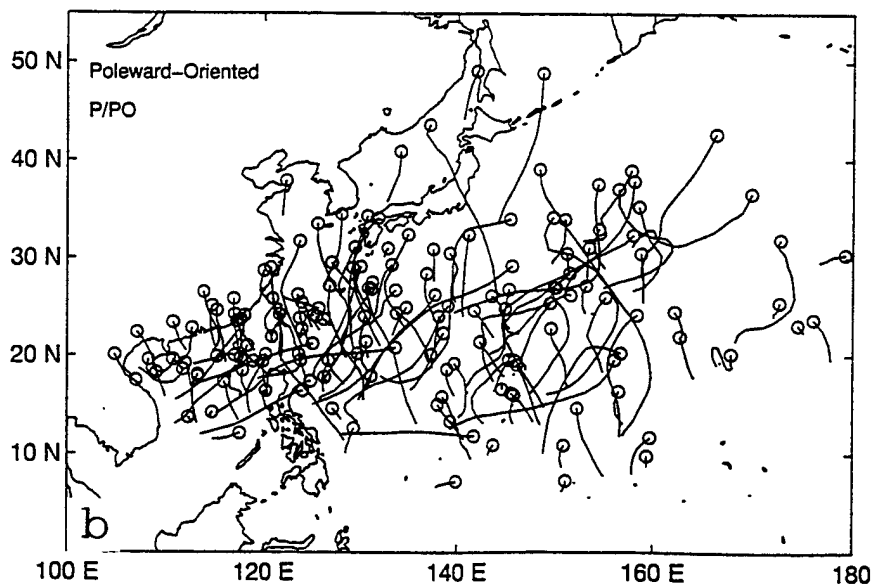
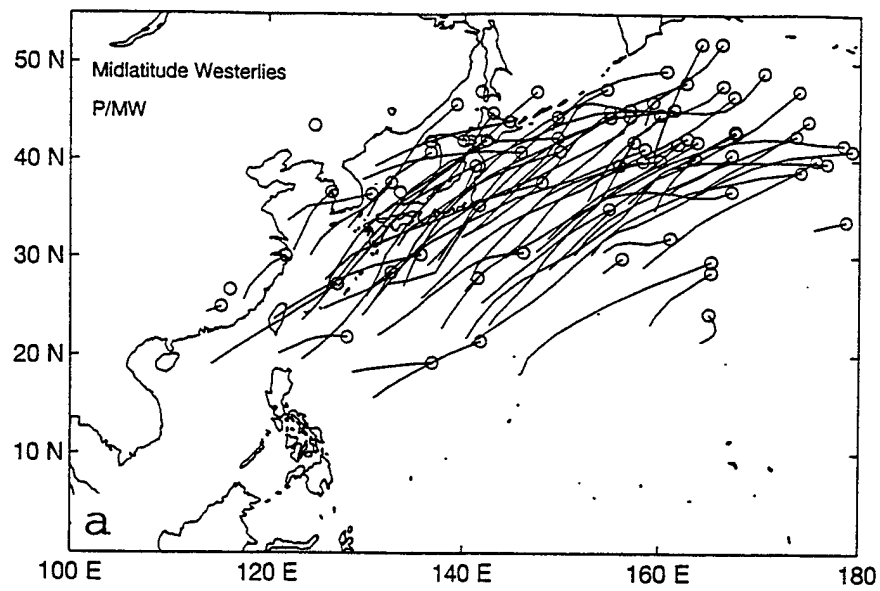


**Figure 1.5.** Storm tracks as in Fig. 1.3, except in the Poleward (P) pattern and the (a) Midlatitude Westerlies (MW) and (b) Poleward-oriented (PO) synoptic regions.

the storm tracks in the P/MW region tend to be consistently poleward, although an eastward track sometimes does occur. About 30% of the synoptic environment characterizations are in the P pattern, with 21% in the PO region, and the remainder in the MW region. Notice that about 73% of all cases are in the S/DR and P/PO combinations alone.

#### **D. PURPOSE OF THESIS**

This thesis will document the performance of both the NOGAPS and the GFDN models during the 1997 western North Pacific typhoon season through individual case studies. A knowledge base that associates types of recurring TC track forecast errors with various TC structures and environment structures will be constructed. Conceptual models and case studies will be presented to illustrate recurring poor performance in either the NOGAPS model, GFDN model, or both mainly during the 1997 western North Pacific typhoon season. These illustrations of the NOGAPS performance and GFDN performance, as well as the description of the conceptual models, will be provided in the context of the Systematic Approach described in Chapter I.C above. This thesis will also provide guidance to JTWC forecasters on how best to use (or not use) NOGAPS and GFDN track predictions. In addition, this thesis will provide feedback to model producers as to situations in which large track errors have occurred, in hopes that the models can be improved in the future.

## II. METHODOLOGY

A forecast track error (FTE) is the distance between the JTWC best-track position and the forecast location of a TC at the same valid time. Another error measure is to separate it into an along-track component and a cross-track component relative to the best-track orientation at the verification time. The NOGAPS and GFDN FTEs were computed at 24 h, 48 h, and 72 h for each TC that developed in the western North Pacific basin during the 1997 TC season. Storms with higher than average FTEs were selected for detailed analysis. Special attention was given to those storms that exhibited consistently large FTEs and had a notable difference between the performance of NOGAPS and GFDN. For example, the NOGAPS track of Tropical Storm Scott (11W) exhibited extremely large 72-h FTEs for several model runs while the GFDN FTEs were considerably lower at the corresponding times (not shown). These NOGAPS and GFDN comparisons had to be done on a 6-h lag basis because of the difference in initialization times. Specifically, the 00 UTC NOGAPS track was compared with the GFDN track that was begun at 06 UTC, and the 12 UTC NOGAPS track was compared with the GFDN track that was begun at 18 UTC. Since the objective here is to examine large track error causes, the small advantage of the GFDN from a later initial position (but essentially the same synoptic data) is not considered to be important.

In 1997, the GFDN forecast fields of 27 of the 31 TCs that formed in the western North Pacific became available for study, and could be compared with the corresponding NOGAPS analyses. Close attention was paid to the forecast vortex circulations versus the

analyzed circulations, and forecast and analyzed intensities, between NOGAPS and GFDN, as well as to forecast separation distances. Consideration was also given to how the initial TC(s) modified the surrounding environment during the forecast interval.

Chapters III through VII will introduce six conceptual models that illustrate how the differences in initial TC specifications and in horizontal/vertical resolution may have lead to different tracks in the two models. Chapter VIII will classify 21 of the analyzed 27 TCs during 1997 into at least one of these conceptual models.

### **III. FALSE DIRECT TROPICAL CYCLONE INTERACTION**

#### **A. IDEALIZED FALSE DIRECT TROPICAL CYCLONE INTERACTION CONCEPTUAL MODEL**

A false direct tropical cyclone interaction occurs when a tropical cyclone (TC) is predicted to interact with another TC (or with another cyclonic circulation) in the forecast model but such an interaction does not occur in nature. Three ways false direct TC interaction may occur in the forecast fields are position-induced, horizontal structure-related interaction of two real TCs/cyclonic circulations, and false second cyclonic circulation. Each of these ways is described below.

##### **1. Position-Induced False Direct TC Interaction**

Position-induced false direct TC interaction may occur in the model forecast when the TC location in the model first-guess field differs from the location of the synthetic observations or specified vortex. In these situations, the model first-guess vortex and the synthetic observation vortex (or specified vortex) tend to rotate cyclonically around one another during the forecast interval. Also, the model forecast surface fields often have a larger vortex than the analyzed fields as a result of a merger of the two vortices (Fig. 3.1d). The predicted TC track is usually degraded when this type of false interaction occurs.

##### **2. Horizontal Structure-Related False Direct TC Interaction**

Horizontal structure-related false direct TC interaction may be predicted by a model when two real TCs/cyclonic circulations are in close proximity (Fig. 3.1a). In these situations, too large TCs/cyclonic circulation diameters, which may become evident in the

**Scenario: Model-predicted direct interaction of TC (DTI) with second, weaker cyclone in equatorial trough**

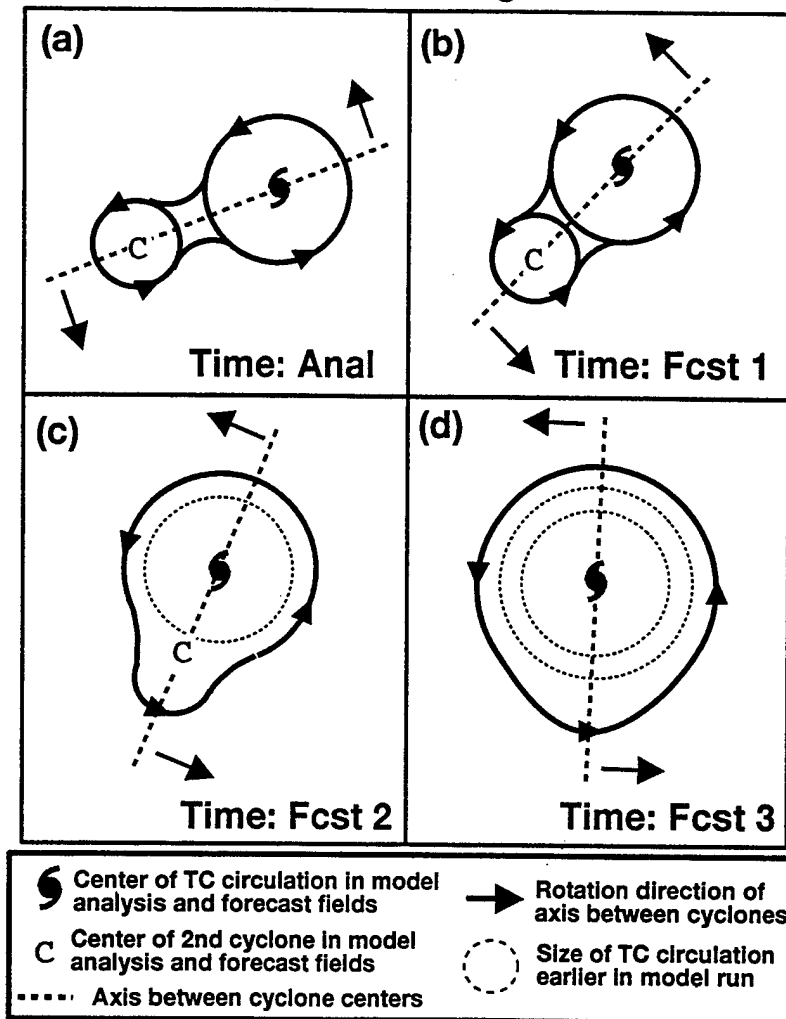


**Figure 3.1.** False TC Interaction conceptual model. This model-predicted TC interaction occurs when two TCs falsely interact with one another (see insert for amplification of this conceptual model).

model forecast fields, can result in a false reduction in the separation distance between the circulations and usually a merger of the two circulations. In these situations, a characteristic cyclonic rotation of the two circulations around each other is noted in the forecast fields (Figs. 3.1a through 3.1d), and is also evident in the predicted TC track. A characteristic of this type of false direct TC interaction in the model forecast is an inability to maintain TC intensity when the TC and the cyclonic circulation begin to interact. This reduction in intensity may shift the TC steering flow to a lower level. The usual result of horizontal structure-related false direct TC interaction is a slow and left of track forecast (an example is given in Fig. 3.7).

### **3. False TC/Second Cyclonic Circulation Direct Interaction**

False TC/second cyclonic circulation direct interaction may be predicted in a model when another forecast circulation is found in close proximity to the TC that does not exist in nature. A cyclonic rotation about the mid-point between the TC and the false second cyclonic circulation is often evident, and the false cyclonic circulation influences the movement and development of the TC in the forecast interval. The result of this type of false direct TC interaction is often a slow and left of track forecast (an example will be given in Fig. 3.10).

## **B. CASE STUDIES**

The following case studies provide examples of the three types of false direct TC interaction described above. The first case study of Super Typhoon (ST) Fred occurred in August 1994 and is an example of position-induced direct tropical cyclone interaction. The second case study of Tropical Storm (TS) Scott occurred in July 1997 and is an example of

horizontal structure-related false direct interaction. The third case study of ST Nestor occurred in June 1997 and is an example of false TC/second cyclonic circulation direct interaction. All the case studies that follow illustrate false direct TC interaction occurring in NOGAPS, since the phenomenon seems to occur most frequently in that model. However, it is emphasized that false direct TC interaction can and has occurred in other operational models that provide TC forecast tracks.

### **1. Super Typhoon Fred (19W)**

ST Fred provides an example of position-induced false direct TC interaction in the NOGAPS model. Notice that ST Fred had formed near  $18^{\circ}$  N,  $145^{\circ}$  E and tracked westward for about two days before beginning a long track to the northwest (Fig. 3.2).

At 12 UTC 14 August 1994 (Fig. 3.3a), the NOGAPS surface analysis has a closed vortex near  $18^{\circ}$  N,  $149^{\circ}$  E and also has an area of low pressure to the west of this vortex. Notice that the 12 UTC 14 August best-track position (Fig. 3.2) for Tropical Depression (TD) 19W is near  $18^{\circ}$  N,  $144^{\circ}$  E, which is actually in the area of low pressure to the west of the closed vortex in the NOGAPS analysis. The distance between the NOGAPS analyzed vortex and the best-track position of TD Fred is about  $5^{\circ}$  long., which suggests that the NOGAPS first-guess location was in error and resulted in a vortex considerably east of the proper location.

Twenty-four hours later, the NOGAPS surface analysis (Fig. 3.3b) has TS Fred near  $19^{\circ}$  N,  $141^{\circ}$  E, which is a westward displacement consistent with the track in Fig. 3.2. However, the NOGAPS 24-h forecast (Fig. 3.3c) has TS Fred near  $20^{\circ}$  N,  $147^{\circ}$  E, which is about  $6^{\circ}$  long. to the east-northeast of the analyzed position. This 24-h forecast track to the

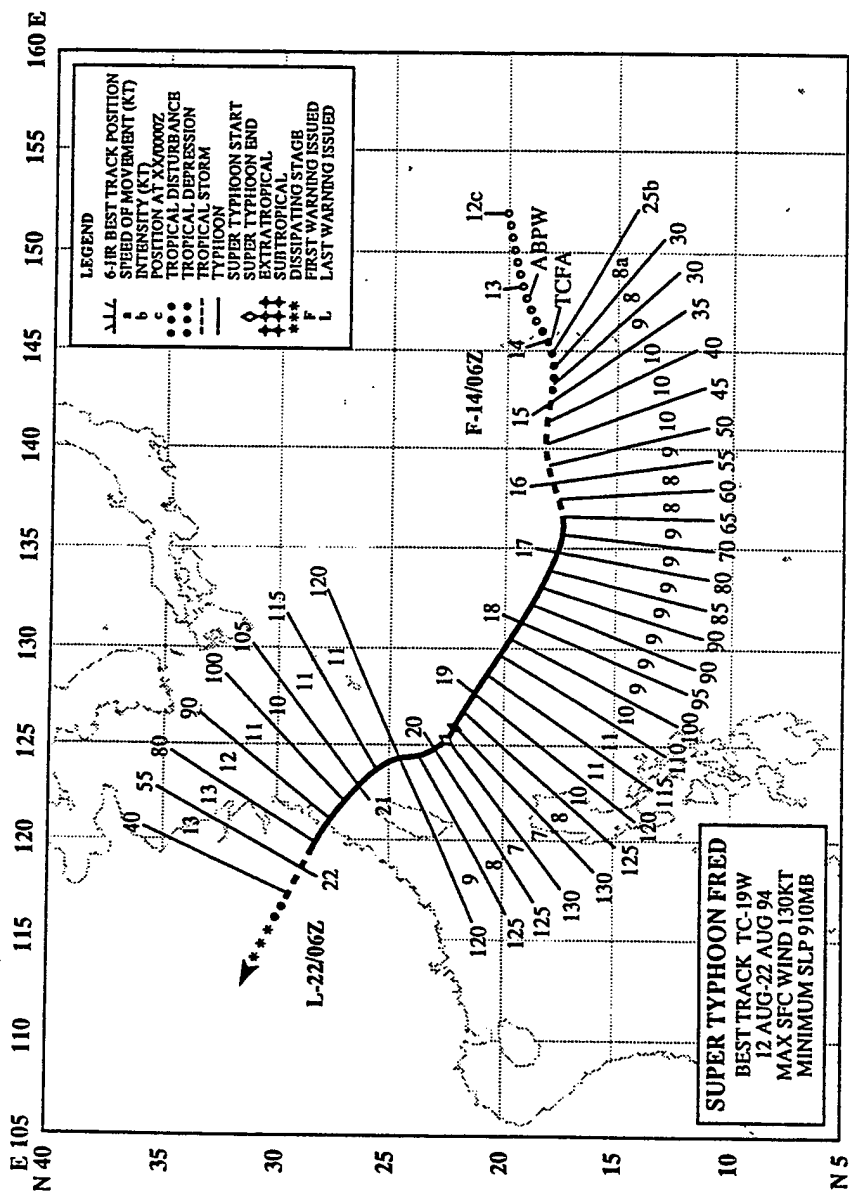
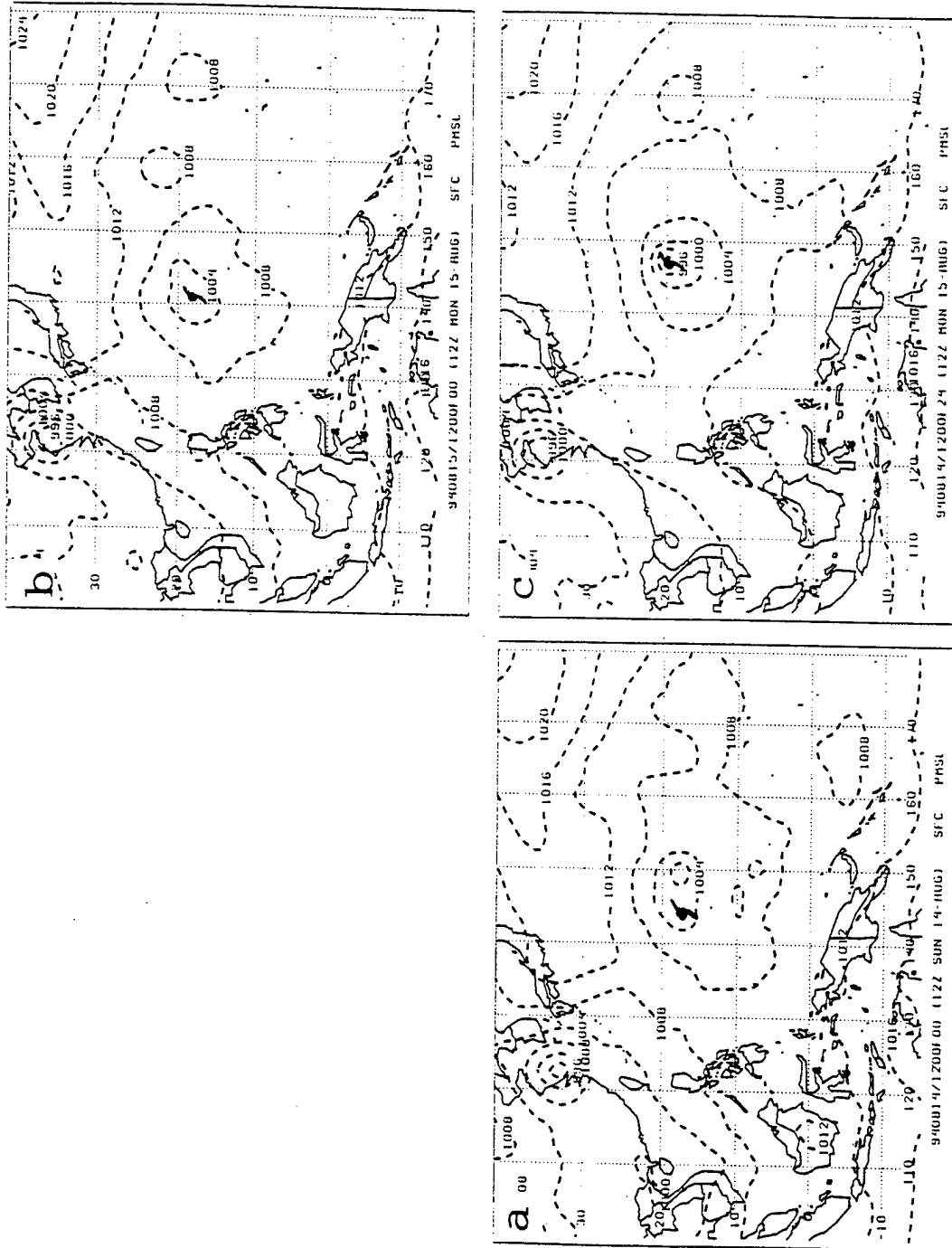
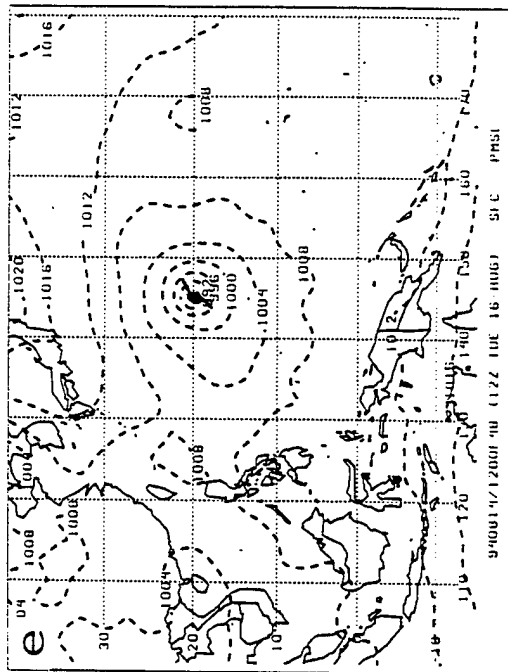
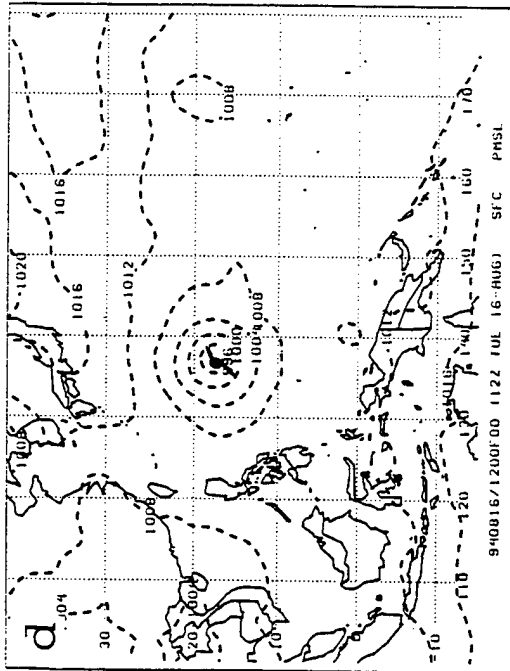
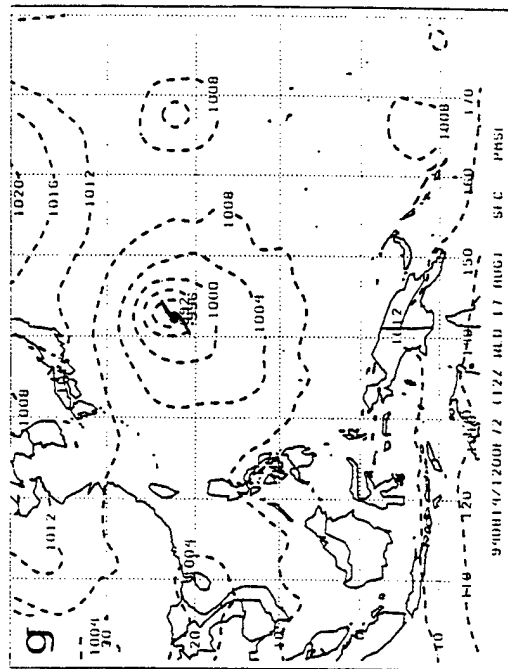
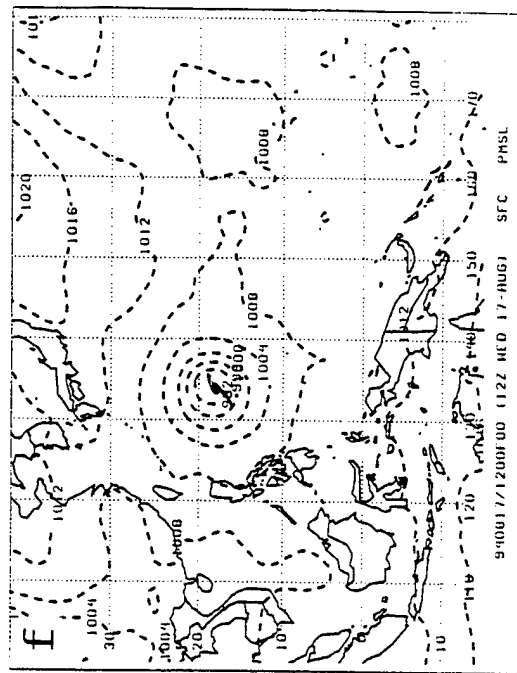


Figure 3.2. Joint Typhoon Warning Center best track for ST Fred 12 August to 22 August 1994. Positions at 00 UTC are indicated along the track with intensities (kt) indicated at the end of radials extending from intermediate 6-h positions, storm translation speeds over 6 h are indicated between these radials (see inset for explanation of symbols).



**Figure 3.3.** NOGAPS surface analysis (dashed, 4 mb interval) at 12 UTC (a) 14 August 1994, (b) 15 August, (d) 16 August, and (f) 17 August. Corresponding forecasts valid at the times of (b), (d), and (f) are given in panels (c), (e), and (g), respectively. Notice the distance between the best-track position (TC symbol) and the analyzed center to the east.



northwest suggests that a cyclonic rotation of the vortex and low pressure in the initial field (Fig. 3.3a) is taking place in the NOGAPS model. Whereas the NOGAPS 24-h predicted central pressure of TS Fred is about 992 mb, the analyzed central pressure of TS Fred is about 1002 mb. That is, the merger of the vortex and low pressure area in the initial conditions appears to result in a deepening of the combined circulation.

At 12 UTC 16 August (Fig. 3.3d), the NOGAPS analysis has TY Fred near  $18^{\circ}$  N,  $137^{\circ}$  E. Notice that the central pressure has decreased to near 994 mb and that the actual movement continues to be westward. The NOGAPS 48-h forecast (Fig. 3.3e) is for a slow westward track from the 24-h forecast location (Fig. 3.3c) and a further decrease in central pressure to about 987 mb. Notice that the NOGAPS 48-h forecast continues to predict a slow and to the right track and that the 48-h forecast central pressure continues to be considerably deeper than the analyzed central pressure.

After another 24 h (Fig. 3.3f), TY Fred is beginning to move northwestward as it continues to deepen. The NOGAPS 72-h forecast (Fig. 3.3g) has TY Fred near  $22^{\circ}$  N,  $143^{\circ}$  E, which is considerably north and east of the analyzed position. Notice that the NOGAPS 72-h forecast central pressure continues to be slightly lower than the NOGAPS analyzed central pressure. It is suggested that the apparent misplacement of the NOGAPS first-guess field has severely degraded the forecast track of ST Fred.

## **2. Tropical Storm Scott (11W)**

TS Scott was an example of false direct TC interaction in the NOGAPS model. Notice that TS Scott had formed near  $24^{\circ}$  N,  $149^{\circ}$  E and had drifted northward for four days and then southeastward for two days before again turning northward (Fig. 3.4). The

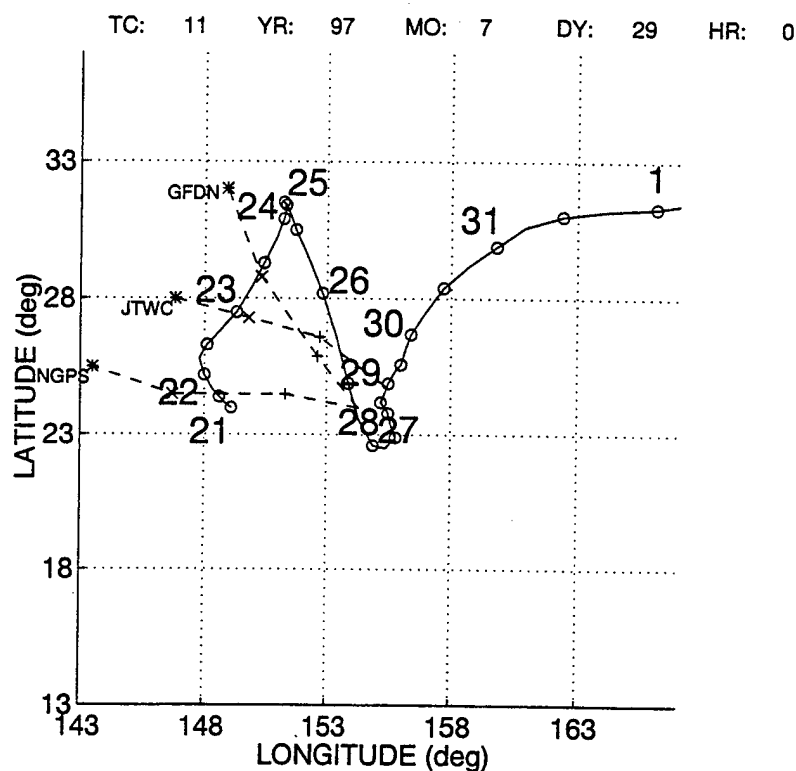


**Figure 3.4.** Best track and predicted tracks for Tropical Storm (TS) Scott from 21 July to 1 August 1997. The best track is a solid line with circles indicating every 00 and 12 UTC position. Large bold numbers are the date next to the 00 UTC position. Dashed lines are forecast tracks for TS Scott by different models (NOGAPS and GFDN) or by JTWC. The NOGAPS and GFDN model forecasts were initiated at 12 and 18 UTC 28 July, respectively. The JTWC forecast was initiated at 00 UTC 29 July. The (+), (x), and (\*) along the forecast track indicate the 24-h, 48-h, and 72-h forecast positions, respectively.

NOGAPS track forecast initiated at 12 UTC 28 July 1997 (Fig. 3.4) had a 72-h FTE of 1050 n mi. The corresponding 66-h FTE for the GFDN track forecast initiated at 18 UTC 28 July (Fig. 3.4) was 778 n mi. Whereas both the NOGAPS and GFDN tracks were westward, the actual motion of the storm was first northward and then eastward.

At 12 UTC 28 July 1997 (Fig. 3.5a), the NOGAPS streamline analysis had TS Scott near  $24^{\circ}\text{N}$ ,  $155^{\circ}\text{E}$ . Notice also a cyclonic circulation to the southwest centered near  $18^{\circ}\text{N}$ ,  $148^{\circ}\text{E}$ . Twenty-four hours later, the NOGAPS streamline analysis (Fig. 3.5b) has TS Scott near  $26^{\circ}\text{N}$ ,  $155^{\circ}\text{E}$ . The isotach maximum to the east-southeast of TS Scott in Fig. 3.5b suggests a steering current from the south-southwest, which is consistent with the observed track direction at 12 UTC 29 July (Fig. 3.4). Notice that the cyclonic circulation initially to the southwest, which is about  $2^{\circ}$  long. wide, has maintained the same orientation. However, the NOGAPS 24-h forecast (Fig. 3.5c) has TS Scott near  $26^{\circ}\text{N}$ ,  $153^{\circ}\text{E}$ , which is west of the actual position. Notice the circulation that was initially to the southwest of TS Scott is now predicted to be closed and to have translated eastward. The extended 20-kt isotach maximum to the south and east of this cyclonic circulation is further evidence that NOGAPS has amplified this circulation. The combination of the forecast westward placement of TS Scott and eastward position of the cyclonic circulation to the southwest suggests a cyclonic rotation as in TC interaction (see Figs. 3.1a-b). It also appears that the separation distance has been reduced, which is further evidence of a false direct TC-like interaction. In this situation, the expectation would be that the TS Scott forecast track would be more influenced by the cyclonic circulation to the southwest than by a steering flow as indicated in Fig. 3.5b. As noted above, the NOGAPS forecast track errors and the track (Fig. 3.4) indicate this

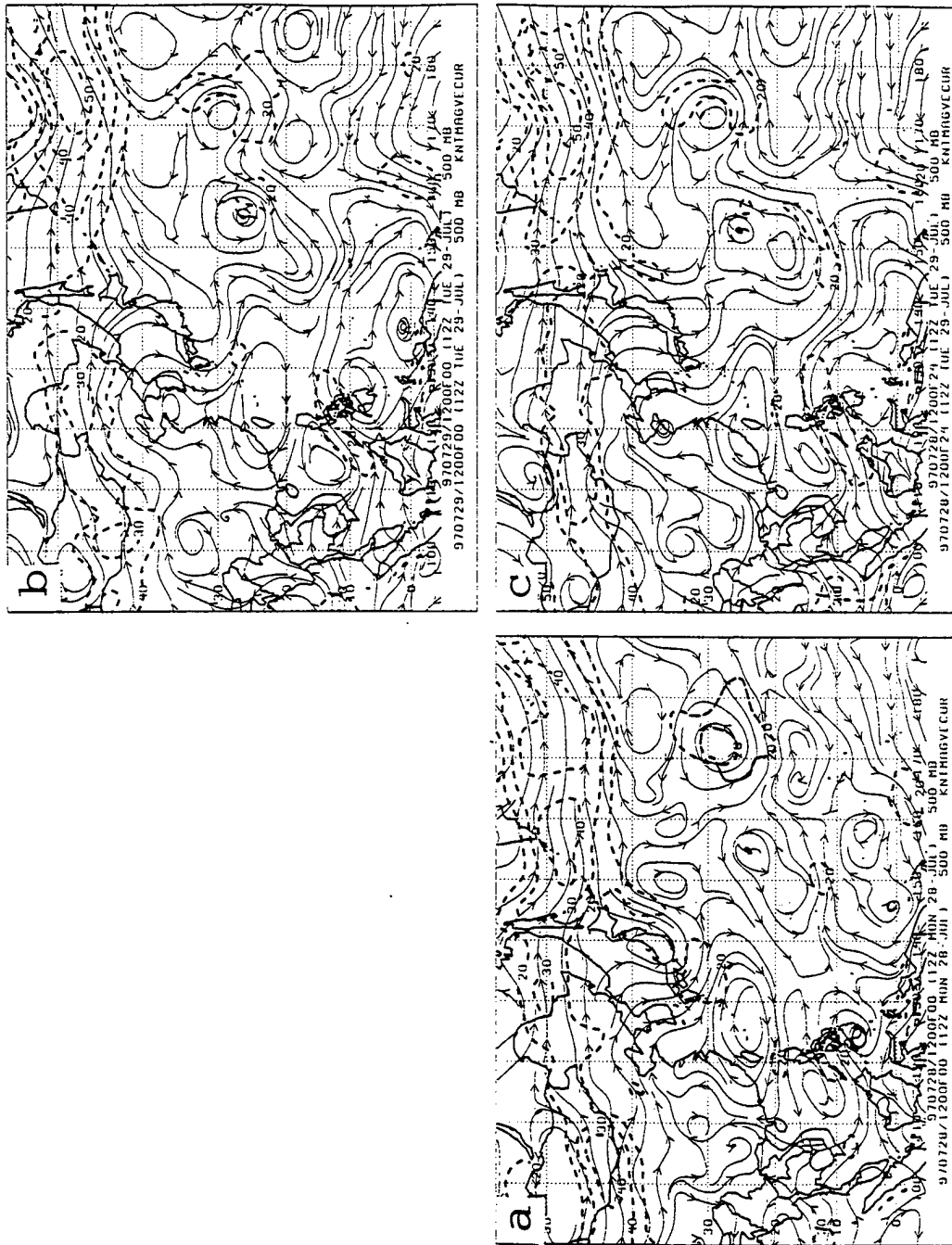
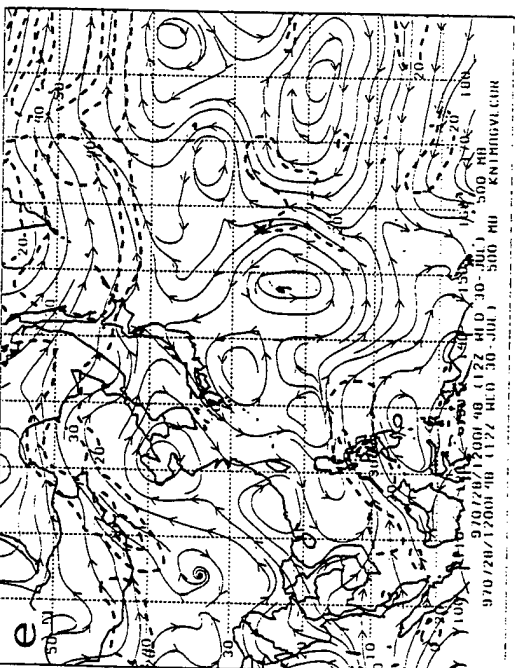
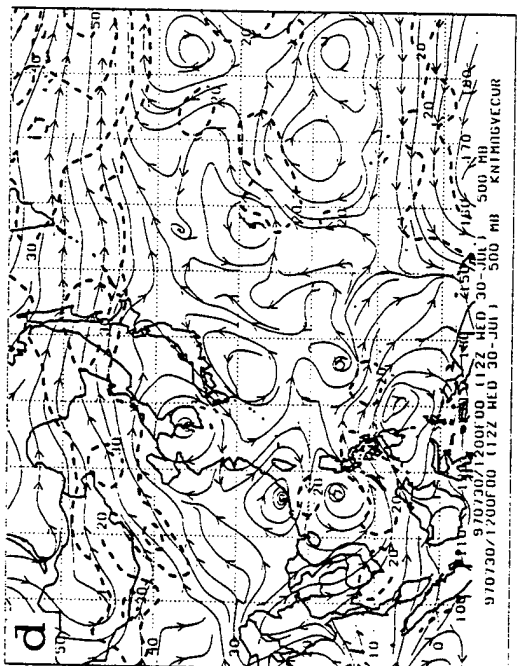
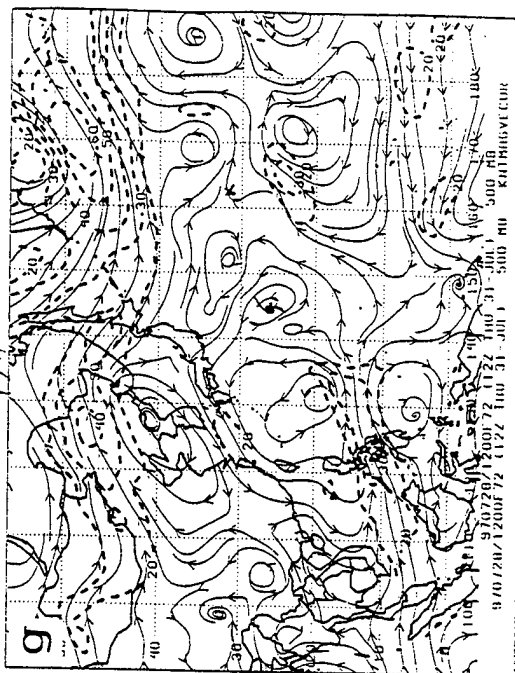
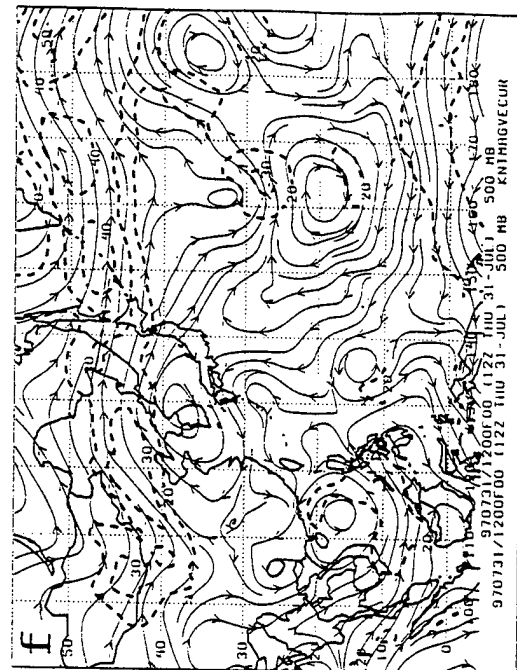


**Figure 3.5.** NOGAPS 500-mb streamline and isotach (dashed 10 kt interval, beginning at 20 kt) analysis at 12 UTC on (a) 28 July 1997, (b) 29 July, (d) 30 July, and (f) 31 July. Corresponding forecasts initiated at time of (a) and verifying at times of (b), (d), and (f) are given in panels (c), (e), and (g), respectively. Notice that TS Scott is over-predicted and merges with a cyclonic circulation to the southwest during the forecast interval.



apparently was the case.

By 12 UTC 30 July (Fig. 3.5d), TS Scott was near  $29^{\circ}\text{N}$ ,  $157^{\circ}\text{E}$  and was moving to the northeast, which is consistent with the 20-kt isotach maximum to the southeast. The cyclonic circulation that was located to the southwest in the 24-h analysis is more diffuse in the 48-h analysis and a ridge has developed between TS Scott and the weak cyclonic circulation. By contrast, the NOGAPS 48-h forecast (Fig. 3.5e) has merged TS Scott with the cyclonic circulation that was to the south-southwest 24-h prior into one large circulation centered near  $24^{\circ}\text{N}$ ,  $148^{\circ}\text{E}$ , which is well west-southwest of the analyzed position. This westward displacement in the 24-48h NOGAPS forecast track (Fig. 3.4) again indicates the motion was dominated by the false direct TC-like interaction with the cyclonic circulation.

After another 24 h (Fig. 3.5f), TS Scott is continuing to move northeastward under the influence of a subtropical anticyclone to the south and the mid-latitude flow to the north. By contrast, the NOGAPS 72-h forecast continued to move TS Scott to the west under the influence of the ridge to the north-northeast (Fig. 3.5g). The false direct TC-like interaction with the cyclonic circulation in the NOGAPS forecast has created an independent circulation entity that is clearly unrepresentative of the actual situation.

At 00 UTC 29 July (Fig. 3.6a), the GFDN 6-h forecast has TS Scott near  $25^{\circ}\text{N}$ ,  $154^{\circ}\text{E}$ . The cyclonic circulation to the southwest in the NOGAPS analyses 12 h prior (Fig. 3.5a) and 12 h later (Fig. 3.5b) is present in the GFDN field as well. Twelve hours later (Fig. 3.6b), when GFDN forecast may be directly compared to the NOGAPS forecast at the same valid time (Fig. 3.5c), the higher resolution GFDN forecast has TS Scott as more intense than in the NOGAPS forecast. The GFDN location of TS Scott is also northeast of the NOGAPS

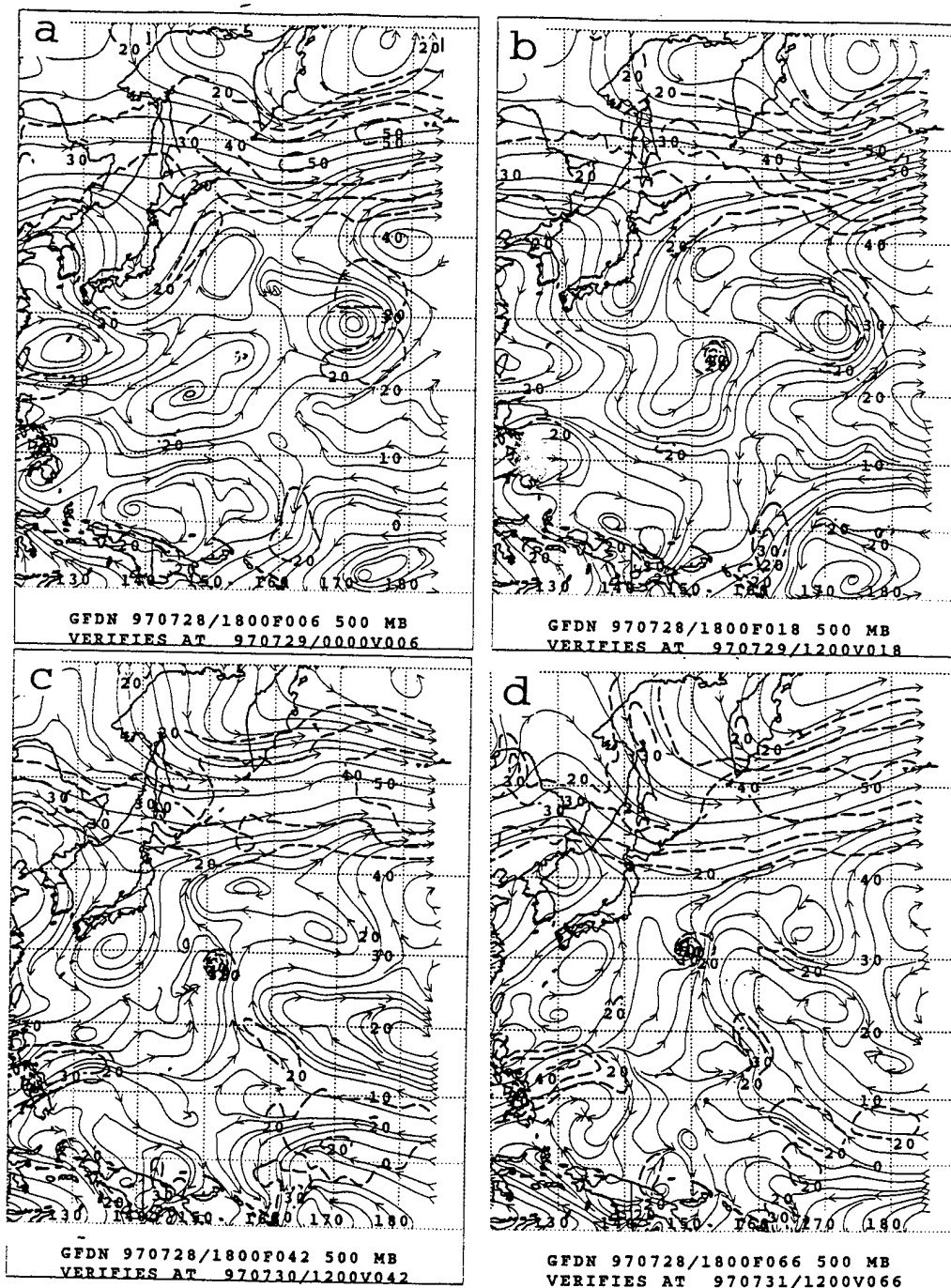


**Figure 3.6.** GFDN 500-mb streamline and isotach (dashed 10 kt interval beginning at 20 kt) predictions initiated at 18 UTC 28 July 1997 and verifying at (a) 00 UTC 29 July, (b) 12 UTC 29 July, and (d) 12 UTC 31 July. Notice that TS Scott maintains a separation distance from the cyclonic circulation to the southwest.

storm location at that time. Notice also the cyclonic circulation to the southwest was in a more western position than was represented in the NOGAPS 24-h forecast (Fig. 3.5c), and appears to verify well with the analysis (Fig. 3.5b). The combination of the northeastward GFDN location of TS Scott and the more western placement of the cyclonic circulation indicates that less of an apparent rotation about a midpoint had occurred in the GFDN forecast. Although the GFDN forecast track (Fig. 3.4) was west of north versus east of north, the FTE is smaller than for NOGAPS.

At 12 UTC 30 July (Fig. 3.6c), the GFDN 42-h forecast has maintained a separation between TS Scott and the cyclonic circulation to the southwest. Although the GFDN track forecast at this time (Fig. 3.4) continues to be west of north, it is somewhat better than the NOGAPS track. As GFDN maintains the higher intensity, the forecast track seems to be influenced by the flow. Unfortunately, the forecast environment is different from the analyzed environment (Fig. 3.5d) and the GFDN forecast continues the erroneous northward track through 66 h (Figs. 3.4 and 3.6d).

The NOGAPS forecast initiated 12 h later at 00 UTC 29 July, and the corresponding GFDN forecast initiated at 06 UTC 29 July, exhibit FTEs very similar to the forecasts discussed above (not shown). However, the 12 UTC 29 July NOGAPS forecast and the corresponding 18 UTC 29 July GFDN forecast differ dramatically. The slow northwestward track in NOGAPS (Fig. 3.7) results in extremely large FTEs. By contrast, the GFDN forecast performed very well (Fig. 3.7). The reason for the poor NOGAPS forecast may be detected early in the forecast period. At 12 UTC 29 July (Fig. 3.8a), the NOGAPS initial analysis has TS Scott near 27°N, 155°E and the cyclonic circulation to the southwest is centered near

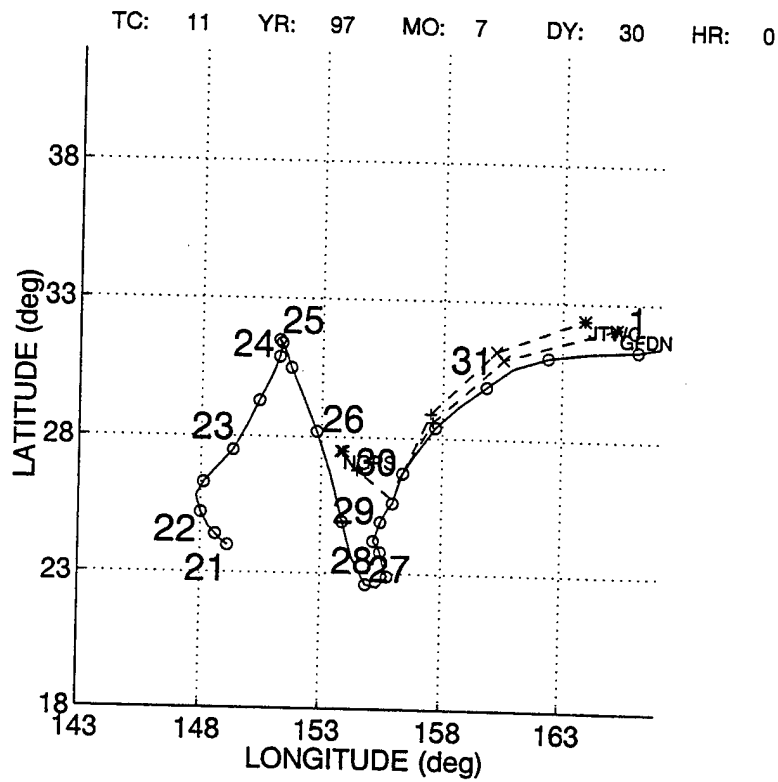


**Figure 3.7.** Best track as in Fig. 3.4, except NOGAPS and GFDN model forecasts initiated at 12 and 18 UTC 29 July, respectively. The JTWC forecast was initiated at 00 UTC 30 July. Notice that the NOGAPS forecast is slow and left of the best track.

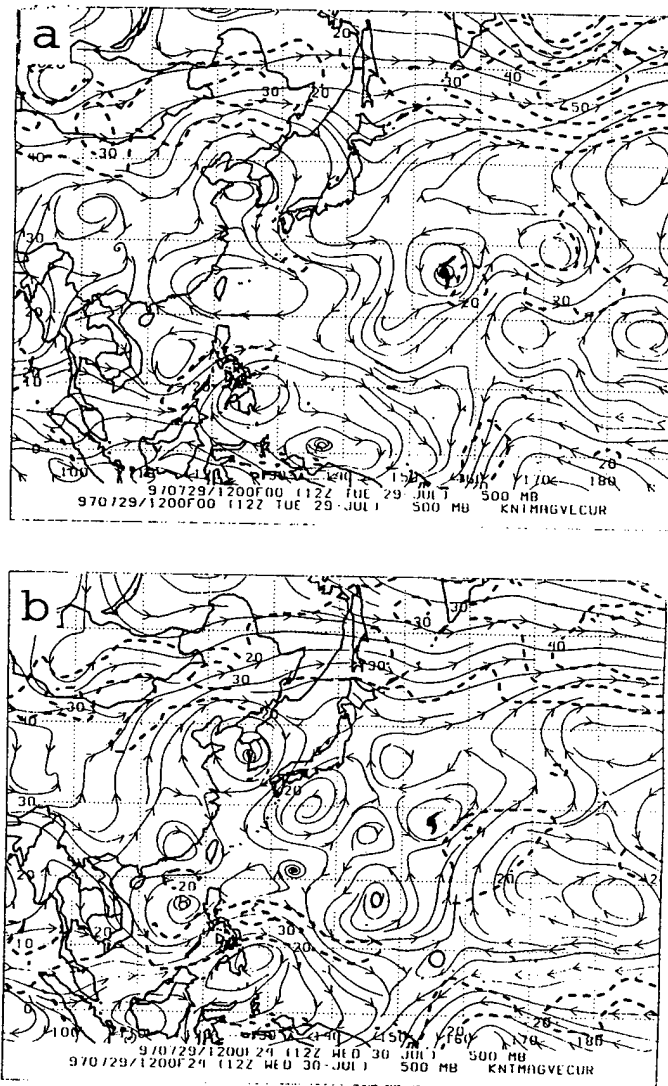


**Figure 3.8.** NOGAPS 500-mb streamline and isotach analyses and predictions as in Fig. 3.5, except (a) an analysis initiated at 12 UTC 29 July 1997 and (b) a 24-h forecast that verifies at 12 UTC 30 July. Notice that TS Scott seems to be interacting with the cyclonic circulation at the analysis time.

20°N, 147°E. The close proximity of these two circulations indicated a possible interaction scenario in which TS Scott and the circulation would again rotate cyclonically relative to each other as in Fig. 19. Indeed, the NOGAPS track forecast (Fig. 3.7) is for a northwest movement of TS Scott during the first 24 h. After 24 h (Fig. 3.8b), the NOGAPS forecast stalls TS Scott as a ridge develops between the storm and the circulation to the southwest.

The GFDN 6-h forecast valid at 00 UTC 30 July (Fig. 3.9a) has TS Scott near 27°N, 155°E (at an intermediate location in the NOGAPS 12 UTC 29 July and 12 UTC 30 July positions in Figs. 3.4b and 3.5d, respectively). Notice that the GFDN forecast has again represented TS Scott as being more compact and of higher intensity than in the NOGAPS analyses because of the higher horizontal resolution and special initial condition specification procedures. However, the NOGAPS representation of the cyclonic circulation to the southwest was similar. Although the depictions are valid 12 h prior and after, a hypothesis as to why the GFDN track forecast is better than for NOGAPS may be inferred. The GFDN compact representation of the vortex allows the separation distance between TS Scott and the cyclonic circulation to the southwest to be larger, and avoids a false TC-like interaction with the cyclonic circulation. The higher intensity in this 500-mb analysis indicates a deeper storm, which results in steering at a higher level in the atmosphere. The combination of increased separation distance and higher steering flow in the GFDN forecast resulted in a correct northeastward TC track movement through 72 h (Fig. 3.7) under the influence of the anticyclone to the east-southeast of TS Scott. Already in the 18-h forecast (Fig. 3.9b), the 20-kt isotachs have merged. By 42 h (Fig. 3.9c), the TS Scott circulation is embedded in a vigorous anticyclonic circulation with an isotach maximum to the south-southeast, which is

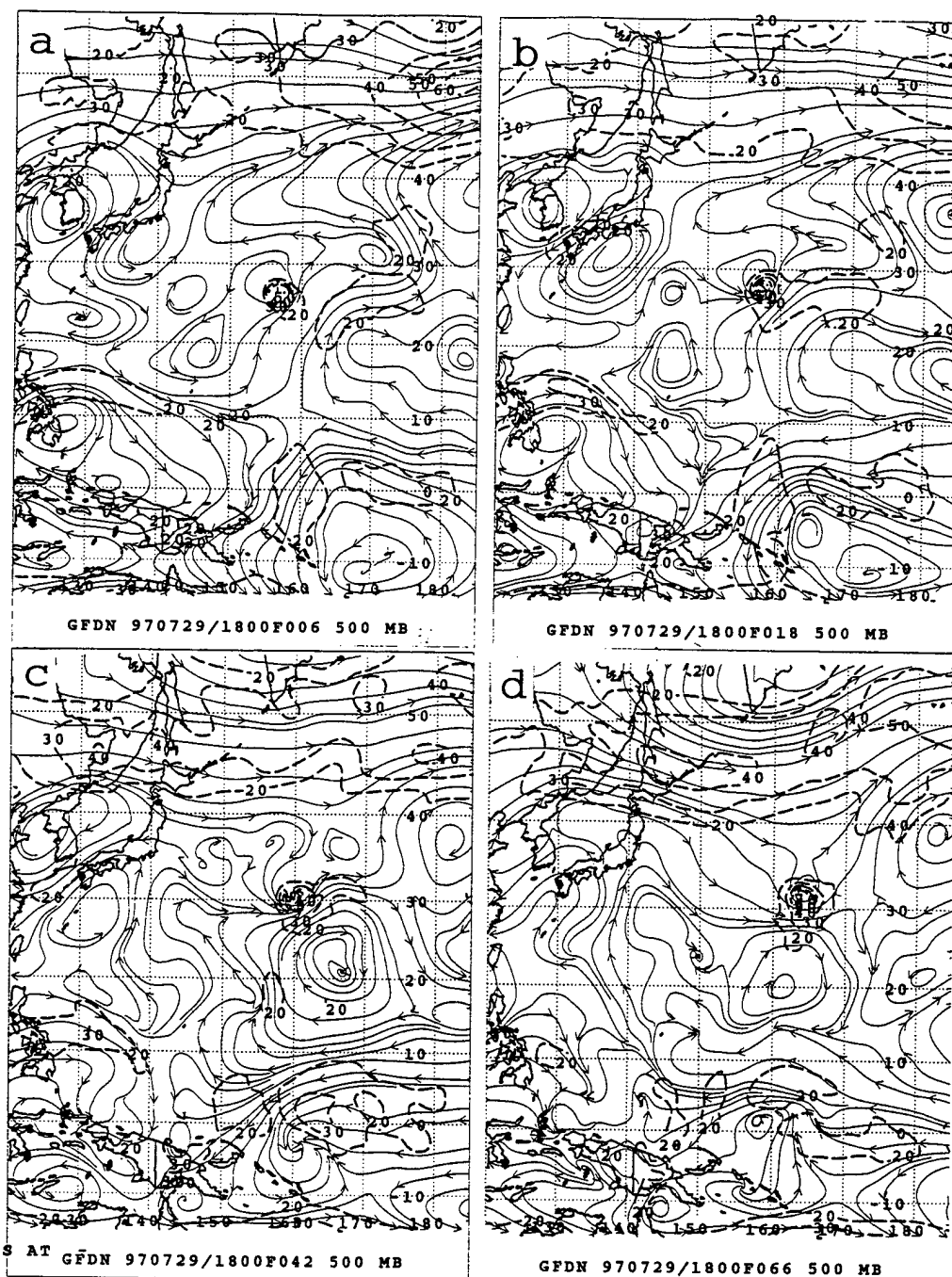


**Figure 3.9.** GFDN 500-mb streamline and isotach predictions as in Fig. 3.6, except GFDN forecast initiated at 18 UTC 29 July 1997 and verifies at (a) 00 UTC 30 July, (b) 12 UTC 30 July, (c) 12 UTC 31 July, and (d) 12 UTC 1 August 1997. Notice that TS Scott remains separated from the cyclonic circulation to the southwest.

consistent with the track forecast at 12 UTC 31 July (Fig. 3.7). This excellent track forecast is continued at 66 h in conjunction with an anticyclone to the south and mid-latitude flow to the north (Fig. 3.9d).

### **3. Super Typhoon Nestor (7W)**

Super Typhoon (ST) Nestor (7W) provides an example of false TC/second cyclonic circulation direct interaction in the NOGAPS model and also provides an example of how the high resolution GFDN model is sometimes able to avert this false interaction. The NOGAPS track forecast initiated at 00 UTC 11 June 1997 (Fig. 3.10) has a 72-h cross-track error of only -45 n mi (left), but has an along-track error of -540 n mi (slow). The corresponding errors for the GFDN 72-h track forecast initiated at 06 UTC 11 June 1997 (Fig. 3.10) were -94 n mi cross-track and -140 n mi along-track.

At 00 UTC 11 June 1997 (Fig. 3.11a), the NOGAPS initial analysis has ST Nestor near 19°N, 145°E. Notice the analysis also has a trough of low pressure extending well to the south of ST Nestor. Twenty-four hours later (Fig. 3.11c), the NOGAPS forecast has ST Nestor near 20°N, 142°E, which is slightly south of the best-track position. The notable difference between the analysis (Fig. 3.11b) and the forecast (Fig. 3.11c) is the representation of the area to the south of the ST Nestor. Whereas the analysis has a small isolated cyclonic circulation near 10°N, 141°E, the forecast has continued to indicate a broad trough of low pressure. Notice this trough of low pressure has rotated to the east and is now located to the south-southeast of ST Nestor. Although fairly subtle due to the lack of a clearly defined cyclonic circulation to the south, false direct interaction seems to be taking place.

By 00 UTC 13 June (Fig. 3.11d), ST Nestor continues to be represented as a compact

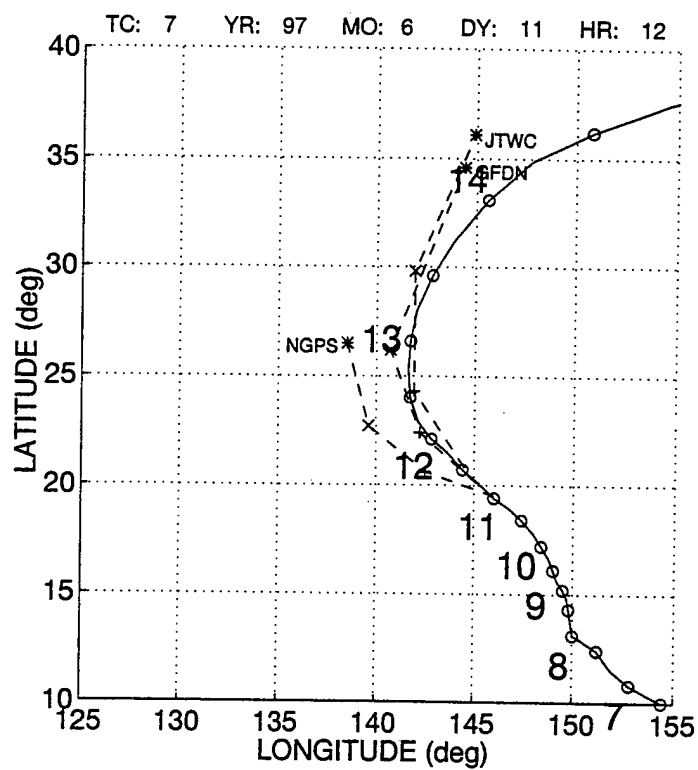


**Figure 3.10.** Best track as in Fig. 3.4, except for ST Nestor, and NOGAPS and GFDN model forecasts initiated at 00 UTC and 06 UTC 11 June 1997, respectively. The JTWC forecast was initiated at 12 UTC 11 June. Notice that the NOGAPS forecast is slow and left of track.

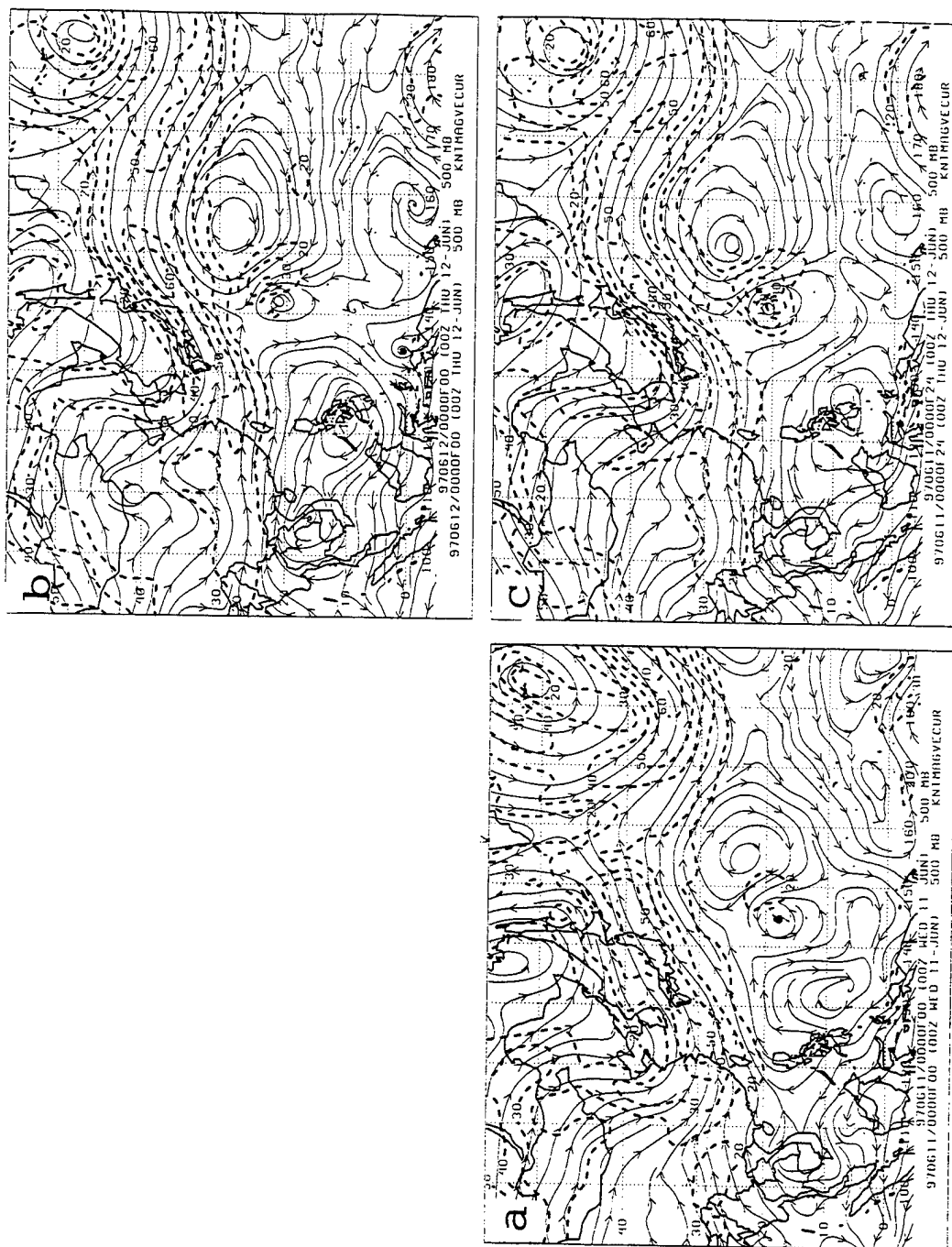
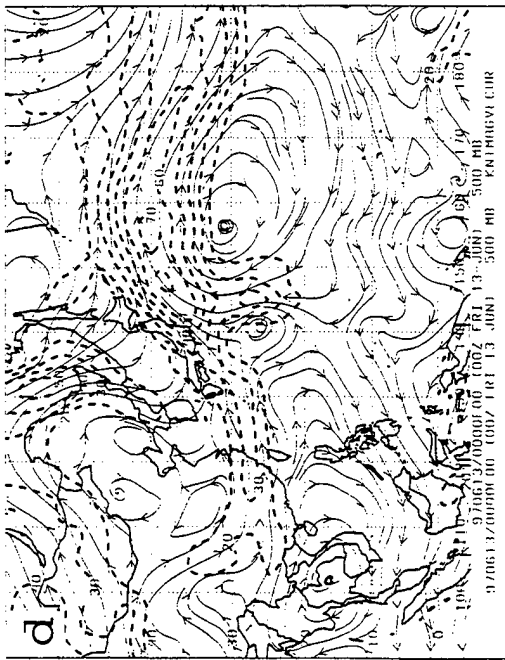
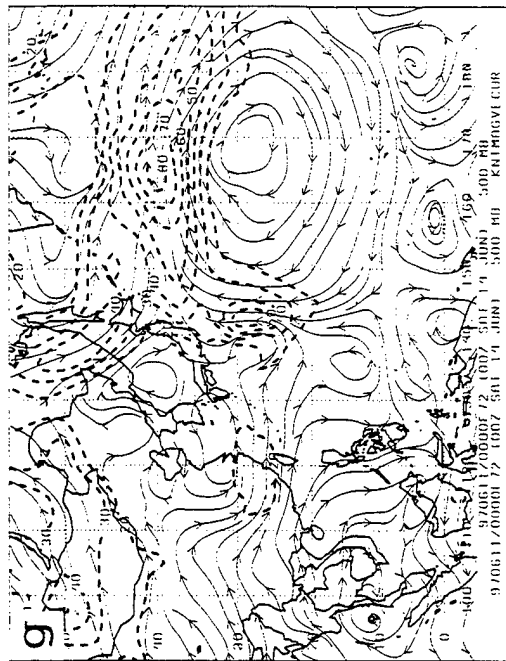
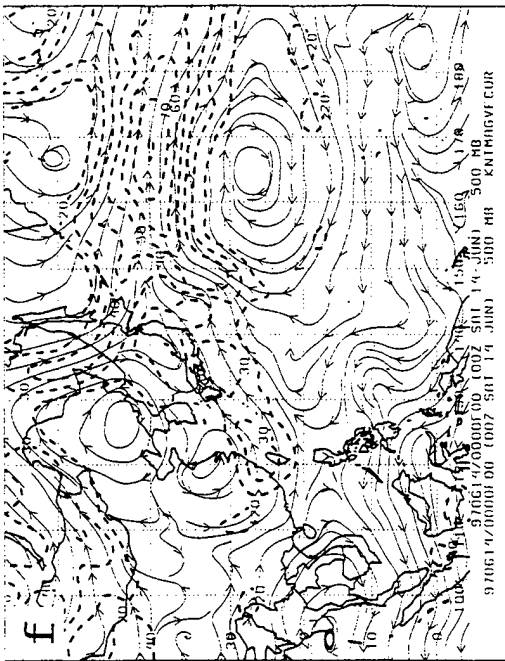


**Figure 3.11.** NOGAPS 500-mb streamline and isotach analyses and predictions as in Fig. 3.5, except analysis in (a) is initiated at 00 UTC 11 June 1997, with continuing analyses in (b-d-f) and forecasts in (c-e-g). Notice the apparent cyclonic rotation about a mid-point between ST Nestor and the trough of low pressure to the south.



cyclonic circulation with a distinct isotach maximum to the east, which is reasonable as Nestor had started to track to the north-northeast (Fig. 3.10). Notice that little evidence of the cyclonic circulation exists to the south. By contrast, the NOGAPS 48-h forecast (Fig. 3.11e) continued to indicate a large area of low pressure to the south-southeast of ST Nestor. The corresponding track forecast continued to be slow and to the left under the influence of the weaker steering from the south. After another 24 h (Fig. 3.11g), the NOGAPS forecast was similar and actually has a separate cyclonic circulation to the south, which does not verify in the analysis (Fig. 3.11f).

At 12 UTC 11 June (Fig. 3.12a), the GFDN 6-h forecast has ST Nestor near  $20^{\circ}\text{N}$ ,  $144^{\circ}\text{E}$ . As expected from the GFDN initial condition technique changing only the field near the actual TC, the trough to the south is represented in a similar fashion as the NOGAPS corresponding analysis, which is intermediate between Figs. 3.11a and 3.11b.

Twelve hours later (Fig. 3.12b), the GFDN field may be directly compared to NOGAPS 24-h forecast in Fig. 3.11c. Notice that the GFDN forecast represents ST Nestor as having a smaller diameter than the corresponding NOGAPS depiction, and also has ST Nestor in a more northerly location. The combination of the smaller diameter of the vortex in GFDN and the more northern placement increases the separation distance from the cyclonic circulation. With this combination, false direct interaction did not take place and the GFDN forecast moves ST Nestor in the correct north-northeast direction (Fig. 3.10). Although the cyclonic disturbance continues to exist near  $12^{\circ}\text{N}$ ,  $146^{\circ}\text{E}$  in the 42-h GFDN forecast (Fig. 3.12c), the break between ST Nestor and the cyclonic circulation is clearly established and no effect on Nestor's movement is evident. No supporting evidence for a

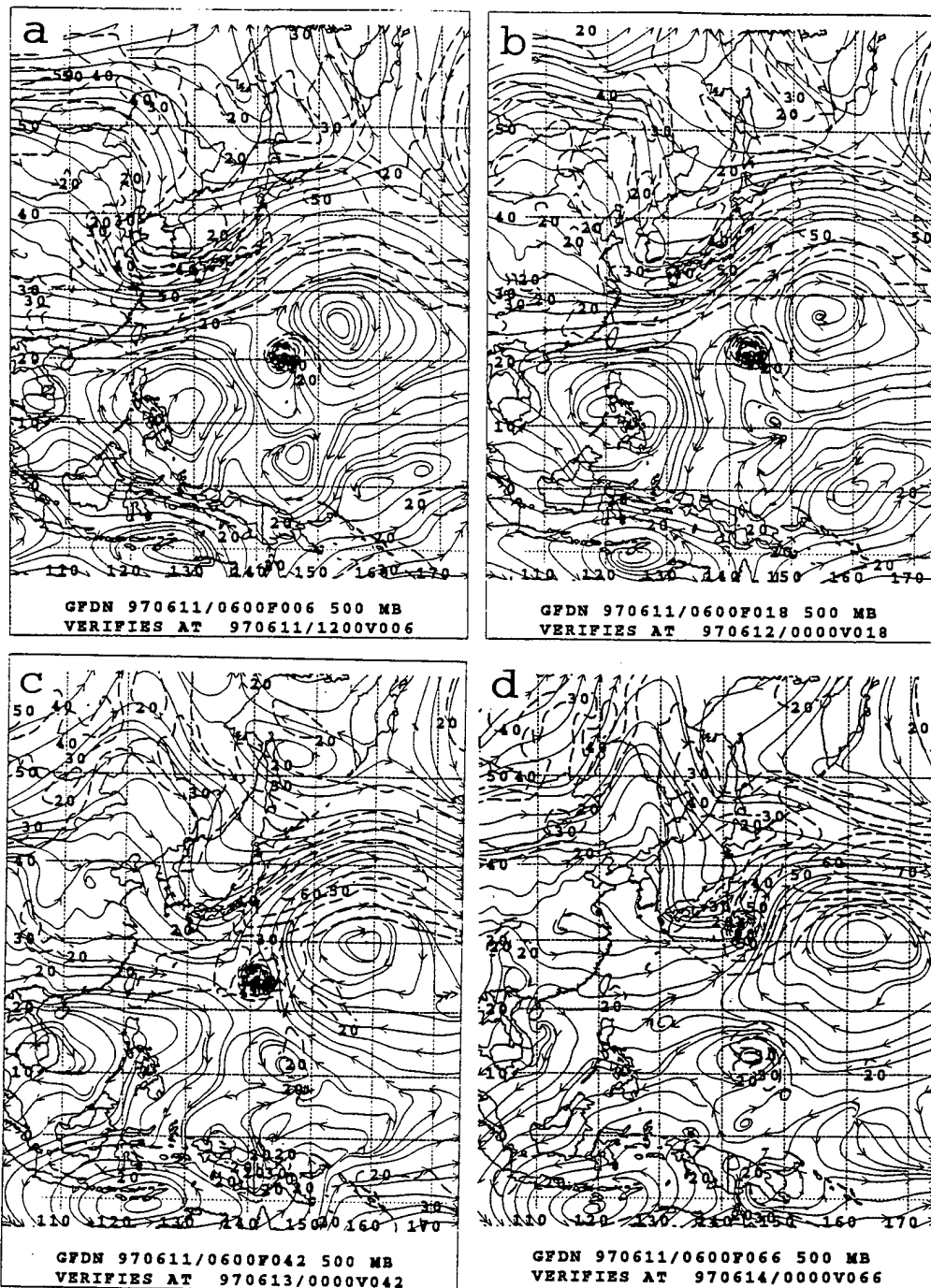


**Figure 3.12.** GFDN 500-mb streamline and isotach predictions as in Fig. 3.6, except forecast initiated for ST Nestor at 06 UTC 11 June 1997 and verifies at (a) 12 UTC 11 June 1997, (b) 00 UTC 12 June, (c) 00 UTC 13 June, and (d) 00 UTC 14 June. Notice that ST Nestor remains separated from the cyclonic circulation to the south.

cyclonic circulation at this location is evident in the verifying analysis (Fig. 3.11d). Although the GFDN then intensifies this cyclonic circulation at 66 h (Fig. 3.12d), again with little support in the verifying analysis (Fig. 3.11f), this is irrelevant to the Nestor track forecast.

#### **IV. TRANSITION INTO THE MIDLATITUDE WESTERLIES**

##### **A. CONCEPTUAL MODEL OF RETARDED TRANSITION INTO MIDLATITUDE WESTERLIES**

When the forecast of the TC structure is inaccurate, the TC track forecast beginning near the subtropical ridge axis and moving into the Midlatitude Westerlies (MW) synoptic region is often degraded (Fig. 4.1). In situations when the TC horizontal structure is under-forecast by a model, the forecast TC vertical extent is often shallower than the actual TC extent. As the TC vertical extent is reduced, the steering current for that system is in a lower atmospheric layer that often results in a slowing of the along-track forecast in the MW region (Figs. 4.1b-c). Conversely, when the TC circulation is over-forecast by a model, the forecast TC vertical extent is often greater than the actual TC extent. As the TC vertical extent is increased, the steering current for that system is over a deeper tropospheric layer, which often results in a faster along-track forecast in the MW region. These degraded track forecasts due to TC structure inaccuracies can occur in the Standard synoptic pattern, in the Poleward pattern, and in the situation when a Standard pattern transforms to a Poleward pattern during the forecast interval.

##### **B. CONCEPTUAL MODEL FOR MOTION-INDUCED SHIFTING OF TC WIND FIELD CENTER**

A motion-induced shifting of a TC wind field center (Fig. 4.2) may be predicted in a coarse-resolution numerical model when the TC intensity is under-forecast. In this conceptual model, the addition of the environmental steering flow and the symmetric TC wind field results in the wind pattern in the vicinity of the TC. Typically, the wind center in

**Scenario: Under-representation of  
recurving TC circulation by model**

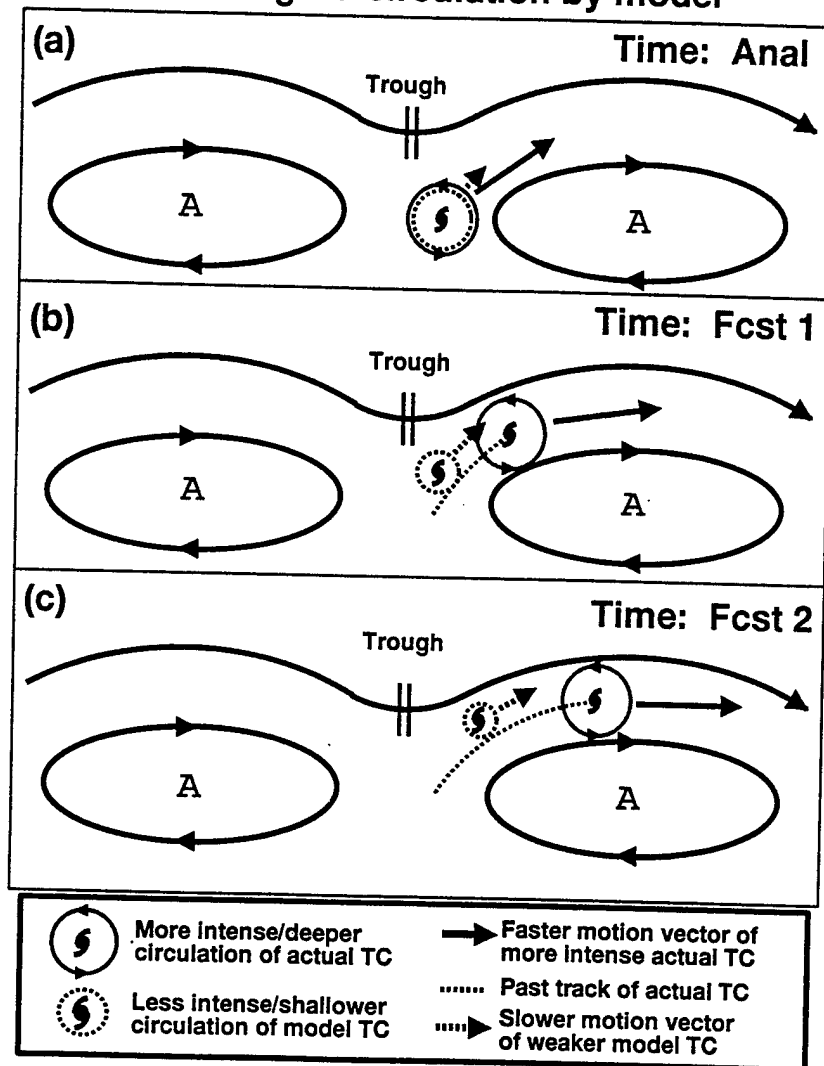
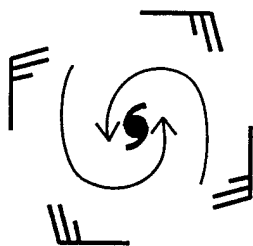


**Figure 4.1.** Conceptual model of an erroneous transition into the MW synoptic region due to model-predicted TC structure inaccuracies (see insert for amplification of this conceptual model).

# Conceptual model for motion-induced shifting of TC wind field center

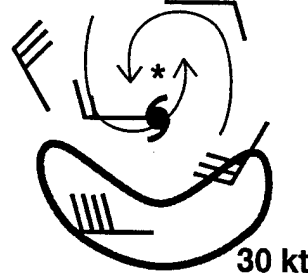
Symmetric TC wind field



Environmental steering flow



TC wind field + steering flow



Location of actual center of TC



Location of TC wind field center



Location of isotach maximum

**Figure 4.2.** Motion-induced shifting of a TC wind field center conceptual model (see insert for explanation of the symbols)

the model is shifted well to the left of the actual TC location because the inner core structure is not resolved. Consequently, the initial position and the resultant model-predicted motion of the TC is consistently shifted to the left of track as in Fig. 4.2.

### **C. 1997 CASE STUDIES**

The following case studies are examples of inaccurate structure forecasts that lead to degraded forecast tracks. The first case occurred in the Standard pattern as Super Typhoon (ST) Keith moved from near the subtropical ridge axis in the Weakened Ridge (WR) region into the MW region. The second case occurred in the Poleward pattern as Typhoon Marie moved across the subtropical ridge axis from the PO region to the MW region.

#### **1. Super Typhoon Keith (29W)**

ST Keith was an example of an inaccurate structure forecast that degraded the forecast TC track. This example illustrates the characteristic effects of both an under-forecast of TC wind structure in the NOGAPS model, and a stronger forecast of TC winds in the GFDN model.

ST Keith formed near  $7^{\circ}$  N,  $176^{\circ}$  E and tracked west-northwestward before recurving to the northeast near  $17^{\circ}$  N,  $135^{\circ}$  E (Fig. 4.3). The NOGAPS track forecast initiated at 00 UTC 5 November (Fig. 4.3) had a 72-h FTE of 680 n mi. The 72-h FTE for the corresponding GFDN track forecast initiated at 06 UTC 5 November (Fig. 4.3) was 426 n mi. Notice the NOGAPS track forecast was slow and that the GFDN track forecast was left of track and fast compared to the actual motion of the storm.

At 00 UTC 5 November (Fig. 4.4a), the NOGAPS 500-mb streamline analysis has ST Keith near  $18^{\circ}$  N,  $135^{\circ}$  E. Notice also that this is a Standard pattern (Fig. 1.2) with ST

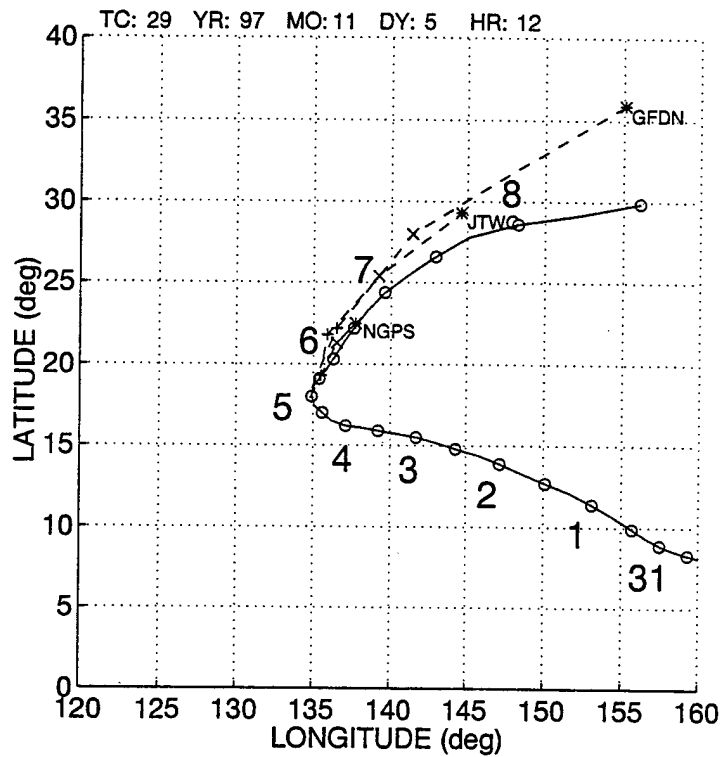


**Figure 4.3.** Best track as in Fig. 3.4, except for ST Keith. NOGAPS and GFDN model forecasts initiated at 00 and 06 UTC 5 November 1997, respectively. The JTWC forecast was initiated at 12 UTC 5 November. Notice that the NOGAPS forecast is behind and that the GFDN forecast is ahead of the verifying position.

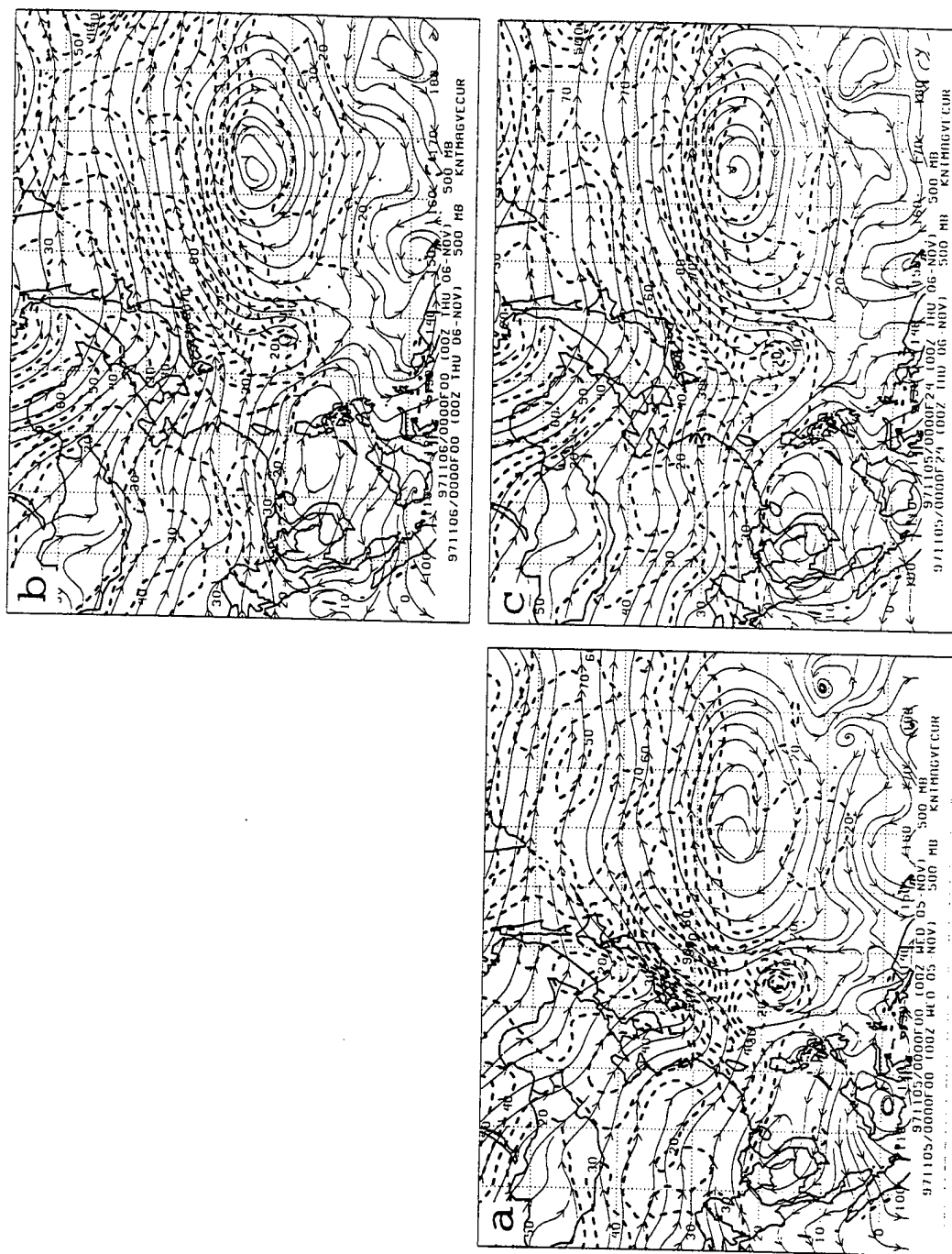
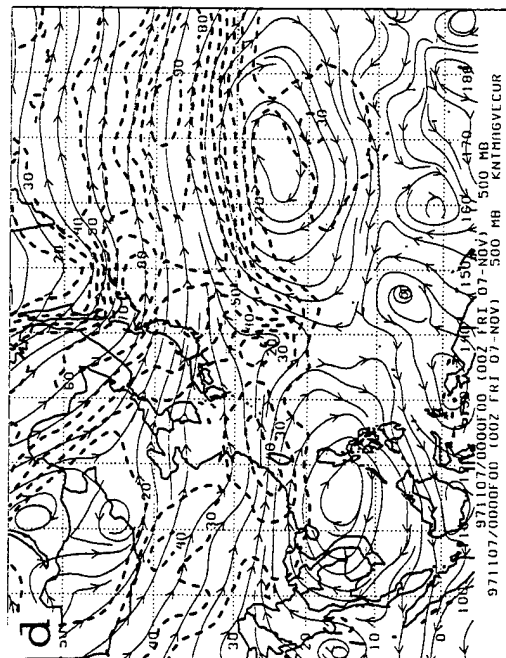
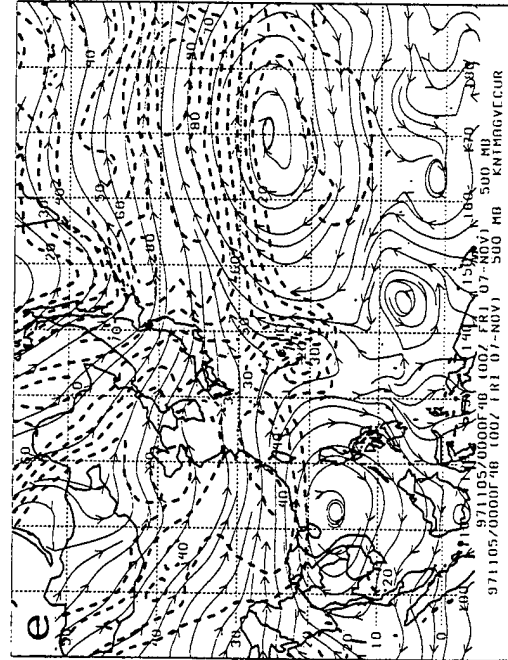


**Figure 4.4.** NOGAPS 500-mb streamline and isotach analyses and predictions as in Fig. 3.5, except the initial analysis (a) is initiated at 00 UTC 5 November 1997, with subsequent analyses in (b-d), and forecasts in (c-e). Notice the structural differences and predicted versus actual positions of ST Keith.



Keith located in the S/WR pattern/region. Twenty-four hours later, the NOGAPS streamline analysis (Fig. 4.4b) has ST Keith near  $21^{\circ}$  N,  $136^{\circ}$  E and beginning to enter the MW region. However, the NOGAPS 24-h forecast (Fig. 4.4c) has ST Keith near  $20^{\circ}$  N,  $134^{\circ}$  E, which is slightly south and west of the actual position and still in the WR region. The isotach maximum to the east of ST Keith in the analysis (Fig. 4.4b) suggests a steering current from the south, which is fairly consistent with the observed direction at 00 UTC 6 November (Fig. 4.3). The isotach maximum to east-southeast of ST Keith in the NOGAPS 24-h forecast (Fig. 4.4c) suggests a steering current from the south-southwest, which is consistent with the best track at 00 UTC 6 November (Fig. 4.3). Notice the value of the isotach maximum on the eastern side of ST Keith in the NOGAPS 24-h analysis (Fig. 4.4b) is slightly larger than the 24-h forecast isotach maximum on the eastern side of ST Keith (Fig. 4.4c). Based on the usual situation that a stronger, more concentrated horizontal wind structure is accompanied with a deeper vertical extent, the NOGAPS 24-h forecast TC structure may be somewhat shallower than in nature. This lower vertical extent, with an assumed slower steering current, is consistent with the NOGAPS 24-h along-track error of -75 n mi (negative values indicate a slow bias).

By 00 UTC 7 November (Fig. 4.4d), ST Keith is analyzed near  $26^{\circ}$  N,  $139^{\circ}$  E and is tracking to the northeast well into the MW region. However, the NOGAPS 48-h forecast (Fig. 4.4e) has ST Keith near  $24^{\circ}$  N,  $137^{\circ}$  E, which is southwest of the actual storm position and barely into the MW region. Notice the difference in isotach positioning between Fig. 4.4d and Fig. 4.4e. The NOGAPS 48-h forecast (Fig. 4.4e) has a more significant isotach maximum to the west-southwest of ST Keith than the NOGAPS analysis (Fig. 4.4d). This

variation in isotach placements and values suggests a difference in TC horizontal structure between analysis and forecast. The isotach maxima on both sides of ST Keith in the NOGAPS 48-h forecast (Fig. 4.4e) suggests steering currents that would oppose one another and inhibit the northeastward progression into the MW region. The NOGAPS -648 n mi along-track error after 48 h (Fig. 4.3) is evidence of this slowing that appears to be due to TC structure inaccuracy. Notice the NOGAPS 00 UTC 7 November 500-mb analysis (Fig. 4.4d) indicates a more significant isotach maxima to the east-southeast of ST Keith that is consistent with the actual northeastward track of the storm.

At 12 UTC 5 November (Fig. 4.5a), the GFDN 6-h forecast has ST Keith near  $19^{\circ}$  N,  $134^{\circ}$  E in the WR region of the Standard pattern (Fig. 1.2). Notice that the predicted isotach maximum is larger than it is in the 00 UTC 5 November NOGAPS 500-mb analysis (Fig. 4.4a). Twelve hours later (Fig. 4.4b) when GFDN may be directly compared to the NOGAPS forecast at the same valid time (Fig. 4.4c), a large difference in maximum isotachs exists. Notice that the higher resolution GFDN has ST Keith more intense than in the NOGAPS analysis at the same valid time (Fig. 4.4b). The larger isotach value of the GFDN 18-h forecast (Fig. 4.5b) implies a deeper storm and suggests a steering current over a deeper layer of the atmosphere than in the NOGAPS analysis (Fig. 4.4b). The vertical structure and subsequent steering current level differences between the GFDN 18-h forecast and the NOGAPS analysis are consistent with the GFDN track having a too fast along-track displacement (Fig. 4.3).

At 00 UTC 7 July (Fig. 4.5c), the GFDN 42-h forecast has ST Keith near  $28^{\circ}$  N,  $139^{\circ}$  E, which is well into the MW region. Notice that the higher resolution GFDN forecast

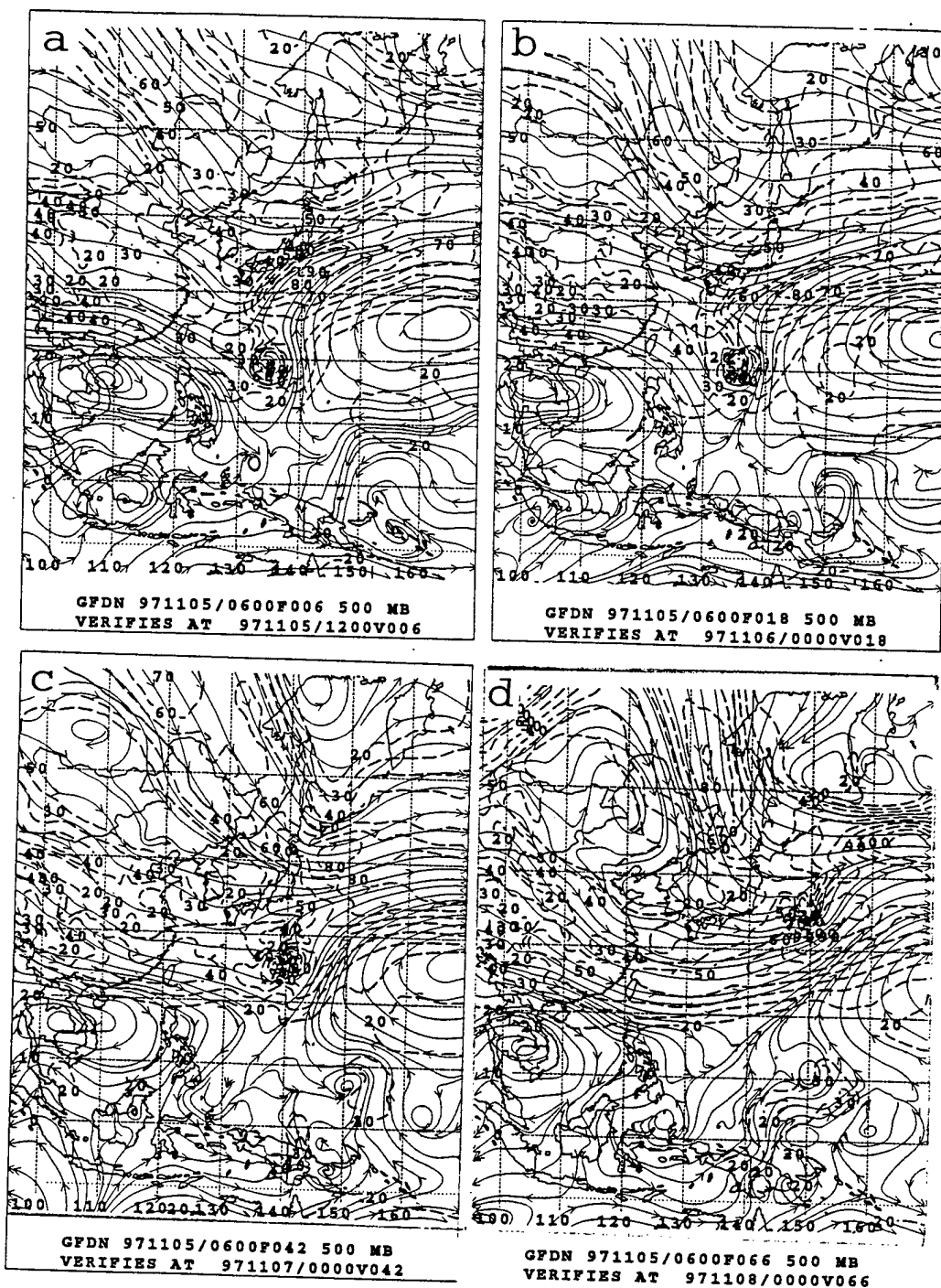


**Figure 4.5.** GFDN 500-mb streamline and isotach predictions as in Fig. 3.6, except forecast initiated for ST Keith at 06 UTC 5 November 1997 and verifies at (a) 12 UTC 5 November, (b) 00 UTC 6 November, (c) 00 UTC 7 November, and (d) 00 UTC 8 November. Notice the large isotach maxima associated with ST Keith, which suggests a predicted over-intensification of Keith.

continues to have larger isotach values than the isotachs of the NOGAPS analysis (Fig. 4.4d) that is valid at the same time. Again the vertical structure difference between the GFDN 42-h forecast and the corresponding NOGAPS analysis seem to be supported by the GFDN along-track error of 97 n mi (Fig. 4.3).

At 00 UTC 8 July (Fig. 4.5d), the GFDN 66-h forecast has ST Keith near  $35^{\circ}$  N,  $150^{\circ}$  E. At this time, the actual storm intensity has dropped to 60 kt at the surface. Notice that the GFDN 66-h forecast isotach maximum exceeding 60 kt at 500 mb may (depending on translation speed) suggest that the intensity of ST Keith has been over-predicted in the GFDN model. Also notice that the TC in the NOGAPS analysis at this time (Fig. 4.4f) is less intense than the GFDN forecast intensity. The GFDN track forecast position of ST Keith at this time (Fig. 4.3) continues to be well ahead of the best-track position.

## **2. Typhoon Marie (6W)**

Typhoon (TY) Marie provides an example of a forecast TC structure error that caused a poor translation from near the subtropical ridge axis in the PO region of the Poleward pattern (Fig. 1.4) into the MW region and also a hypothesized motion-induced shifting of the TC wind field center (Fig. 4.2). TY Marie also provides an example of a forecast TC structure error in the NOGAPS model that is believed to cause a motion-induced shifting of the TC wind field center. Notice that TY Marie had formed near  $10^{\circ}$  N,  $161^{\circ}$  E and had tracked generally northward for five days before curving to the northeast near  $23^{\circ}$  N,  $161^{\circ}$  E (Fig. 4.6). Whereas the NOGAPS track forecast initiated at 12 UTC 30 May (Fig. 4.6) has a 48-h FTE of 396 n mi, the 48-h FTE for the corresponding GFDN track forecast initiated at 18 UTC 30 May (Fig. 4.6) was only 170 n mi. Notice that both the NOGAPS and GFDN

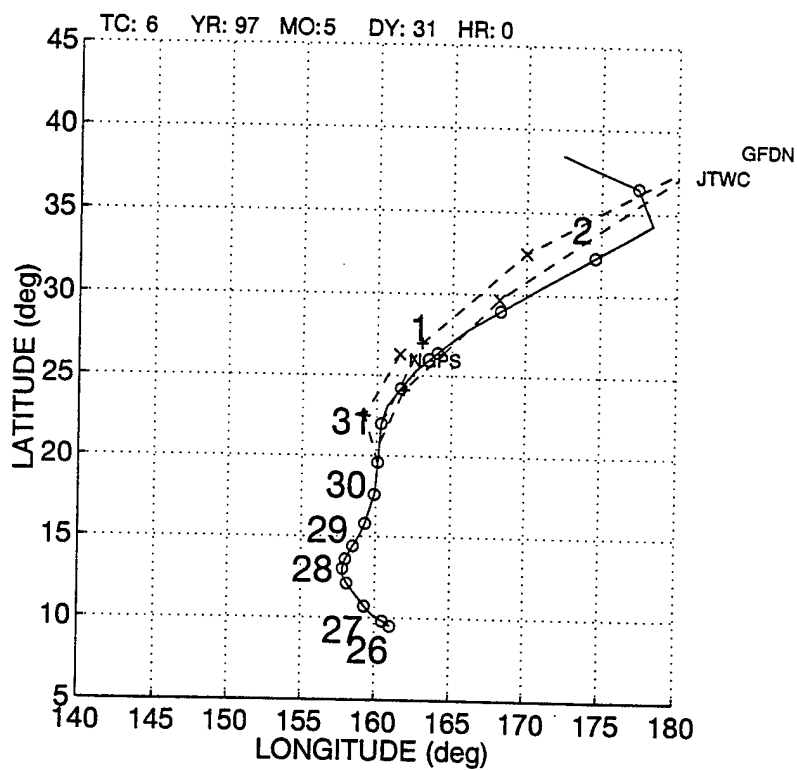


**Figure 4.6.** Best track as in Fig. 3.4, except for TY Marie. NOGAPS and GFDN model forecasts initiated at 12 and 18 UTC 30 May 1997, respectively. The JTWC forecast was initiated at 00 UTC 31 May 1997. Notice that the NOGAPS forecast track is behind and left of the best track.

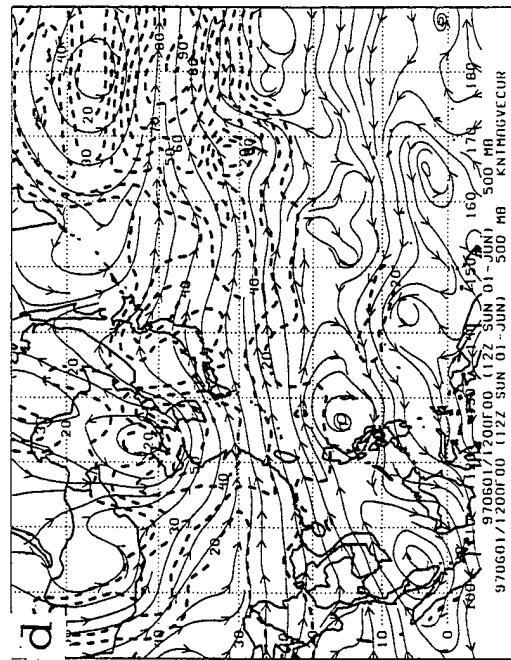
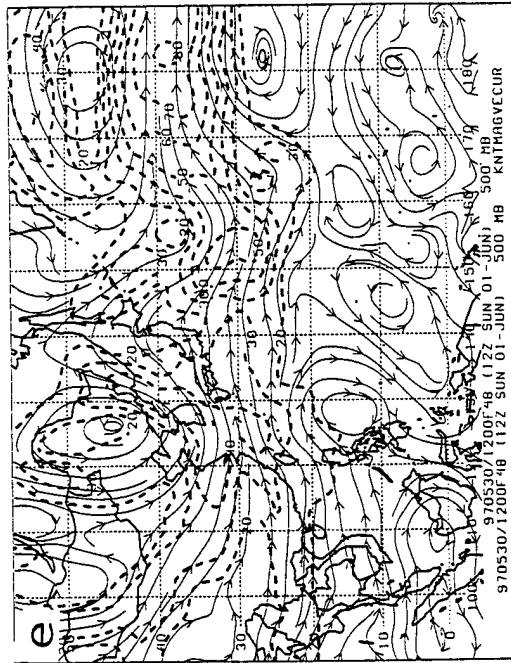
track forecasts are slightly left of track. While both track forecasts are slow, the NOGAPS track forecast is considerably behind the best-track position at this time.

At 12 UTC 30 May (Fig. 4.7a), the NOGAPS 500-mb streamline analysis has TY Marie near  $20^{\circ}$  N,  $158^{\circ}$  E. Notice that TY Marie is located in the Poleward-Oriented (PO) region of the Poleward pattern. Twenty-four hours later, the NOGAPS analysis (Fig. 4.7b) has TY Marie near  $23^{\circ}$  N,  $161^{\circ}$  E near the northern portion of the PO region. However, the NOGAPS 24-h forecast (Fig. 4.7c) has TY Marie near  $21^{\circ}$  N,  $160^{\circ}$  E, which is also in the PO region but is south and west of the analyzed position. The isotach maxima to the east of TY Marie in Figs. 4.7b and 4.7c suggest a steering current from the south-southeast that is consistent with the actual storm movement and with the NOGAPS 24-h forecast track (Fig. 4.6). However, the value of the isotach maximum in the NOGAPS analysis (Fig. 4.7b) is greater than the isotach maximum in the NOGAPS 24-h forecast (Fig. 4.7c). This suggests that the NOGAPS 24-h forecast structure of TY Marie may be somewhat shallower than it actually is. This is consistent with the NOGAPS 24-h forecast along-track error of -162 n mi because a shallower TC may be advected more slowly by a lower atmospheric steering current. In addition, the NOGAPS 24-h forecast cross-track error of -40 n mi (i.e., to the left as in Fig. 4.2) is consistent with a motion-induced shifting of the TC wind field center for this under-forecast typhoon. By contrast, the GFDN 24- and 48-h positions have almost no cross-track bias, which is expected because the horizontal resolution is adequate to resolve the inner vortex structure.

By 12 UTC 1 June (Fig. 4.7d), the NOGAPS analysis has TY Marie near  $30^{\circ}$  N,  $169^{\circ}$  E and in the MW region of the Poleward pattern. However, the NOGAPS 48-h forecast (Fig.



**Figure 4.7.** NOGAPS 500-mb streamline and isotach analyses and predictions as in Fig. 3.5, except for an analysis at (a) 12 UTC 30 May 1997, and subsequent analyses in (b-d), and forecasts in (c-e). Notice that TY Marie is analyzed more intense than forecast and that the analyzed position is ahead of the forecast position at the same valid times.



4.7e) has TY Marie near  $27^{\circ}$  N,  $162^{\circ}$  E, which is also in the MW region but is considerably southwest of the actual position. Again, TY Marie seems to be more intense in the NOGAPS 48-h analysis than in the NOGAPS 48-h forecast, which is consistent with the NOGAPS forecast 48-h along-track error of -392 n mi and cross-track error of -56 n mi.

At 00 UTC 31 May (Fig 4.8a), the GFDN 6-h forecast has TY Marie near  $21^{\circ}$  N,  $160^{\circ}$  E and in the PO region of the Poleward pattern. Notice that the isotach maximum is considerably larger than it is in the 12 UTC 30 May NOGAPS analysis (Fig. 4.7a). Twelve hours later (Fig. 4.8b) when GFDN forecast may be directly compared to the NOGAPS forecast at the same valid time (Fig. 4.7c), a considerable difference is found in the isotach maxima values in close proximity to TY Marie. Notice that the higher resolution GFDN forecast has TY Marie more concentrated than in the NOGAPS 24-h forecast. The larger isotach maximum of the GFDN 18-h forecast suggests a deeper structure with a larger steering current velocity over a deeper atmospheric layer. This vertical structure difference between the GFDN 18-h forecast and the NOGAPS 24-h forecast, and the assumed different steering current levels, are consistent with the smaller GFDN 24-h forecast along-track error of only -11 n mi.

By 12 UTC 1 June (Fig. 4.8c), the GFDN 42-h forecast has TY Marie near  $30^{\circ}$  N,  $166^{\circ}$  E, which is in the MW region of the Poleward pattern. Notice that the higher resolution GFDN 42-h forecast has a larger isotach maximum value in the vicinity of TY Marie than in the NOGAPS 48-h forecast (Fig. 4.7e). The TC vertical structure of the GFDN 42-h forecast seems to be more representative of the 65-kt surface wind speeds of Typhoon Marie than the NOGAPS 48-h forecast does at this time. Again, this disparity of vertical structure

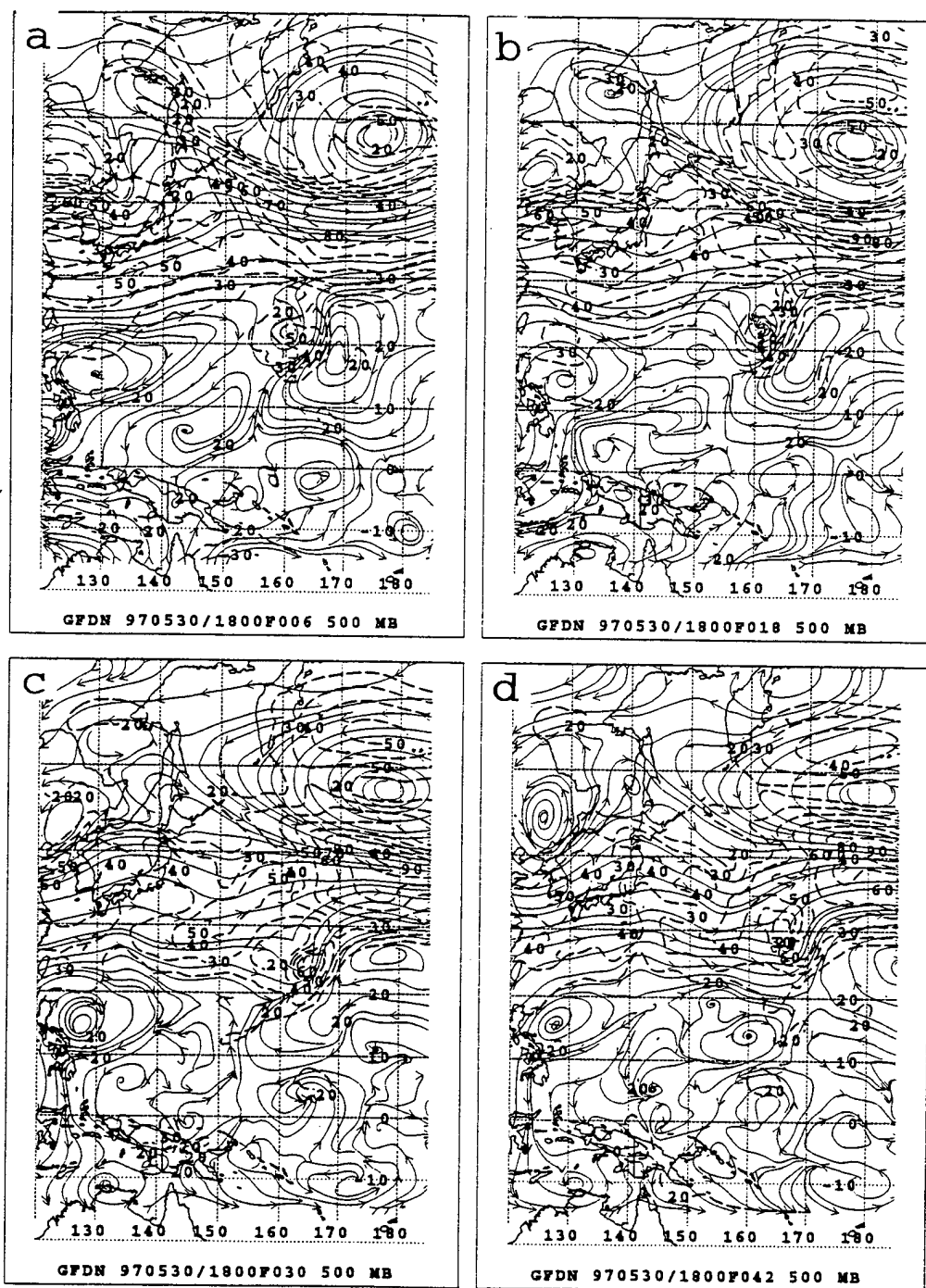


**Figure 4.8.** GFDN 500-mb streamline and isotach predictions as in Fig. 3.6, except the forecast was initiated for TY Marie at 18 UTC 30 May 1997 and verifies at (a) 00 UTC 31 May, (b) 12 UTC 31 May, (c) 00 UTC 1 June, and (d) 12 UTC 1 June. Notice that TY Marie is more compact and has larger isotach maxima in this forecast interval than in the corresponding NOGAPS forecast interval (Fig. 4.7).

between the GFDN 42-h forecast and the NOGAPS 48-h forecast is consistent with the lower value (-165 n mi) of GFDN along-track error at this time.

#### **D. STATISTICS/VARIATIONS**

Of the 27 storms during the 1997 typhoon season in the western North Pacific that were analyzed, six storms were classified under the idealized conceptual model of section A. Two of these cases have been described in section C. In addition, three storms were classified under the conceptual model of section B. One of these cases was described in section C. Whereas some cases of typhoons exhibited the same types of errors found in section A, some slight differences from this idealized conceptual model were also found. The main differences were in the forecast field variations of the idealized conceptual model. The case of ST Nestor is briefly described to show some of this forecast field variability relative to the idealized conceptual model.

ST Nestor formed near  $6^{\circ}$  N,  $169^{\circ}$  E and generally moved northwestward to near  $27^{\circ}$  N,  $142^{\circ}$  E before recurving to the northeast (Fig. 4.9). At 00 UTC 12 June (Fig. 4.10a), the NOGAPS 500-mb streamline analysis has ST Nestor near  $31^{\circ}$  N,  $142^{\circ}$  E and in the WR region of the Standard pattern. Notice that the subtropical ridge axis is tilted from northeast to southwest, that a small cyclonic circulation is located about  $10^{\circ}$  lat. to the south of ST Nestor, and that a peripheral ridge is building to the southeast of ST Nestor. Twenty-four hours later (Fig. 4.10b), the NOGAPS analysis has ST Nestor near  $26^{\circ}$  N,  $141^{\circ}$  E and just north of the tilted ridge axis. Thus, ST Nestor is in the MW region of a Poleward pattern. Notice the isotach maximum to the east of ST Nestor indicates a steering current from the south, which is consistent with the storm movement to the north at this time (Fig. 4.9). The

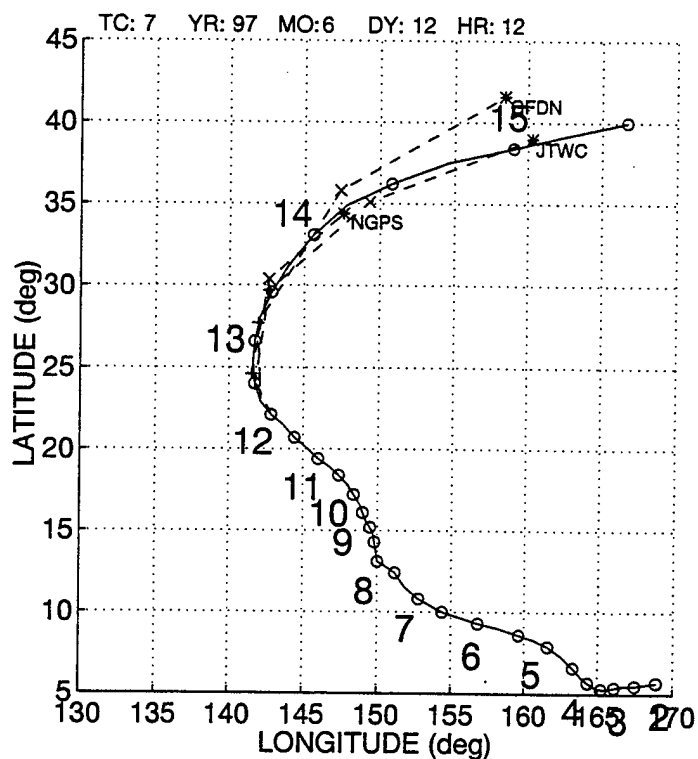


**Figure 4.9.** Best track as in Fig. 3.4, except for ST Nestor. NOGAPS and GFDN model forecasts initiated at 00 UTC and 06 UTC 12 June 1997, respectively. The JTWC forecast was initiated at 12 UTC 12 June. Notice that the NOGAPS forecast is significantly behind the best track through 72 h.

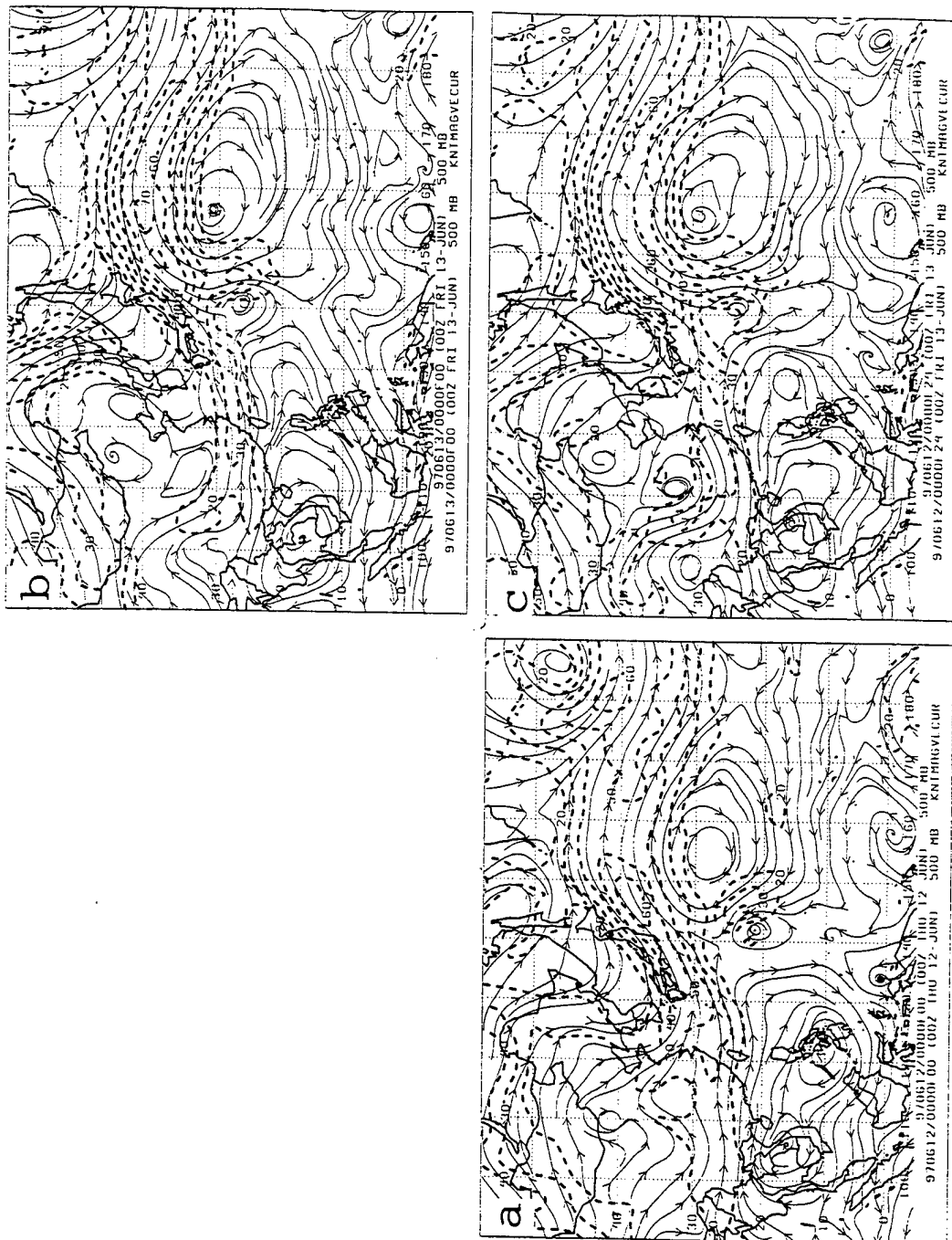


**Figure 4.10.** NOGAPS 500-mb streamline and isotach analyses and predictions as in Fig. 3.5, except from (a) an initial analysis at 00 UTC 12 June 1997, and subsequent analysis in (b) and forecast in (c). Notice that ST Nestor is forecast to be too slow along-track at 24 h.

NOGAPS 24-h forecast (Fig. 4.10c) has ST Nestor near  $24^{\circ}$  N,  $141^{\circ}$  E, which is south of the actual position at this time. In fact, the NOGAPS prediction remains significantly behind the positions through 72 h (Fig. 4.9). Notice the 24-h predicted isotach maximum to the east of ST Nestor is similar in value and position to the analyzed isotach maximum. However, an isotach maximum is predicted to the southwest of ST Nestor that is not verified in the analysis. This predicted isotach to the southwest hints at a structural difference from the analysis and a component of steering flow from the northwest that might slow ST Nestor's northward track.

Although the forecast fields vary somewhat from the idealized conceptual fields, the basic concept of a structural inaccuracy in the forecast degrading the NOGAPS forecast TC track as the storm transitions from the WR region to the MW region is still apparent. This is supported by the NOGAPS 72-h forecast along-track error of -597 n mi versus the corresponding GFDN along-track error of only -147 n mi.



## **V. ERRONEOUS INDIRECT TROPICAL CYCLONE INTERACTION**

### **A. BACKGROUND**

The key circulation in an indirect TC interaction (ITI) is an anticyclone located between the two TCs that arises from Rossby wave dispersion associated with the western TC (Fig. 5.1a). Without the presence of the eastern TC, the poleward steering flow across the western TC associated with this anticyclone would lead to a poleward track deflection from the typical  $285^\circ$  heading for a TC south of the subtropical anticyclone in the S pattern (Fig. 1.2). The ITI effect on the eastern TC is an equatorward steering flow such that the eastern TC may even move south of west. However, the cyclonic relative vorticity advection to the northwest of the approaching eastern TC will tend to weaken the anticyclone between the two TCs, and may even cause a break between this anticyclone and the subtropical anticyclone. The ITI effect on the western TC is to decrease its poleward steering flow, and thus tend to cause the track of the western TC to become more westward. Weakening of the anticyclone will also decrease the equatorward steering flow across the eastern TC, which may then turn poleward (Carr *et al.* 1997).

### **B. ERRONEOUS INDIRECT TROPICAL CYCLONE INTERACTION CONCEPTUAL MODEL**

Erroneous ITI (Fig. 5.1b) may occur in the model forecast when the anticyclone between the two TCs is predicted to be weakened more than it actually is weakened in nature. Apparently, as the energy of the predicted anticyclone between the two TCs is transferred too quickly to the TC to the east, this anticyclone weakens too rapidly and the

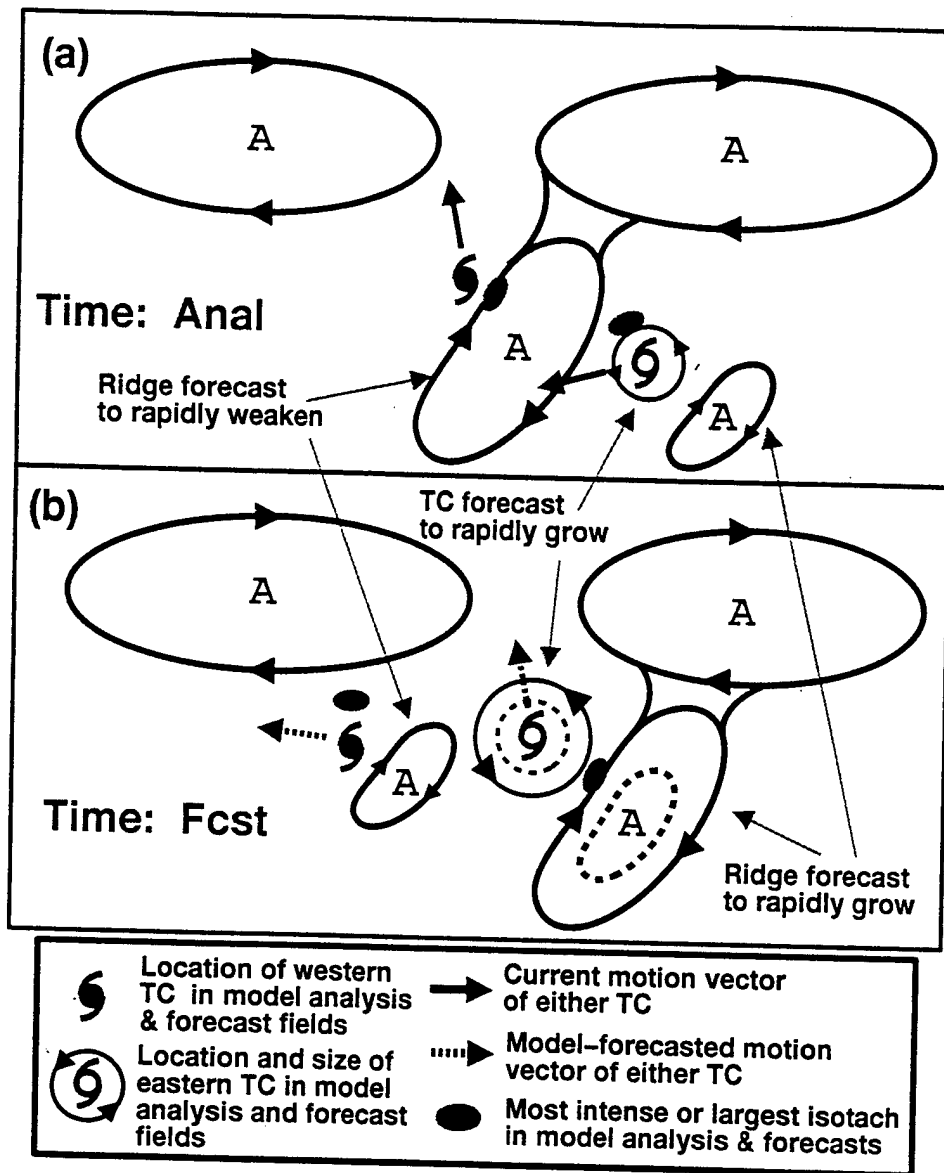


**Figure 5.1.** Schematics of the (a) actual indirect TC interaction (ITI) scenario, and (b) erroneous (ITI) conceptual model. Bold arrows indicate the direction the TC moves in each case, and (A) indicates anticyclone. Notice that the anticyclone between the two TCs in the erroneous ITI conceptual model is under-developed in comparison to the anticyclone between the two TCs in the actual scenario, and that the TC motion is different in each schematic.

horizontal extent of the eastern TC is over-predicted in the model. When the eastern TC is over-predicted, greater values of cyclonic relative vorticity are forecast to be advected to the west of the TC and the forecast anticyclone between the two TCs is weakened further. When this occurs, the predicted motion of both TCs may be altered. The predicted motion of the eastern TC tends to be influenced by both the weakened anticyclone to its west and by a developing anticyclone to its east-southeast. The typical forecast motion for the eastern TC in this scenario is a more northward track than observed in nature (Fig. 5.1b). The predicted motion of the western TC tends to be influenced by the weakened anticyclone to its east and is typically more westward than the observed TC motion (Fig. 5.1b).

### **C. CASE STUDIES**

#### **1. TY Zita (17W) and TY Amber (18W)**

The following case study of the interaction between TY Zita (western TC) and TY Amber (eastern TC) that occurred in August 1997 provides an example of erroneous ITI in the NOGAPS model and an example of how the GFDN model handled the same interaction. Notice that TY Zita had formed near  $18^{\circ}$  N,  $116^{\circ}$  E and initially moved eastward before turning west-northwestward (Fig. 5.2a). Notice also that TY Amber had formed near  $14^{\circ}$  N,  $135^{\circ}$  E and moved northwestward (Fig. 5.2b). The NOGAPS forecast initiated at 00 UTC 22 August (Fig. 5.2a) predicts a movement for TY Zita that is left of the best track, whereas the GFDN forecast track initiated at 06 UTC 22 August (Fig. 5.2a) predicts a movement that is right of the best track. For TY Amber (Fig. 5.2b), the NOGAPS track forecast initiated at 00 UTC 22 August, and the corresponding GFDN track forecast initiated at 06 UTC 22 August both predict a movement that is right of the best track.

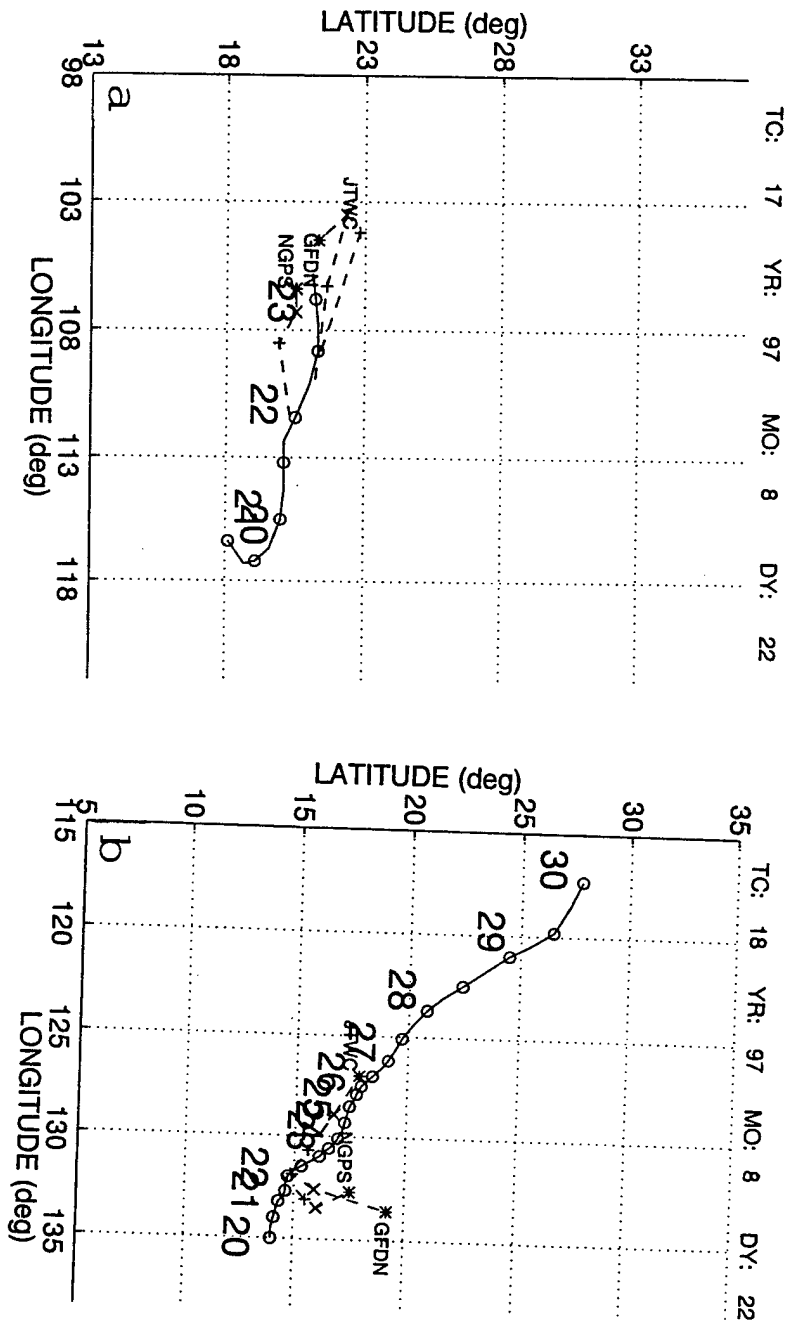


**Figure 5.2.** Best tracks as in Fig. 3.4, except for (a) TY Zita and (b) TY Amber. NOGAPS and GFDN model forecasts are initiated at 00 UTC and 06 UTC 22 August 1997, respectively. The JTWC forecast was initiated at 12 UTC 22 August. Notice that the NOGAPS forecast (a) is left of track for TY Zita and (b) is left of track for TY Amber. Notice that the GFDN forecast in (b) is right of track for TY Amber.

At 00 UTC 22 August (Fig. 5.3a), the NOGAPS 500-mb streamline analysis has TY Zita near  $19^{\circ}$  N,  $115^{\circ}$  E and has TY Amber near  $14^{\circ}$  N,  $132^{\circ}$  E. Notice that an anticyclone is centered near  $8^{\circ}$  N,  $123^{\circ}$  E and that it extends north-northeastward between TY Zita and TY Amber. Notice also that a smaller anticyclone is centered near  $11^{\circ}$  N,  $143^{\circ}$  E, which is to the southeast of TY Amber. This west-to-east wavetrain of TC-anticyclone-TC-anticyclone is well south of the subtropical ridge, which extends east/west along  $29^{\circ}$  N. Twenty-four hours later, the NOGAPS analysis (Fig. 5.3b) has TY Zita near  $19^{\circ}$  N,  $107^{\circ}$  E and has TY Amber near  $16^{\circ}$  N,  $131^{\circ}$  E. Notice that the anticyclone between the two TCs is analyzed to extend northward to near  $17^{\circ}$  N,  $121^{\circ}$  E, whereas the NOGAPS 24-h forecast (Fig. 5.3c) predicts the same anticyclone to extend northward to near  $15^{\circ}$  N,  $121^{\circ}$  E. Notice also that the NOGAPS 24-h forecast of the horizontal circulation of TY Amber is slightly greater than the analyzed circulation. The weakened anticyclone between TY Zita and TY Amber is consistent with the over-forecast of TY Amber in the NOGAPS 24-h forecast due to the advection of cyclonic relative vorticity to the west of TY Amber. In addition, the NOGAPS 24-h forecast positions of TY Amber (right of track) and TY Zita (left of track) are consistent with the steering currents that are obtained when the predicted anticyclone between the two typhoons is under-developed.

At 00 UTC 24 August, TY Zita is dissipating over land and the NOGAPS 500-mb streamline analysis (Fig. 5.3d) has TY Amber near  $16^{\circ}$  N,  $129^{\circ}$  E. Notice that the anticyclone located near  $8^{\circ}$  N,  $119^{\circ}$  E continues to extend northward between the dissipating western TC and Typhoon Amber. The NOGAPS 48-h forecast (Fig. 5.3e) has Typhoon Amber near  $17^{\circ}$  N,  $133^{\circ}$  E, which is again to the right of the best track (Fig. 5.2b). In

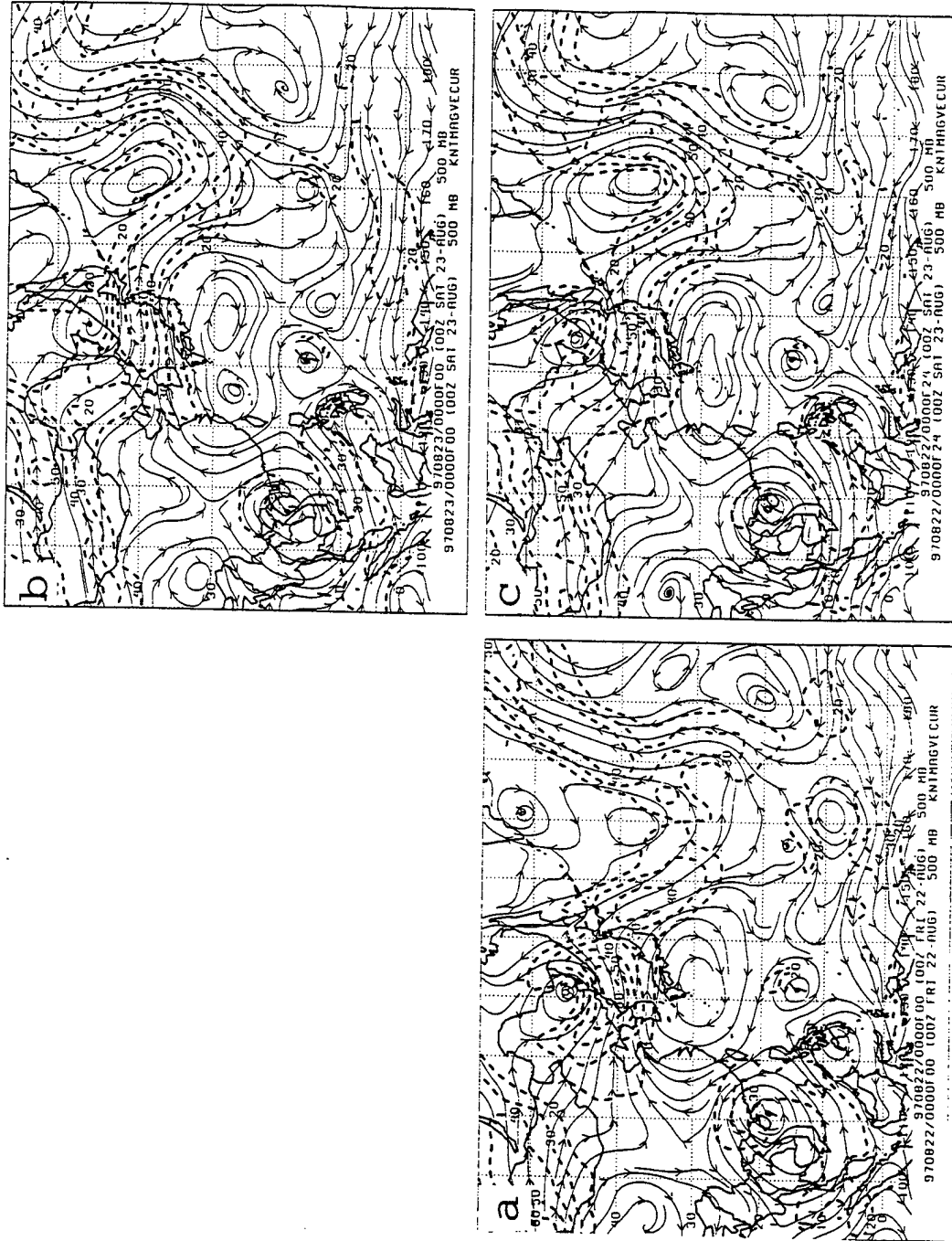
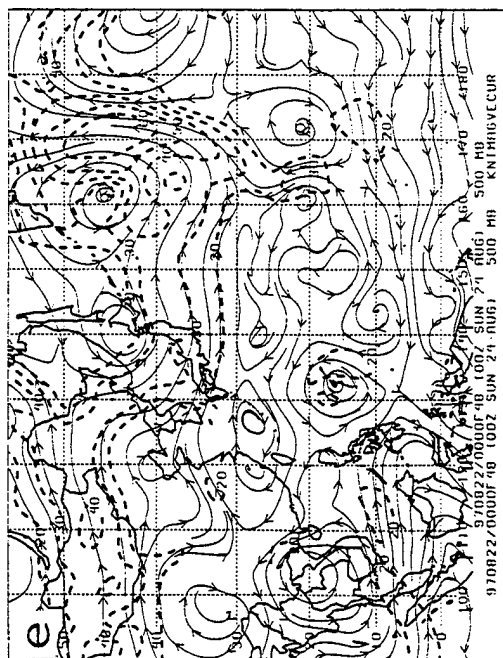
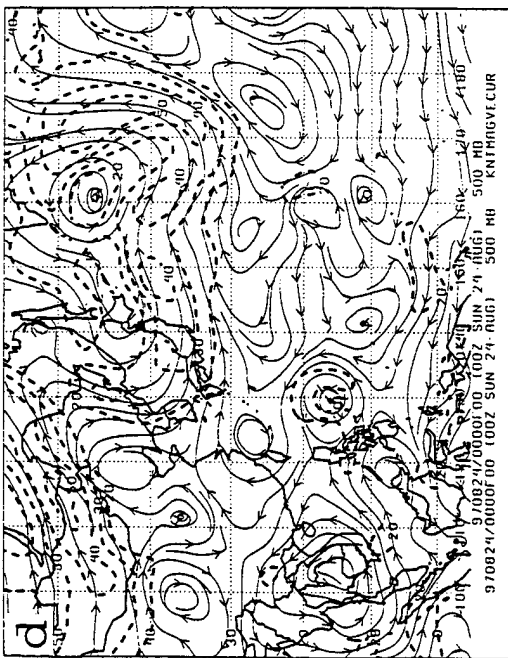
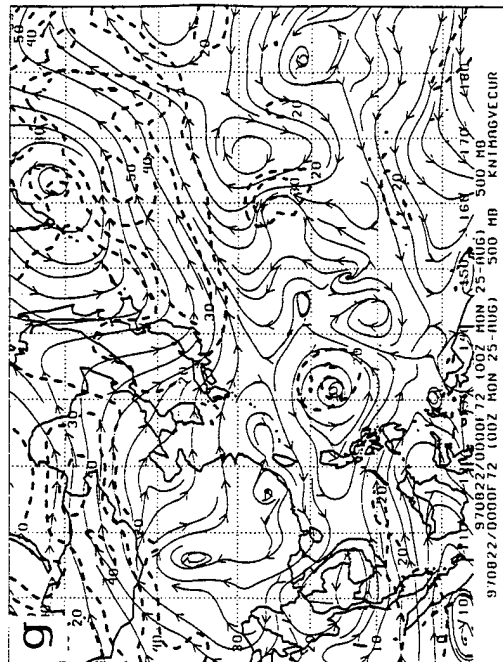
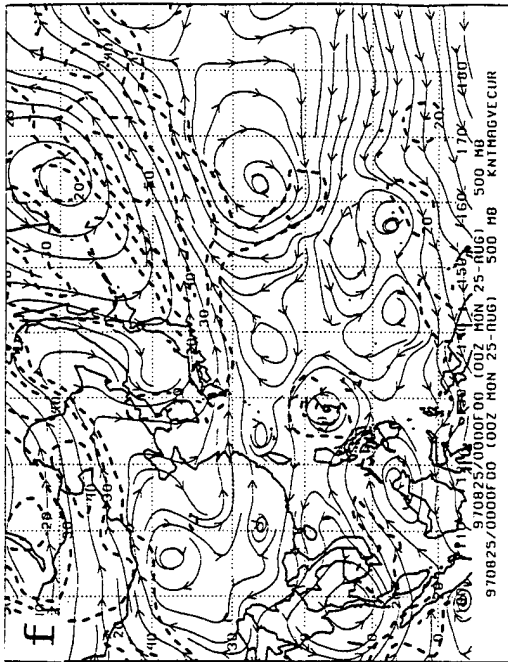


**Figure 5.3.** NOGAPS 500-mb streamline and isotach analyses and predictions as in Fig. 3.5, except from an initial analysis (a) at 00 UTC 22 August 1997, and subsequent analyses in (b-d-f) and forecasts in (c-e-g). Notice the difference in predicted anticyclone size versus analyzed anticyclone size throughout the series of charts.



addition, the NOGAPS 48-h forecast continues to over-develop Typhoon Amber, which is expected to contribute to decreasing the anticyclone amplitude to its west. Also, the anticyclone located to the southeast of TY Amber is slightly more developed in the NOGAPS 48-h forecast (Fig. 5.3e) than it is in the NOGAPS analysis (Fig. 5.3d). The combination of the 48-h predicted decrease in the anticyclone amplitude to the west of TY Amber and the enhanced anticyclone to the southeast of TY Amber is consistent with the continued NOGAPS 48-h forecast movement to the right of the best track (Fig. 5.2b).

After another 24 h (Fig. 5.3f), the NOGAPS analysis has TY Amber near  $17^{\circ}$  N,  $128^{\circ}$  E, whereas the NOGAPS 72-h forecast (Fig. 5.3g) has TY Amber near  $17^{\circ}$  N,  $131^{\circ}$  E. That is, the NOGAPS 72-h track forecast position (Fig. 5.2b) continues to be located to the right of the best track. Notice that TY Amber and the anticyclone to the southeast continue to be over-developed in the NOGAPS 72-h forecast, and that the anticyclone to the west of Typhoon Amber again is under-developed.

At 12 UTC 22 Aug (Fig. 5.4a), the GFDN 6-h forecast has TY Zita near  $20^{\circ}$  N,  $109^{\circ}$  E, TY Amber near  $14^{\circ}$  N,  $132^{\circ}$  E, and an anticyclone centered near  $8^{\circ}$  N,  $122^{\circ}$  E that extends northward between the two typhoons to near  $15^{\circ}$  N,  $122^{\circ}$  E. Twelve hours later (Fig. 5.4b), when the GFDN forecast may be directly compared to the NOGAPS 24-h forecast at the same valid time (Fig. 5.3c), the higher resolution GFDN has TY Zita more intense than the 24-h NOGAPS prediction, which is more consistent with the observed 50-kt surface winds at that time. Unfortunately, TY Zita begins to dissipate over land at this time and a comparison of GFDN performance versus NOGAPS for this western TC in this ITI scenario is difficult. The one notable difference between the two models is the ability of

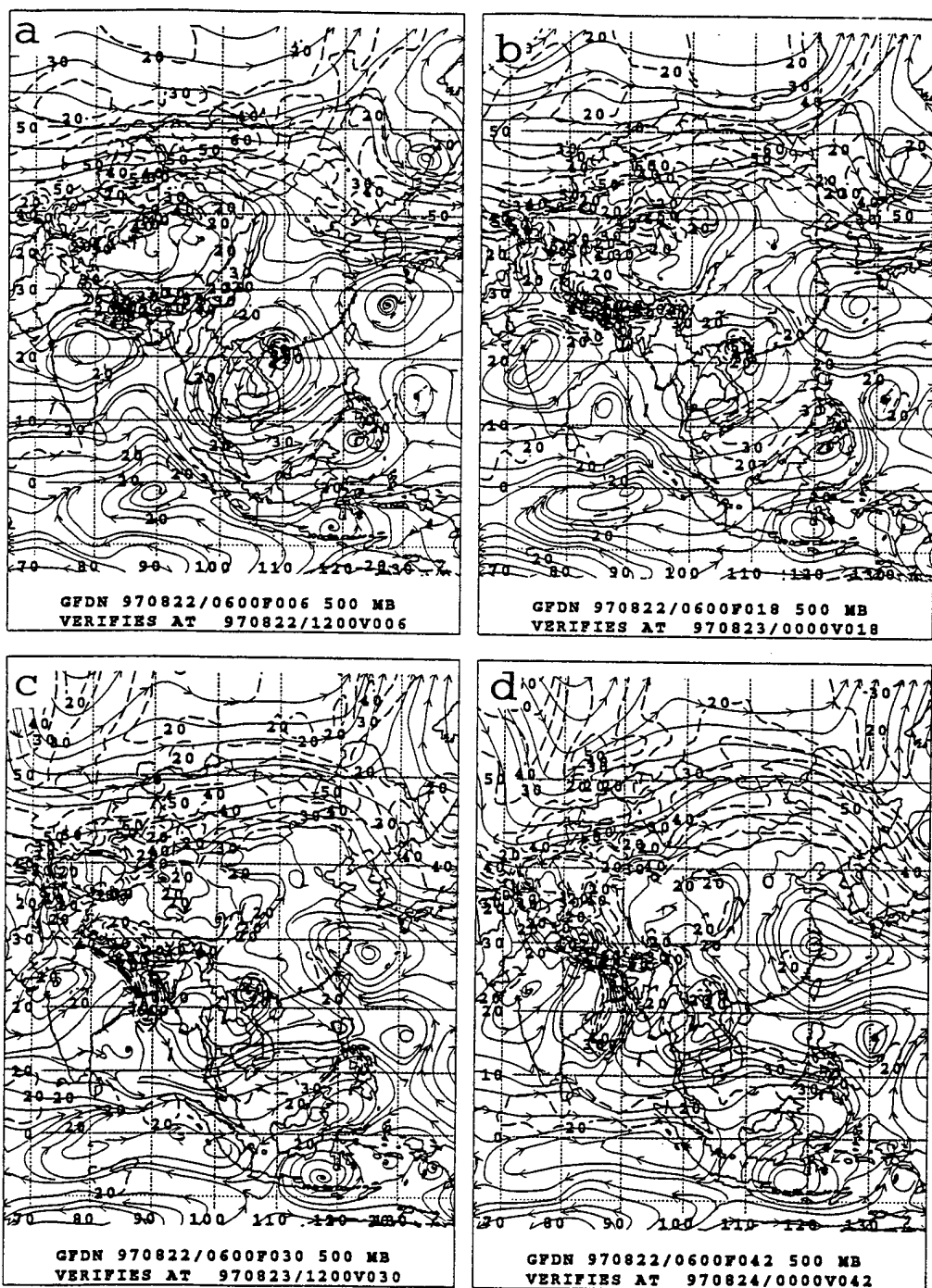


**Figure 5.4.** GFDN 500-mb streamline and isotach predictions as in Fig. 3.6, except for a forecast for TY Zita initiated at 06 UTC 22 August 1997, and verifies at (a) 12 UTC 22 August, (b) 00 UTC 23 August, (c) 12 UTC 23 August, and (d) 00 UTC 24 August. Notice that TY Amber (eastern TC) is predicted to move north too soon.

GFDN to maintain a more proper intensity for the circulation over land.

The GFDN initial condition technique of changing only the field near TY Zita results in an identical representation of the circulation to the east. That is, both the anticyclone under-development and the over-development of TY Amber were predicted in the GFDN 42-h forecast interval (Figs. 5.4a through 5.4d). Recall that the GFDN nested grid is placed over TY Zita, so that the TY Amber region is on the coarse mesh and no special initialization of Amber is made to get a better horizontal structure than exists in the NOGAPS analysis. The GFDN integration with TY Amber as the target storm also exhibited a right of track error (Fig. 5.2b) as did the NOGAPS prediction, presumably for the same reasons.

## **2. ST Bing (19W) and TY Amber (18W) Remnants**

The following case study of ST Bing (19W) and TY Amber (18W) remnants provides an example of erroneous ITI in both the NOGAPS and GFDN models. Notice that ST Bing had formed near 10°N, 160°E and moved west-northwestward for three days, turned poleward for another three days, and then recurved to the northeast (Fig. 5.5). The NOGAPS track forecast initiated at 12 UTC 28 August (Fig. 5.5) had a 72-h FTE of 393 n mi. The 72-h FTE for the corresponding GFDN track forecast that was initiated at 18 UTC 28 August (Fig. 5.5) was 159 n mi. Notice that both the NOGAPS track forecast and the GFDN track forecast predicted an erroneous poleward movement for ST Bing (eastern TC), which is consistent with an erroneous ITI.

At 12 UTC 28 August (Fig. 5.6a), the NOGAPS 500-mb streamline analysis has ST

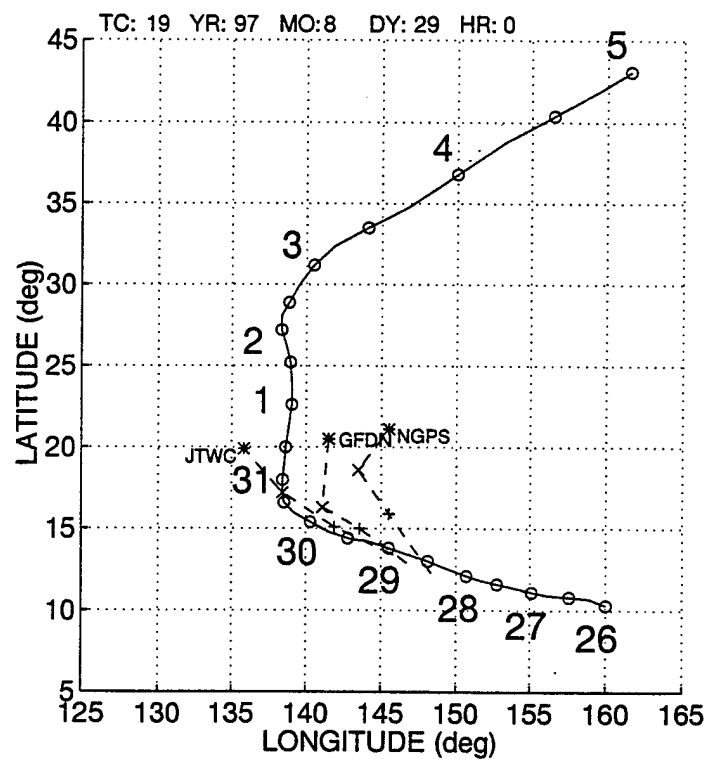


**Figure 5.5.** Best track as in Fig. 3.4, except for ST Bing. NOGAPS and GFDN model forecasts initiated at 12 and 18 UTC 28 August 1997, respectively. The JTWC forecast was initiated at 00 UTC 29 August 1997. Notice that both NOGAPS and GFDN predict a northward movement too soon.

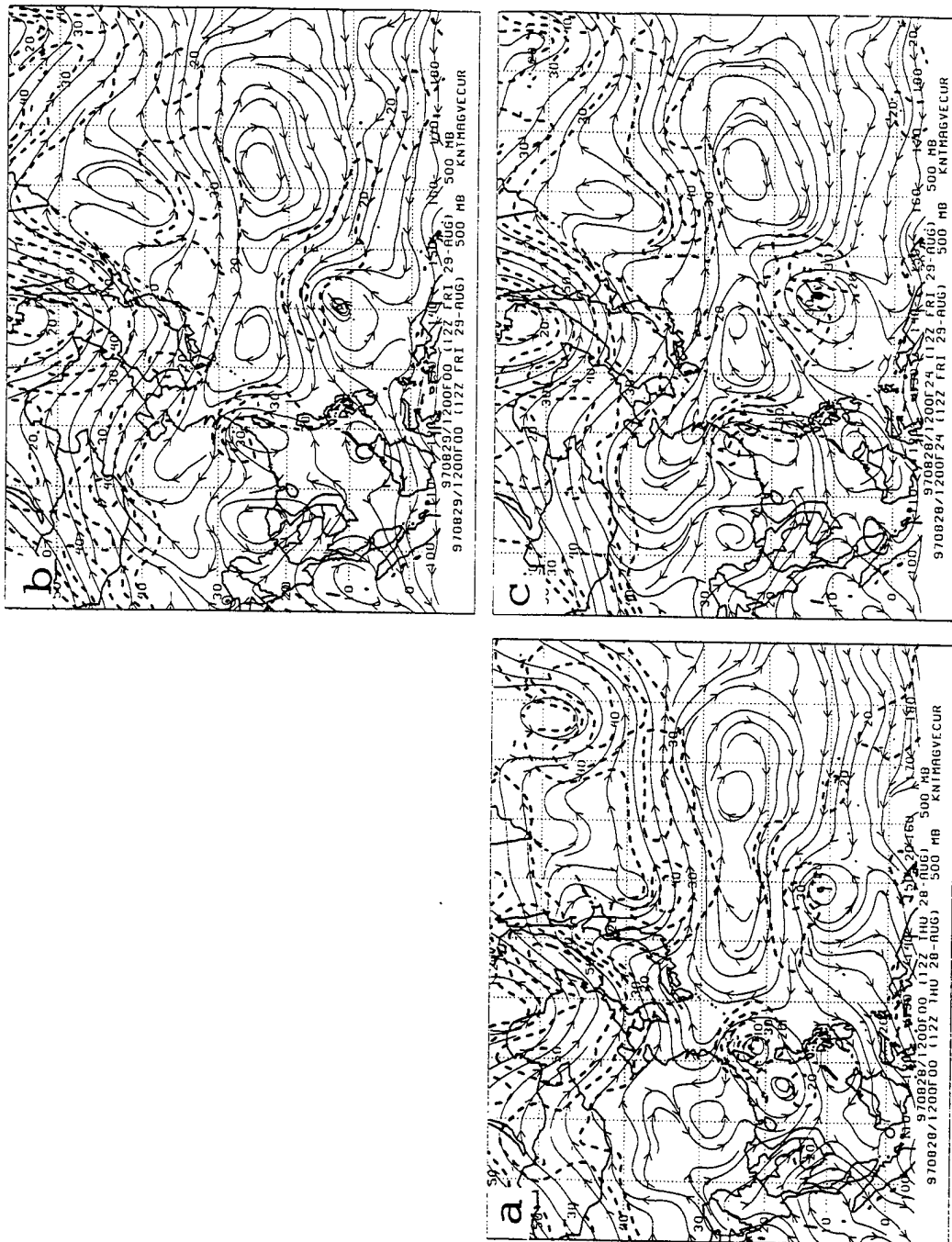
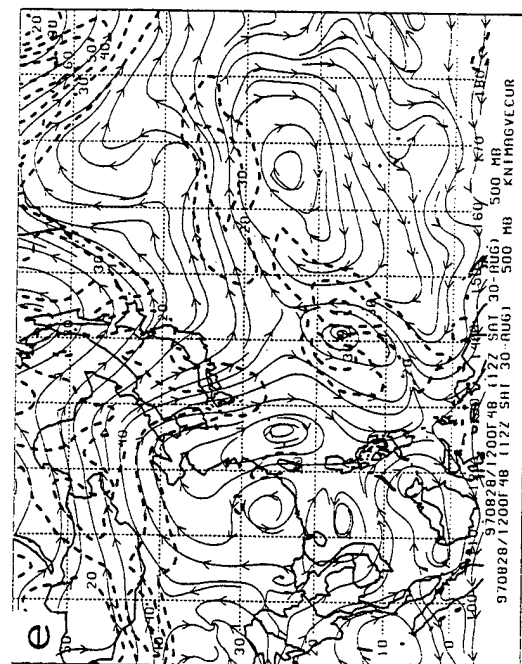
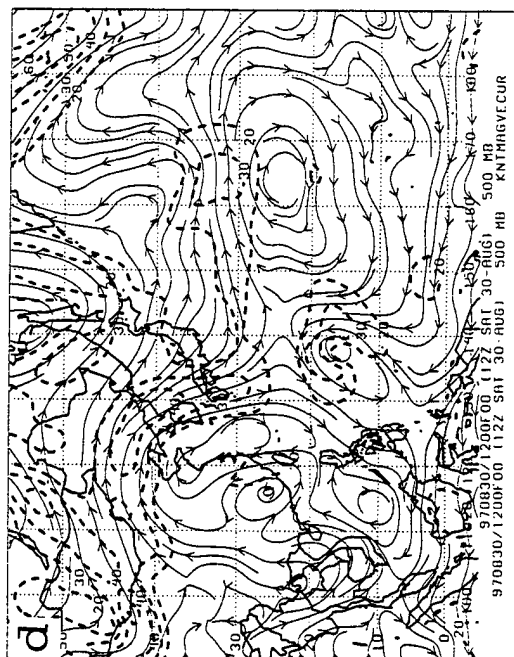


**Figure 5.6.** NOGAPS 500-mb streamline and isotach analyses and predictions as in Fig. 3.5, except from (a) an analysis at 12 UTC 28 August 1997, and subsequent analyses in (b-d) and forecasts in (c-e). Notice that the NOGAPS predictions build a peripheral anticyclone to the southeast of ST Bing too quickly and that the predicted 48-h position is north and east of the analyzed position.



Bing near  $11^{\circ}\text{N}$ ,  $148^{\circ}\text{E}$ . Notice that this is a S pattern with ST Bing located in the DR region. Twenty-four hours later, the NOGAPS analysis (Fig. 5.6b) has ST Bing near  $12^{\circ}\text{N}$ ,  $141^{\circ}\text{E}$ . Notice that a peripheral ridge is building to the southeast of ST Bing, which suggests a possible change from the S synoptic pattern to the P synoptic pattern. However, the analyzed isotach maximum to the north of ST Bing indicates a steering current that remains from the east, and therefore this is still a S synoptic pattern. The NOGAPS 24-h forecast (Fig. 5.6c) has ST Bing near  $13^{\circ}\text{N}$ ,  $144^{\circ}\text{E}$ , which is north and east of the actual position. Notice that the horizontal extent of ST Bing is over-predicted (note the 40-kt isotach to the northeast of Bing), which suggests that energy has transferred too quickly to ST Bing from the anticyclone between ST Bing and the remnants of TY Amber. Notice that the peripheral anticyclone to the southeast of ST Bing has developed, which suggests a continued too rapid energy transfer from the west. Notice also that this peripheral ridge has connected to the subtropical anticyclone to the northeast. The isotach maximum to the northeast suggests a steering flow from the southeast, which is consistent with the forecast northwestward progression of ST Bing. Thus, the NOGAPS model forecast has begun the transition from S/DR to P/PO and erroneous ITI seems to have started.

By 12 UTC 30 August (Fig. 5.6d), the NOGAPS analysis has ST Bing near  $17^{\circ}\text{N}$ ,  $138^{\circ}\text{E}$ . Notice that the peripheral anticyclone to the south-southeast of ST Bing has connected to the subtropical anticyclone to the northeast and that the analyzed isotach maxima are located to the east-southeast and west-northwest. The analyzed isotach maximum to the east-southeast is larger than the isotach maximum to the west-northwest, which indicates a more prevalent steering current from the south-southwest and this is

consistent with the poleward motion of ST Bing (Fig. 5.5). Thus, the transition from S/DR to P/PO has been completed. The NOGAPS 48-h forecast (Fig. 5.6e) continues to over-develop the horizontal extent of ST Bing, and consequently the predicted anticyclone to the south-southeast is again over-developed as energy is apparently transferred from ST Bing to the predicted anticyclone to the southeast too quickly. The strongest forecast isotach maximum in the vicinity of ST Bing is located to the east and is fairly consistent with the NOGAPS-predicted northeastward progression of the storm after 48 h (Fig. 5.5), which again suggests that erroneous ITI is occurring in the NOGAPS forecast.

At 00 UTC 29 August (Fig. 5.7a), the GFDN 6-h forecast has ST Bing near  $11^{\circ}\text{N}$ ,  $144^{\circ}\text{E}$  in the DR region of the S pattern. Notice that the predicted horizontal extent of ST Bing is similar to the representation of the circulation in the NOGAPS initial analysis (Fig. 5.6a), but that the GFDN-predicted isotach maximum is to the northeast instead of to the north as in the NOGAPS analysis. Twelve hours later (Fig. 5.7b) when the GFDN 18-h forecast may be directly compared to the NOGAPS analysis at the same valid time (Fig. 5.6b), the GFDN-predicted horizontal extent of ST Bing is slightly larger than the NOGAPS analyzed horizontal extent of ST Bing. Notice also that the GFDN 18-h forecast (Fig. 5.7b) predicts a more significant isotach maximum to the east of ST Bing, which suggests an intensification of the peripheral ridge to the southeast as energy is transferred too quickly (from the anticyclone between ST Bing and the remnants of TY Amber) to ST Bing.

By 00 UTC 30 August (Fig. 5.7c), the GFDN 30-h forecast has ST Bing near  $15^{\circ}\text{N}$ ,  $143^{\circ}\text{E}$  and continues to develop the peripheral ridge to the southeast. Although the predicted isotach values to the east of ST Bing are larger than those predicted 12 h before (Fig. 5.7b),

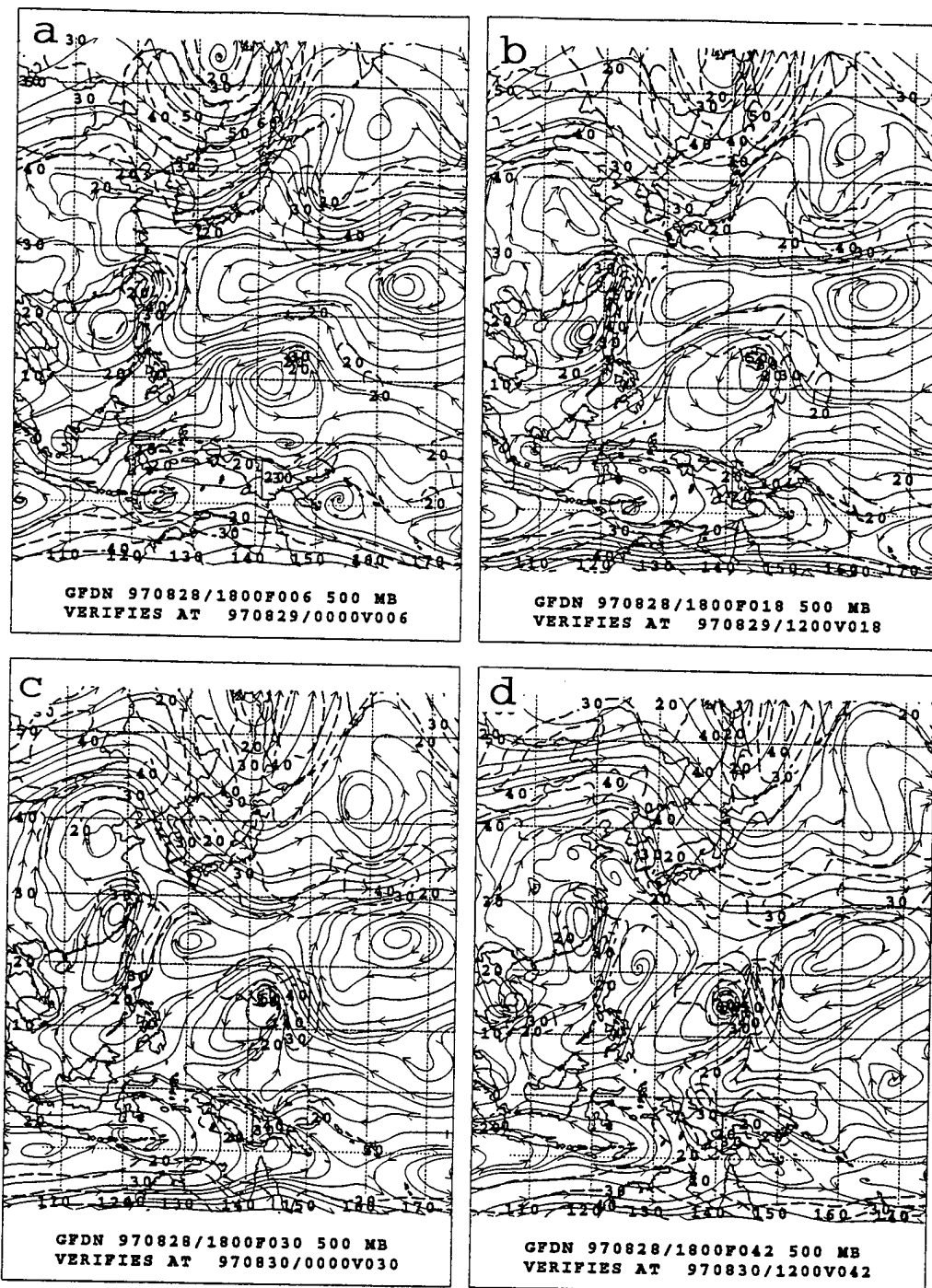


**Figure 5.7.** GFDN 500-mb streamline and isotach predictions as in Fig. 3.6, except forecast for ST Bing initiated at 18 UTC 28 August 1997, and verifies at (a) 00 UTC 29 August, (b) 12 UTC 29 August 1997, (c) 00 UTC 30 August 1997, and (d) 12 UTC 30 August. Notice that GFDN predicts a transition from S/DR to P/PO too quickly and ST Bing moves poleward too soon.

slightly larger forecast isotach values continue to be located on the north side of the storm, which indicates that the transition from S/DR to P/PO has not fully occurred yet. This also suggests that erroneous ITI may be occurring at a later time in the GFDN forecast interval than it did in the corresponding NOGAPS forecast interval. The placement of these 30-h predicted isotach maxima are consistent with the forecast and actual progression of ST Bing at this time. Twelve hours later (Fig. 5.7d), the GFDN 42-h forecast has ST Bing near 15°N, 141°E. Notice that the predicted horizontal extent of ST Bing is now clearly larger than the horizontal extent of ST Bing in the corresponding NOGAPS analysis (Fig. 5.6d). Notice also that the GFDN 42-h predicted isotach maximum to the east of ST Bing is larger than the corresponding NOGAPS analyzed isotach maximum in that location. The GFDN 42-h forecast steering current from the south-southwest is consistent with the inaccurate forecast track of ST Bing to the northeast after this time. As illustrated in Fig. 5.5, this forecast movement (due to the over-predicted horizontal extent of ST Bing and the over-developed peripheral ridge to the southeast of ST Bing) is consistent with an erroneous ITI by the GFDN model.

#### **D. 1997 STATISTICS/VARIATIONS**

Of the 27 storms in the western North Pacific during the 1997 typhoon season that were analyzed, five pairs of storms were classified under the conceptual model of section B. Four of these pairs (including Zita-Amber and Bing-Amber) of storms exhibited the same general errors that were described in the conceptual model. The following case study of the interaction between TY Ivan (27W) and TY Joan (28W) provides an example of a variation to the erroneous ITI conceptual model that was described in section B.

The western TC in this interaction, TY Ivan, formed near  $7^{\circ}\text{N}$ ,  $167^{\circ}\text{E}$  and moved west-northwest for 9 days before recurving to the northeast (Fig. 5.8a). The eastern TC in this interaction, TY Joan, formed near  $4^{\circ}\text{N}$ ,  $178^{\circ}\text{E}$  and moved west-northwest for 10 days before recurving to the northeast (Fig. 5.8b). The GFDN forecast for TY Ivan initiated at 18 UTC 15 October (Fig. 5.8a) has a 72-h cross-track error of 359 n mi to the right, whereas the corresponding NOGAPS forecast initiated at 12 UTC 15 October (Fig. 5.8a) has a 72-h cross-track error of only 100 n mi. However, the GFDN forecast for TY Joan initiated at 18 UTC 15 October (Fig. 5.8b) has a 72-h cross-track error of -140 n mi (i.e., to the left), and the corresponding NOGAPS forecast initiated at 12 UTC 15 October (Fig. 5.8b) has a 72-h cross-track error of 153 n mi.

At 12 UTC 15 November (Fig. 5.9a), the NOGAPS 500-mb streamline analysis has TY Ivan near  $11^{\circ}\text{N}$ ,  $139^{\circ}\text{E}$  and has TY Joan near  $11^{\circ}\text{N}$ ,  $159^{\circ}\text{E}$ . Notice that a southward lobe of the subtropical ridge extends between the two typhoons and that it connects to an anticyclone that is centered near  $2^{\circ}\text{N}$ ,  $150^{\circ}\text{E}$ . Notice also that both typhoons are of similar size and intensity, and that each has an isotach maximum located on the northern side, which indicates a steering flow from the east, and this is consistent with the observed track directions of both storms (Figs. 5.8a and 5.8b). Twenty-four hours later, the NOGAPS streamline analysis (Fig. 5.9b) has TY Ivan near  $12^{\circ}\text{N}$ ,  $134^{\circ}\text{E}$  and has TY Joan near  $12^{\circ}\text{N}$ ,  $154^{\circ}\text{E}$ . Notice that both typhoons have been analyzed to intensify slightly and that the isotach maximum (steering flow) continues to be consistent with the observed tracks of the typhoons (Figs. 5.8a and 5.8b). Notice also that the anticyclone between the two typhoons has basically maintained the same orientation. The NOGAPS 24-h forecast (Fig. 5.9c) has

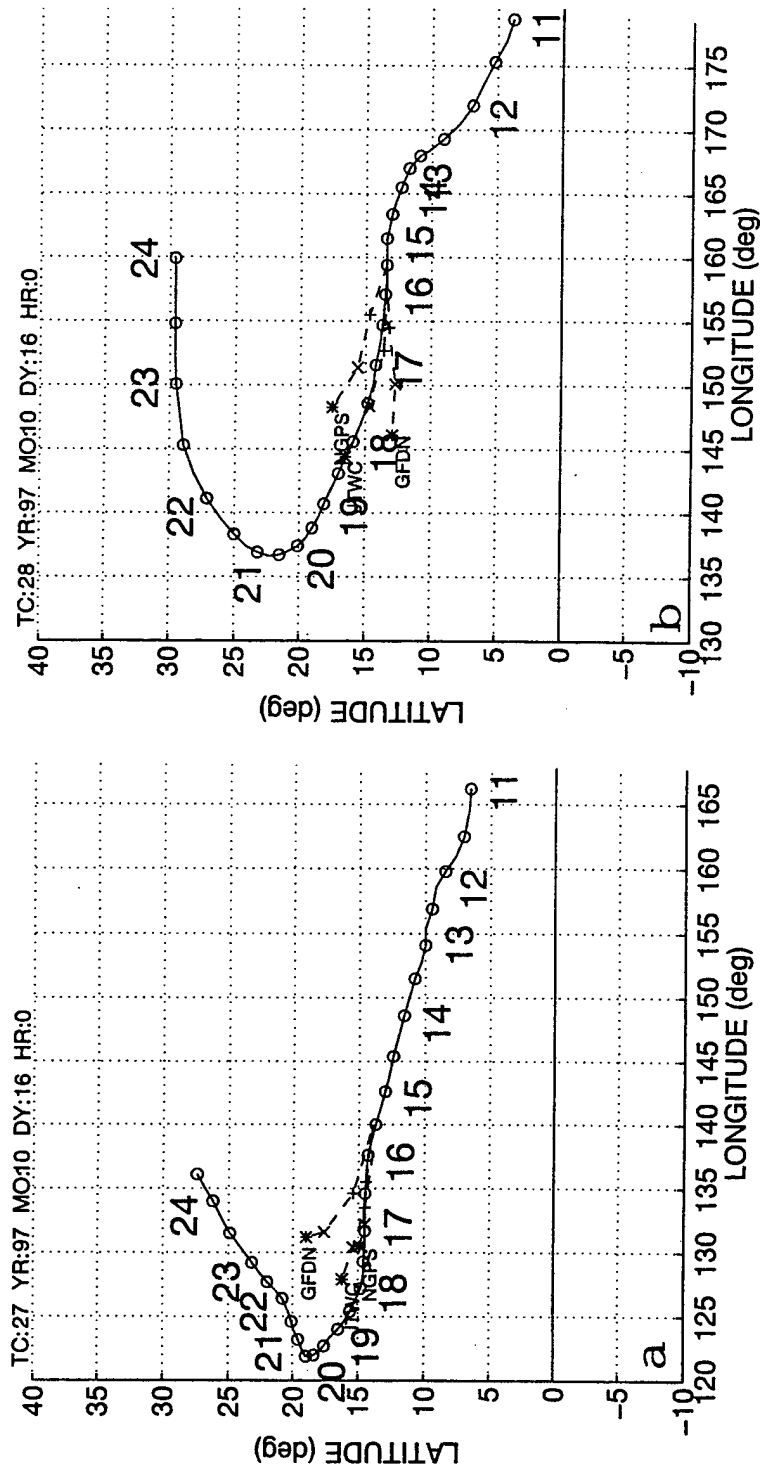


**Figure 5.8.** Best track as in Fig. 3.4, except for (a) TY Ivan and (b) TY Joan. NOGAPS and GFDN model forecasts are initiated at 12 and 18 UTC 15 October 1997, respectively. The JTWC forecast was initiated at 00 UTC 16 October 1997. Notice that the GFDN forecast (a) is right of track and (b) left of track.

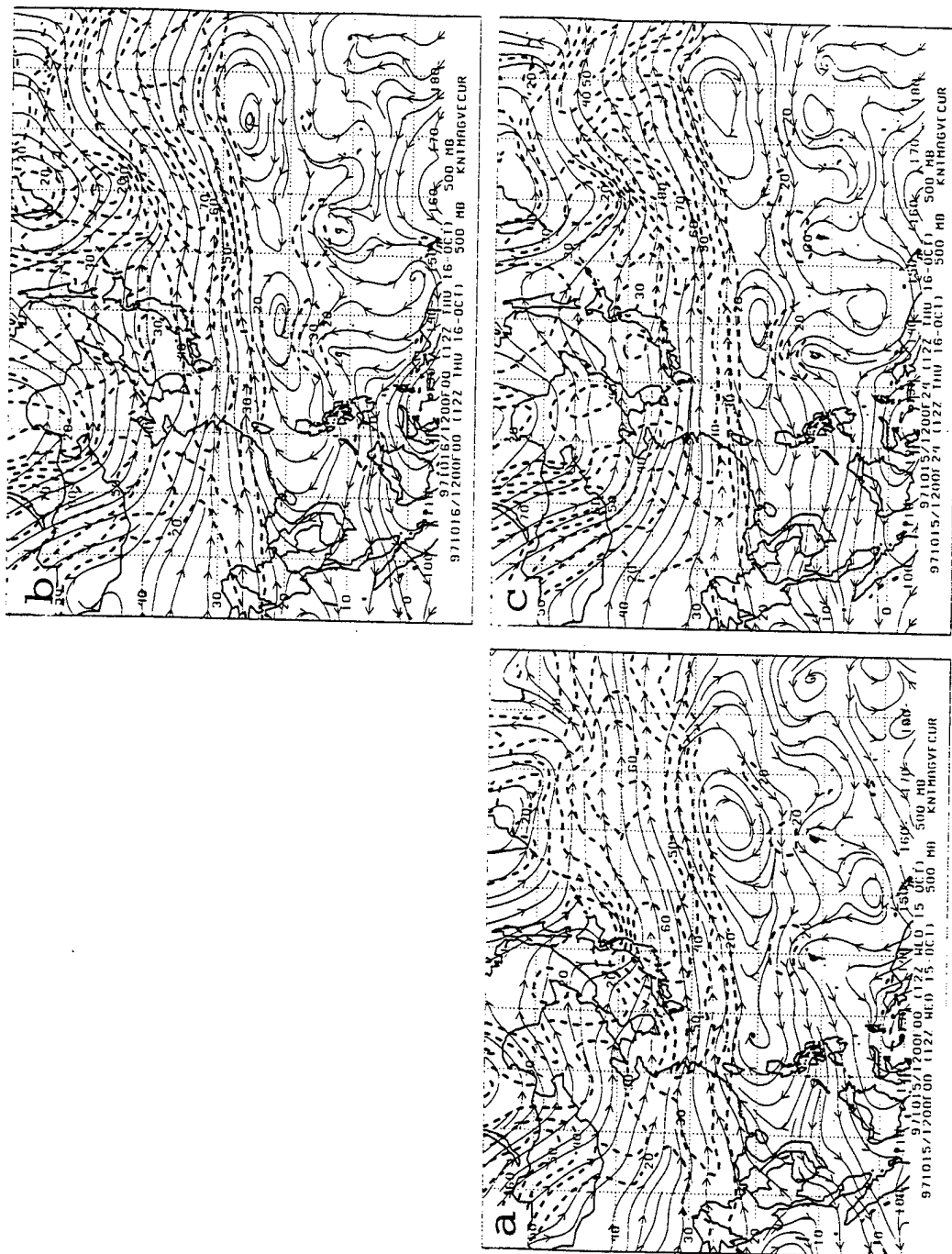
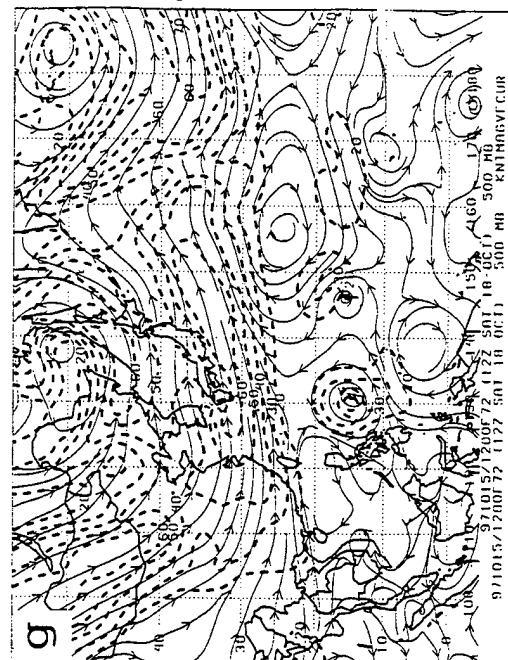
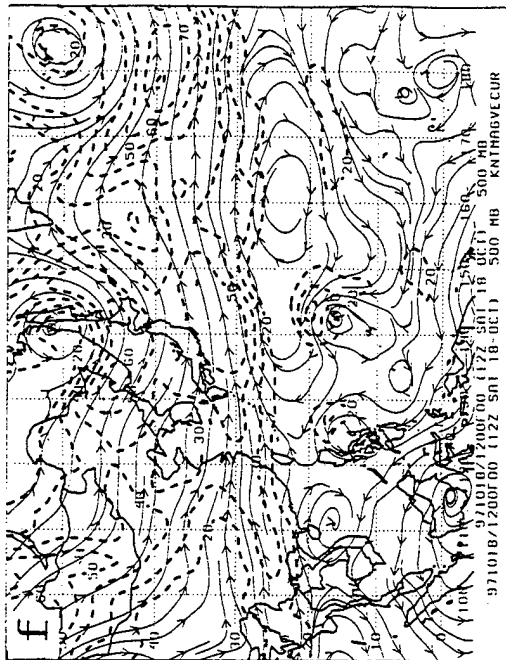
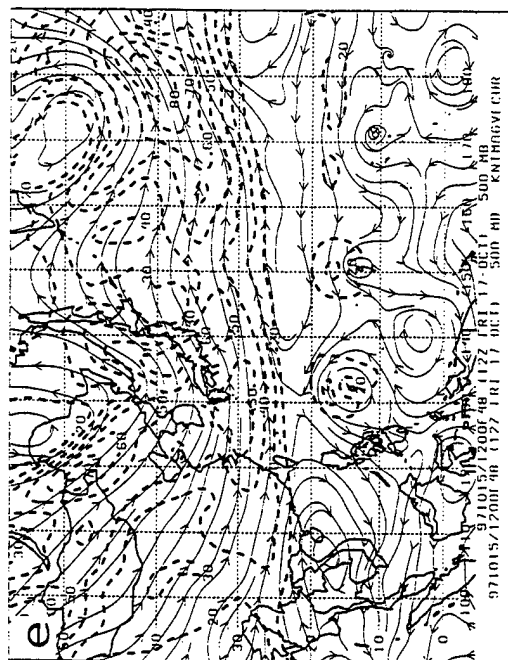
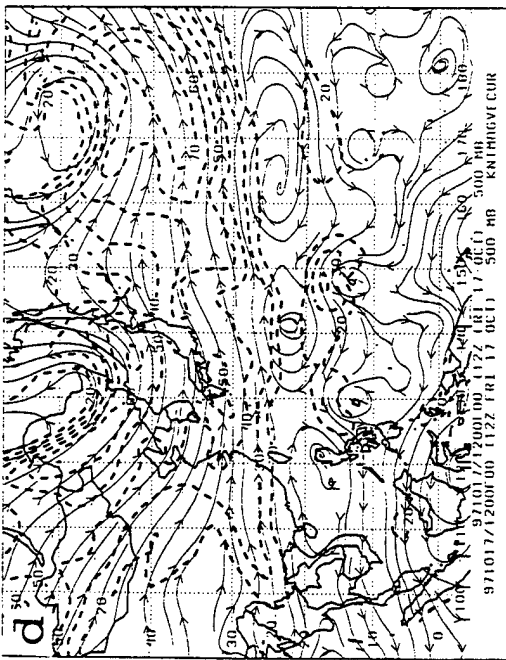


**Figure 5.9.** NOGAPS 500-mb streamline and isotach analyses and predictions as in Fig. 3.5, except from (a) an initial analysis at 12 UTC 15 October 1997, subsequent analyses in (b-d-f) and forecasts in (c-e-g). Notice that the 72-h predicted position for TY Joan is right of the best track.



TY Ivan near  $12^{\circ}\text{N}$ ,  $135^{\circ}\text{E}$  and has TY Joan near  $12^{\circ}\text{N}$ ,  $155^{\circ}\text{E}$ . Notice that the 24-h predicted anticyclone between the two typhoons has weakened slightly as compared to the analyzed anticyclone. This forecast of the slightly weakened anticyclone is consistent with the 24-h forecast track displacement of TY Joan somewhat to the right (65 n mi) of the best track at that time (Fig. 5.8b). At this time, the NOGAPS 24-h forecast cross-track error for TY Ivan (Fig. 5.8a) of only -2 n mi does not indicate any effect of the slight weakening of the 24-h forecast anticyclone.

By 12 UTC 17 October (Fig. 5.9d), the NOGAPS streamline analysis has TY Ivan near  $12^{\circ}\text{N}$ ,  $130^{\circ}\text{E}$  and has TY Joan near  $12^{\circ}\text{N}$ ,  $148^{\circ}\text{E}$ . Notice that TY Ivan maintains the same intensity while TY Joan is analyzed as more intense. The NOGAPS 48-h forecast (Fig. 5.9e) has TY Ivan near  $13^{\circ}\text{N}$ ,  $132^{\circ}\text{E}$  and TY Joan near  $13^{\circ}\text{N}$ ,  $150^{\circ}\text{E}$ . Notice that the anticyclone to the south of the two typhoons has been over-developed and broken away from the subtropical anticyclone to the north in the NOGAPS 48-h forecast. Notice also that TY Ivan is forecast slow (48-h forecast along-track error of -168 n mi), which may be attributed to the forecast over-development of the anticyclone to the southeast (notice the 20-kt isotach extends around Ivan to the southeast). The breaking away of the anticyclone between the two typhoons in the NOGAPS 48-h forecast is consistent with TY Joan being forecast on a right of track movement (Fig. 5.8b). Another factor in a more poleward track may be the steering influence of the developing anticyclone to the east-southeast near  $10^{\circ}\text{N}$ ,  $158^{\circ}\text{E}$ . After another 24 h (Fig. 5.9f), the NOGAPS analysis continues to maintain the anticyclone between the two typhoons. However, the NOGAPS 72-h forecast (Fig. 5.9g) clearly has broken the subtropical anticyclone from the anticyclone that is now predicted to be centered

near 5°N, 139°E. The motion of TY Ivan continues to be influenced by the steering current associated with the over-predicted anticyclone to the south, and now has a -281 n mi along-track error at 72 h (Fig. 5.8a). The NOGAPS 72-h forecast position for TY Joan is 153 n mi to the right and 258 n mi behind the best track (Fig. 5.8b), which is consistent with the breaking of the anticyclone between the two typhoons and the resultant steering current from the combination of the anticyclone to the southeast and the subtropical anticyclone to the northeast (Fig. 5.9g).

At 00 UTC 16 October (Fig. 5.10a), the 6-h GFDN forecast for the target TY Ivan in the fine mesh has the storm near 13°N, 138°E, whereas the second storm (TY Joan) is represented on the coarse mesh near 12°N, 157°E. Twelve hours later (Fig 5.10b), when GFDN forecast may be directly compared to the NOGAPS analysis at the same valid time (Fig. 5.9b), the higher resolution GFDN forecast has a more compact circulation for TY Ivan than in the NOGAPS forecast. Notice that the area east of TY Ivan is similar to the NOGAPS 24-h forecast, which is expected due to the initial vortex specification in GFDN of only the western TC in this case.

After another 24 h (Fig. 5.10c), the GFDN 42-h forecast again predicts a stronger circulation for TY Ivan than in the corresponding NOGAPS analysis (Fig. 5.9d). Notice that the GFDN 42-h forecast for TY Joan is under-developed (and therefore unable to hinder the development of the predicted anticyclone between the two TCs) and that the predicted anticyclone between TY Ivan and TY Joan is more developed than in the NOGAPS 48-h analysis. Consequently, the steering flow for TY Ivan is predicted to be from the south, which is fairly consistent with the GFDN forecast movement (Fig. 5.8a). With the predicted

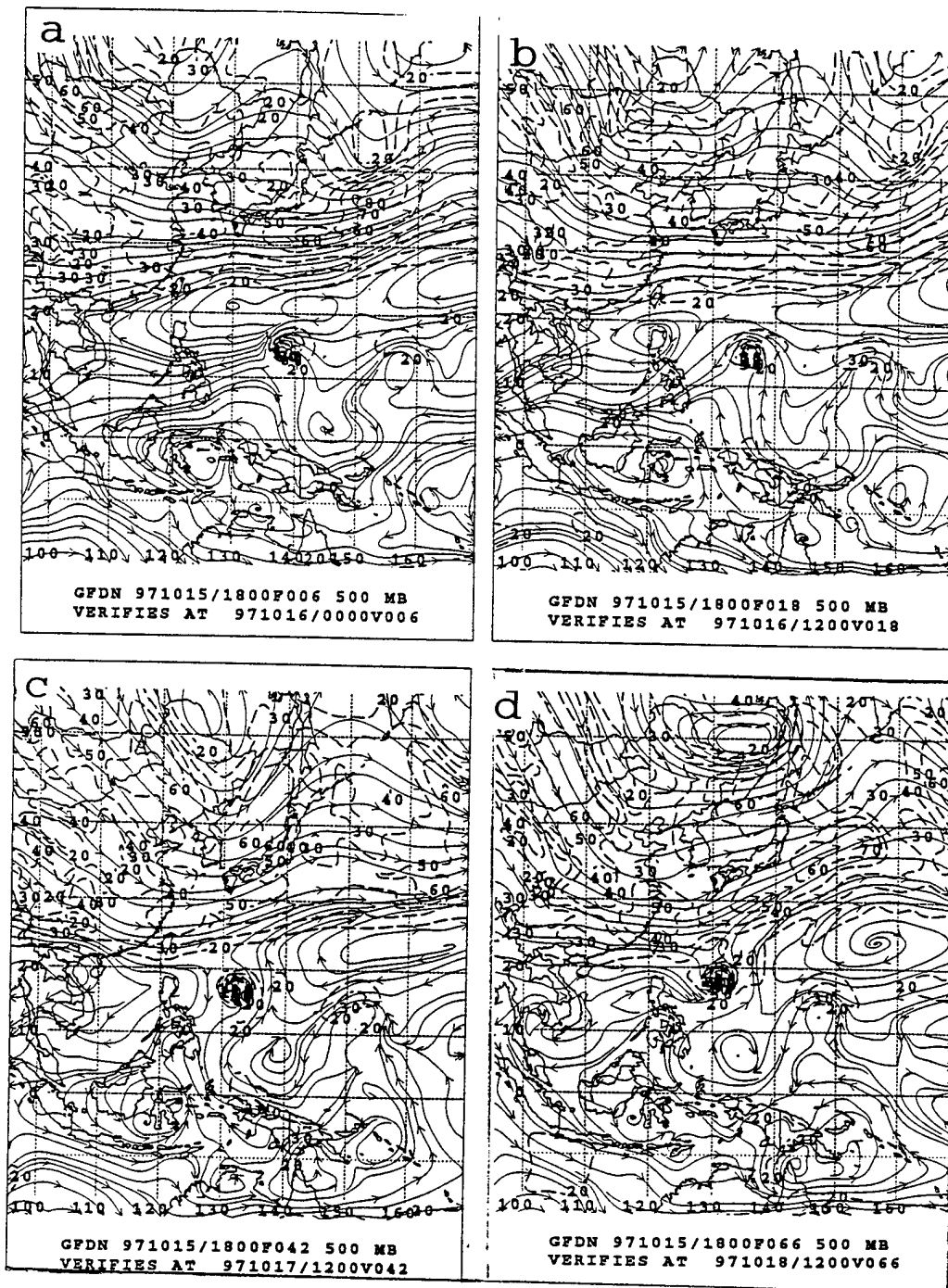


**Figure 5.10.** GFDN 500-mb streamline and isotach predictions as in Fig. 3.6, except for a forecast for TY Ivan initiated at 18 UTC 15 October 1997, and verifies at (a) 00 UTC 16 October, (b) 12 UTC 16 October, (c) 12 UTC 17 October, and (d) 12 UTC 18 October. Notice that TY Ivan is predicted right of the best track at 72 h.

anticyclone in this location, the steering current for TY Joan is from the east on the coarse grid in this GFDN integration. Such a steering current is also consistent with the 48-h west of along-track displacement (Fig. 5.8b) for the GFDN forecast when TY Joan was the target storm. After another 24 h (Fig. 5.10d), the GFDN 66-h forecast again predicts a stronger circulation for TY Ivan than in the corresponding analysis (Fig. 5.9f). Notice also that the anticyclone between TY Ivan and TY Joan is over-developed in the GFDN 66-h forecast, so that a transition from S/DR to P/PO is predicted. Such a poleward steering current is again consistent with the GFDN 72-h forecast right of track error (Fig. 5.8a) for TY Ivan. Although TY Joan is not the target storm in this GFDN integration, the isotach maximum to the north of TY Joan (Fig. 5.10d) is consistent with the predicted track from the east in the GFDN forecast when TY Joan was the target storm and the cross-track error was -140 n mi (Fig. 5.8b). Evidently, the same physical processes affected the track of TY Joan when it was the target storm as in the sequence in Fig. 5.10 with TY Ivan the target storm.

In this case study of TY Ivan and TY Joan, the GFDN prediction of the horizontal structure of TY Ivan is much stronger than the prediction of TY Joan throughout the forecast interval. As a result, the anticyclone that is located between the two typhoons is over-intensified throughout the forecast interval. The erroneous ITI conceptual model of section B describes the anticyclone between the two TCs as being under-forecast due to the over-forecast of the eastern TC. The resultant GFDN forecast tracks of TY Ivan (right of best track) and TY Joan (left of best track) are opposite to those forecast tracks described in section B. That is, whereas the conceptual model indicates that the western TC motion is predicted to be left of the best track (and the eastern TC right of the best track), TY Ivan

(western TC) is falsely predicted to the right of the best track (and TY Joan left of best track) by GFDN. This is reasonable because the key circulation, the anticyclone between the two TCs is described as weakening in the conceptual model, whereas it is predicted to be maintained in the GFDN forecast with TY Ivan as the target storm (Fig. 5.10), and when TY Joan was the target storm (not shown).

## **VI. TOO RAPID S/DR TO P/PO TRANSITION**

### **A. TOO RAPID S/DR TO P/PO TRANSITION CONCEPTUAL MODEL**

A too rapid transition from the S/DR to the P/PO synoptic pattern/region (Fig. 6.1) may occur in the model forecast when the horizontal extent of a TC, while in S/DR, is over-predicted. When the horizontal extent of a TC is over-predicted, an anticyclone to the east-southeast of the TC tends to over-develop and connect to the subtropical anticyclone that is to the north of the TC. When this occurs, the synoptic pattern may change from the S (Fig. 1.2) to the P pattern (Fig. 1.4) with the TC located in the PO region. If the predicted steering current is changed too soon to a poleward flow, the forecast motion for the TC has an incorrect northern component.

### **B. CASE STUDY**

The following case study of ST Ginger (24W) is an example of a too rapid transition from the S/DR to the P/PO synoptic pattern/region.

ST Ginger formed near  $10^{\circ}$  N,  $174^{\circ}$  E and initially moved westward for a day, tracked northwestward for about five days, and then recurved to the northeast (Fig. 6.2). The NOGAPS track forecast initiated at 00 UTC 23 September (Fig. 6.2) had a 72-h FTE of 306 n mi. Notice the NOGAPS track forecast was to the right of the best track as a result of moving poleward too soon.

At 00 UTC 23 September (Fig. 6.3a), the NOGAPS 500-mb streamline analysis has ST Ginger near  $10^{\circ}$  N,  $169^{\circ}$  E, and this is in the DR synoptic region of a S pattern. Notice that the subtropical ridge axis is tilted northeast to southwest and that a broad isotach

## S/DR to P/PO Transition

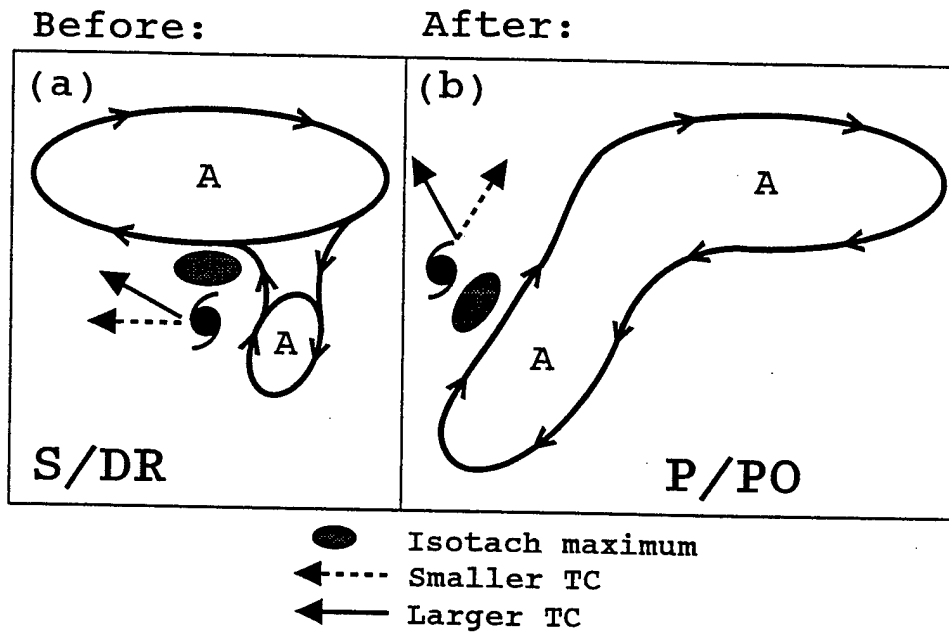


**Figure 6.1.** Conceptual model of a too-rapid transition from the Standard/Dominant Ridge (S/DR) pattern/synoptic region combination to the Poleward/Poleward-oriented (P/PO) synoptic pattern/region combination. The arrows (straight solid, and straight dashed) indicate the TC direction of motion, the A indicates anticyclone and the arrows on the curved lines indicate circulation motion around the anticyclone.

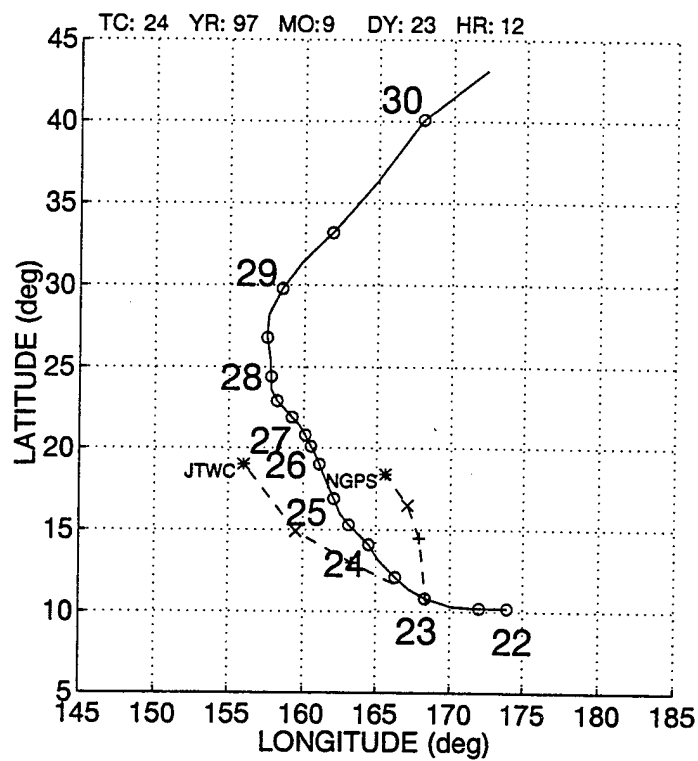


**Figure 6.2.** Best track as in Fig. 3.4, except for ST Ginger. NOGAPS model forecast was initiated at 00 UTC 23 September 1997 and the JTWC forecast was initiated at 12 UTC 23 September 1997. Notice that the NOGAPS model predicted a poleward motion too soon.

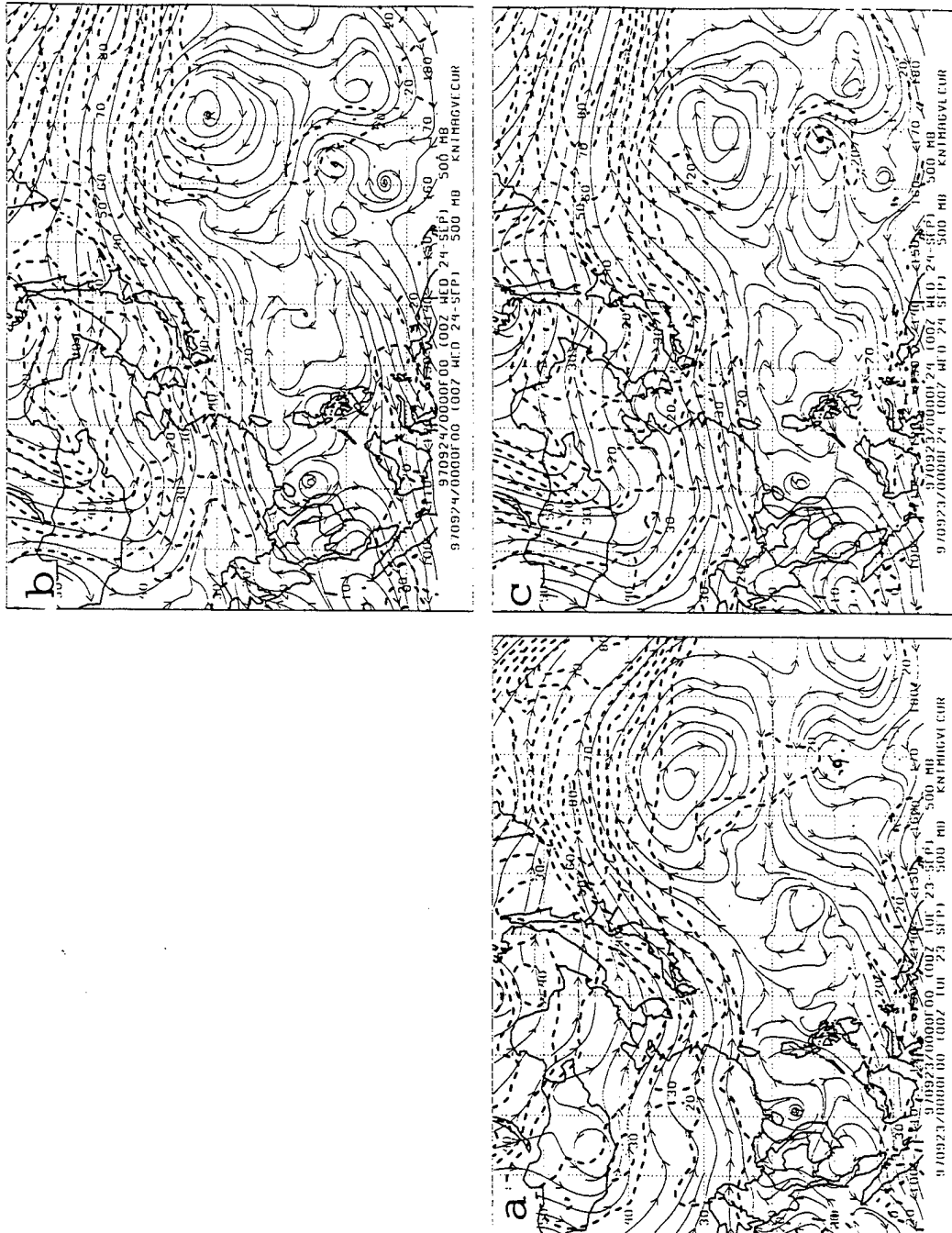


**Figure 6.3.** NOGAPS 500-mb streamline and isotach analyses and predictions as in Fig. 3.5, except from (a) an analysis at 00 UTC 23 September 1997, and a subsequent analysis in (b) and forecast in (c). Notice that TY Ginger moves poleward too quickly early in the forecast interval.

maximum has been analyzed on the northern side of ST Ginger, which indicates a steering current from the east. However, this is not consistent with the actual northwestward motion of the storm. The large horizontal extent of ST Ginger might suggest that the beta effect is influencing the motion of the typhoon at this time. Twenty-four hours later (Fig. 6.3b), the NOGAPS analysis has ST Ginger near  $11^{\circ}\text{N}$ ,  $163^{\circ}\text{E}$ . The developing peripheral anticyclone to the south and east, plus the isotach shift to the eastern side of Ginger, indicate the beginning of a transition from S/DR to P/PO. The NOGAPS 24-h forecast (Fig. 6.3c) has ST Ginger near  $12^{\circ}\text{N}$ ,  $168^{\circ}\text{E}$ , which is already north and east of the analyzed position (Fig. 6.2). Notice that the NOGAPS 24-h forecast has a slightly larger horizontal extent, a larger peripheral anticyclone to the southeast, and a larger isotach maximum to the east for ST Ginger than in the corresponding NOGAPS analysis (Fig. 6.3b). This suggests that the NOGAPS prediction has too quickly transitioned from S/DR to P/PO, which is consistent with the NOGAPS forecast of a northward motion of ST Ginger too soon.

### **C. STATISTICS**

Of the 27 storms in the western North Pacific during the 1997 typhoon season that were analyzed, 2 storms (including TY Ginger) were classified under the conceptual model of section A.



## **VII. ERRONEOUS TC RECURVATURE THROUGH A THIN SUBTROPICAL RIDGE**

### **A. ERRONEOUS RECURVATURE CONCEPTUAL MODEL**

Erroneous recurvature of a TC through a thin subtropical ridge (Fig. 7.1) may be predicted in a model forecast when a TC is predicted either to be stronger than or larger in horizontal extent than actually occurs in nature. In this conceptual model, the over-represented TC is initially located in a S/DR synoptic pattern/region (Fig. 1.2). As the TC progresses and is erroneously forecast to increase in horizontal extent, the model forecast tends to move the TC northwestward (into the WR synoptic region) instead of the actual westward movement (remaining in the DR synoptic region). The cyclonic vorticity advection to the northwest of the over-represented TC may weaken the thin subtropical ridge, move through the WR region (Fig. 7.1b), and recurve to the northeast (Fig. 7.1c).

### **B. CASE STUDY**

The following case study of TY Mort (31W) provides an example of erroneous recurvature of a TC through a thin subtropical ridge in the GFDN model. TY Mort formed near 11°N, 147°E and generally tracked west-northwestward before dissipating (Fig. 7.2). Notice that the GFDN forecast initiated at 06 UTC 11 November predicts a false recurvature to the northeast for TY Mort. Because the NOGAPS-predicted track of TY Mort was not available due to data recovery problems approximate predictions at 48 h and 72 h are taken from the fields (Fig. 7.3e and g). These NOGAPS forecasts verify very well and do not indicate a false recurvature to the northeast as in the GFDN forecast.

**Scenario: Model-predicted recurvature through thin ridge due to over-representation of TC size**

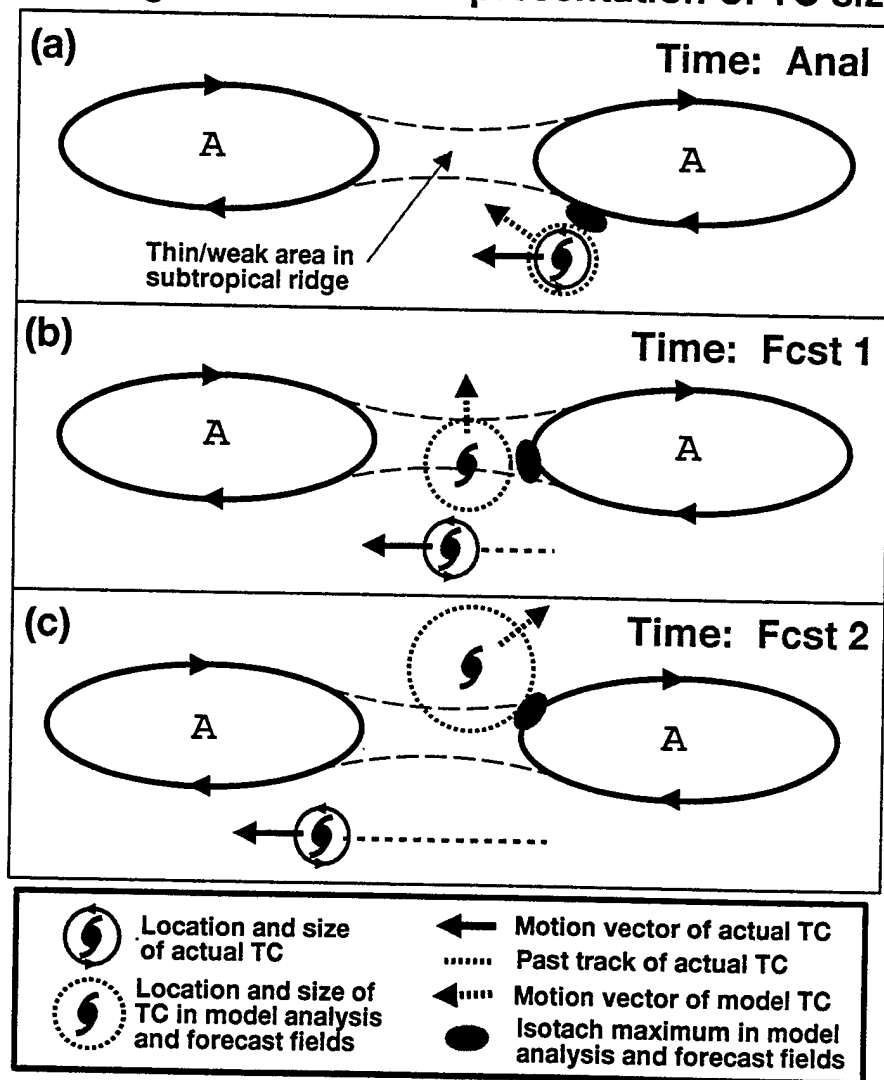


**Figure 7.1.** Conceptual model of a model-predicted recurvature through a thin subtropical ridge due to over-representation of TC size (see insert for explanation of the symbols).

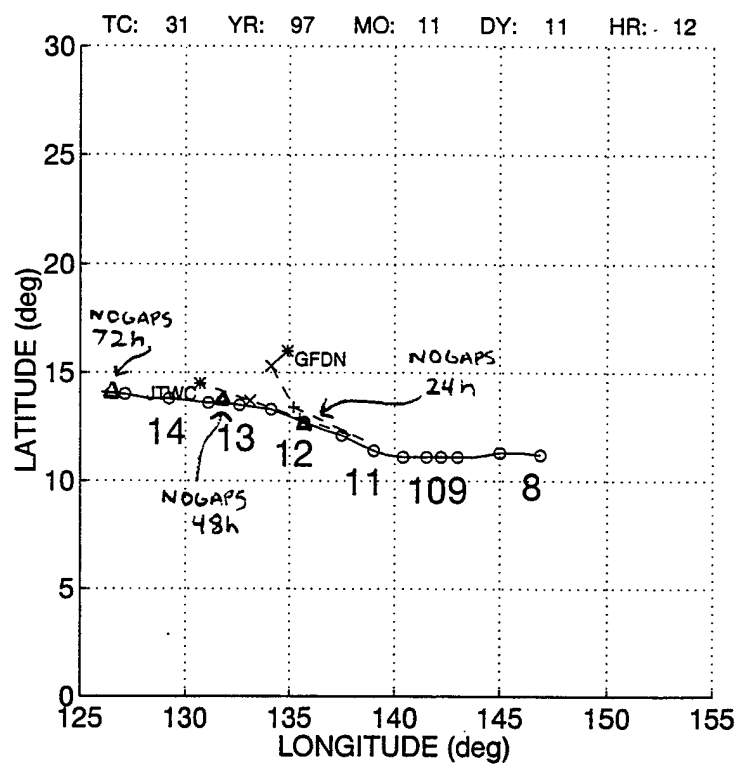


**Figure 7.2.** Best track as in Fig. 3.4, except for TY Mort and NOGAPS 24, 48, and 72h forecast positions are plotted as triangles. GFDN model forecast was initiated at 06 UTC 11 November 1997. The JTWC forecast was initiated at 12 UTC 11 November 1997. Notice that GFDN erroneously predicts a poleward motion.

At 00 UTC 11 November (Fig. 7.3a), the NOGAPS 500-mb streamline analysis has TY Mort near  $10^{\circ}\text{N}$ ,  $139^{\circ}\text{E}$  in the DR region of the S synoptic pattern. Notice the break in the thin subtropical ridge to the northwest of TY Mort. The analyzed isotach maximum to the north of TY Mort suggests a steering current from the east, which is consistent with the actual westward motion of the storm. Twenty-four hours later, the NOGAPS analysis (Fig. 7.3b) has TY Mort near  $10^{\circ}\text{N}$ ,  $135^{\circ}\text{E}$ , which is still in the DR region of the S pattern. Notice that the analyzed isotach maximum now extends to the southeast of TY Mort, which indicates a steering flow from the east-southeast that is consistent with the actual storm movement to the west-northwest. The NOGAPS 24-h forecast (Fig. 7.3c) has TY Mort in nearly the same position as in the analysis (Fig. 7.3b). Notice that the location of TY Mort is to the south of the WR region in the S pattern.

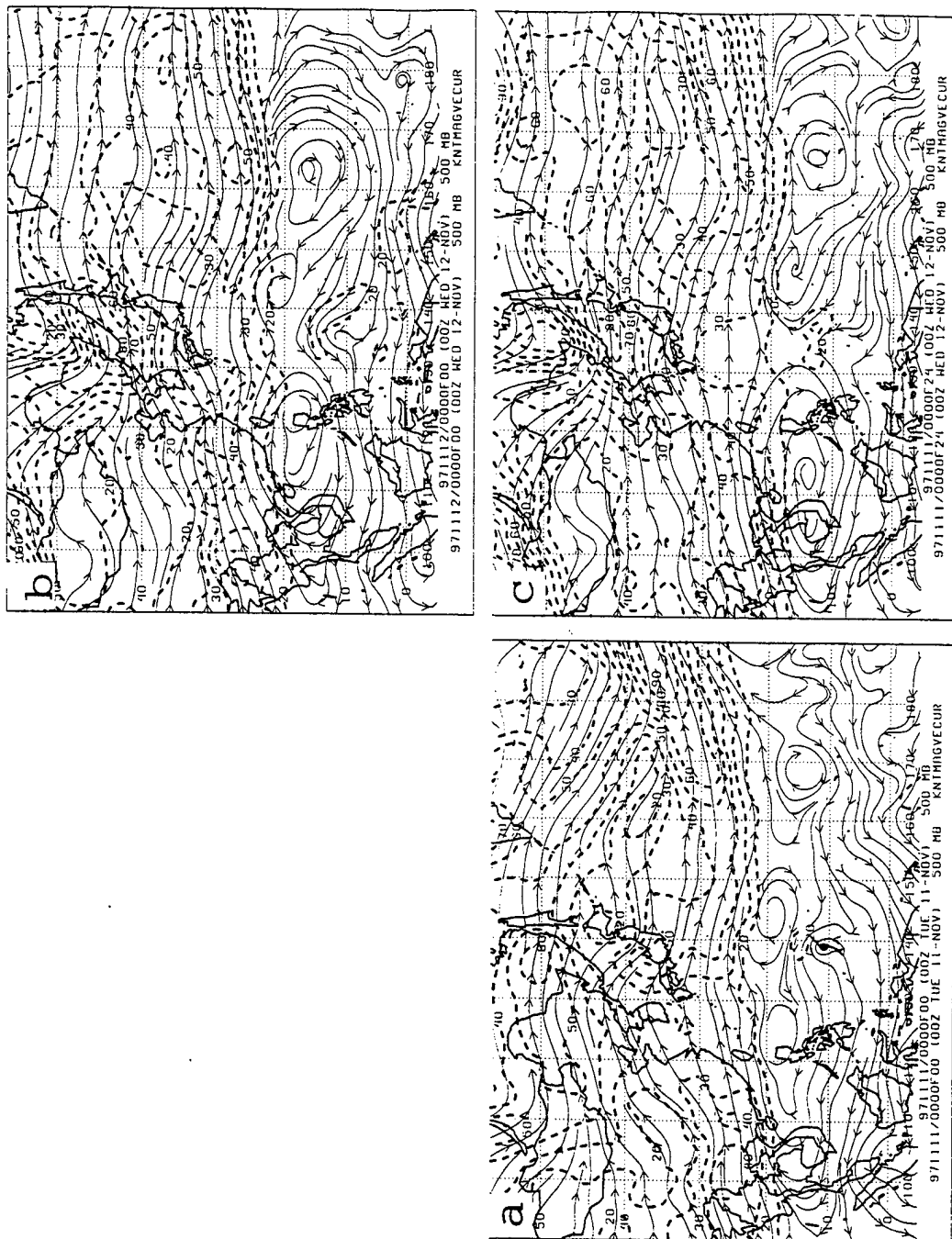
After another 24-h (Fig. 7.3d), the NOGAPS analysis has TY Mort near  $13^{\circ}\text{N}$ ,  $132^{\circ}\text{E}$ , which is still south of the WR region in the S pattern. The NOGAPS 48-h forecast (Fig. 7.3e) again has predicted TY Mort to be in nearly the same location as the analyzed position of TY Mort in the corresponding NOGAPS analysis (Fig. 7.3d). Notice that the NOGAPS 48-h predicted horizontal extent and isotach placements for TY Mort are also very similar to those in the corresponding analysis. At 00 UTC 14 November (Fig. 7.3f), the NOGAPS analysis has TY Mort near  $13^{\circ}\text{N}$ ,  $128^{\circ}\text{E}$ , which is still in the DR region of the S pattern. The NOGAPS 72-h forecast (Fig. 7.3g) has TY Mort near  $13^{\circ}\text{N}$ ,  $127^{\circ}\text{E}$ , which is again in very good agreement with the corresponding analysis. Notice that both the 72-h forecast horizontal extent and the circulation strength in Fig. 7.3g continue to be very similar to the analyzed horizontal extent and the circulation strength in Fig. 7.3f. The apparent result

of a properly forecast size and circulation strength for TY Mort by NOGAPS is a very good 72-h forecast track.

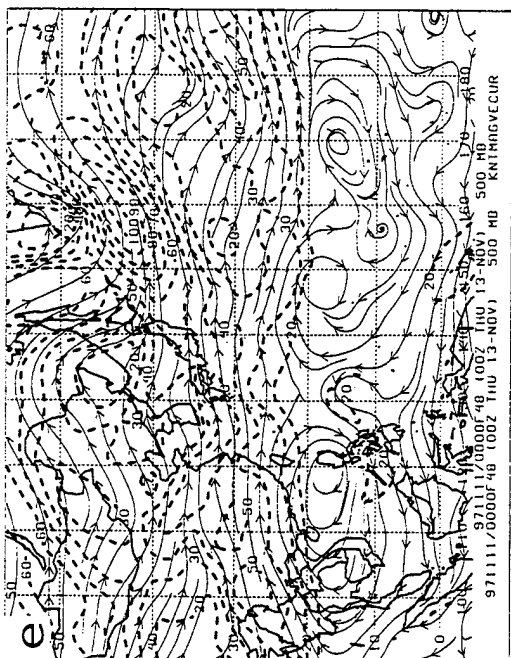
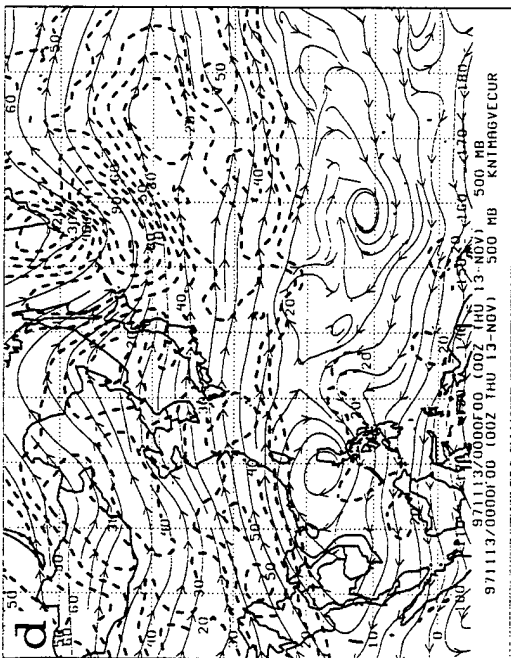
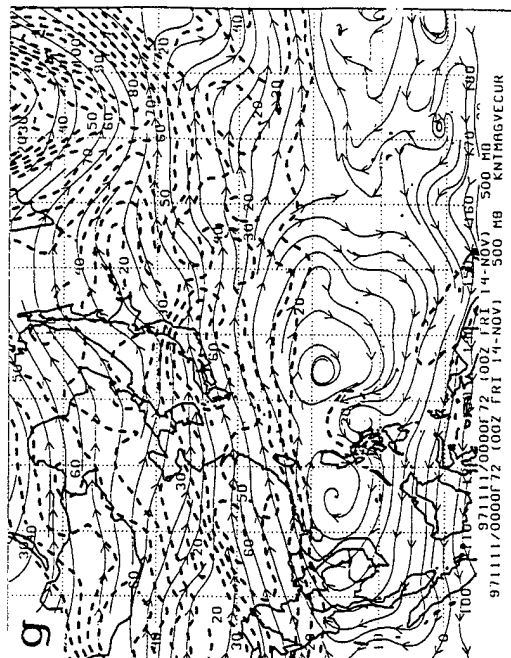
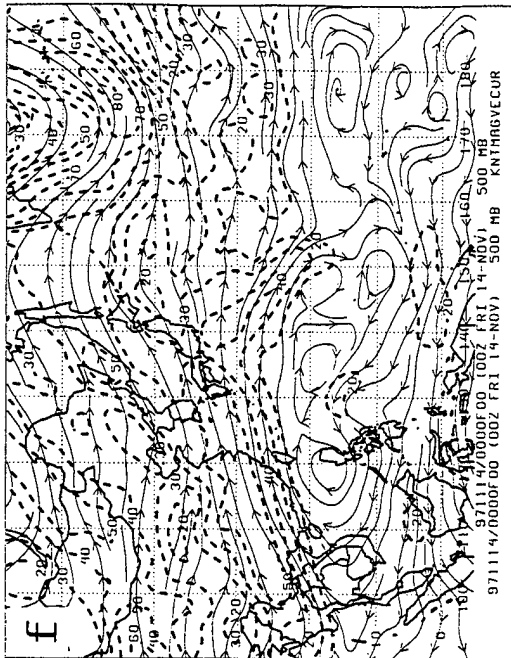
At 12 UTC 11 November (Fig. 7.4a), the GFDN 6-h forecast has TY Mort near  $11^{\circ}\text{N}$ ,  $127^{\circ}\text{E}$  in the DR region of the S pattern. Twelve hours later (Fig. 7.4b) when GFDN may be directly compared to the NOGAPS analysis at the same valid time (Fig. 7.3b), a slight difference in maximum isotachs exists. Notice that the higher resolution GFDN has TY Mort as having a slightly stronger circulation than the NOGAPS analysis at the same valid time, but that only a minor difference in the positioning of TY Mort is found.

Twelve hours later (Fig. 7.4c), the GFDN 30-h forecast predicts a continued strengthening of the circulation. Notice that the GFDN 30-h forecast has TY Mort near  $14^{\circ}\text{N}$ ,  $134^{\circ}\text{E}$ , which is north and east of the actual position at this time (Fig. 7.2). Since the GFDN vortex is moving northwestward and is approaching the break in the subtropical anticyclone (Fig. 7.4c), the predicted TC is in the WR region of the S pattern.

By 00 UTC 14 November (Fig. 7.4d), the GFDN 66-h forecast again predicts a strengthening of TY Mort at 500 mb, which is not consistent with the decreasing surface winds of TY Mort at this time. Notice that the GFDN 66-h forecast has TY Mort near  $16^{\circ}\text{N}$ ,  $135^{\circ}\text{E}$ , which is north and east of the predicted position 12 h prior and indicates a northeastward recurvature as in Fig. 7.2. The over-strengthening of TY Mort in the GFDN forecast has apparently resulted in an erroneous northeastward recurvature through the thin subtropical ridge.



**Figure 7.3.** NOGAPS 500-mb streamline and isotach analyses and predictions as in Fig. 3.5, except from (a) an analysis at 00 UTC 11 November 1997, and subsequent analyses in (b-d-f) and forecasts in (c-e-g). Notice that the NOGAPS-predicted positions throughout the forecast interval are very good.



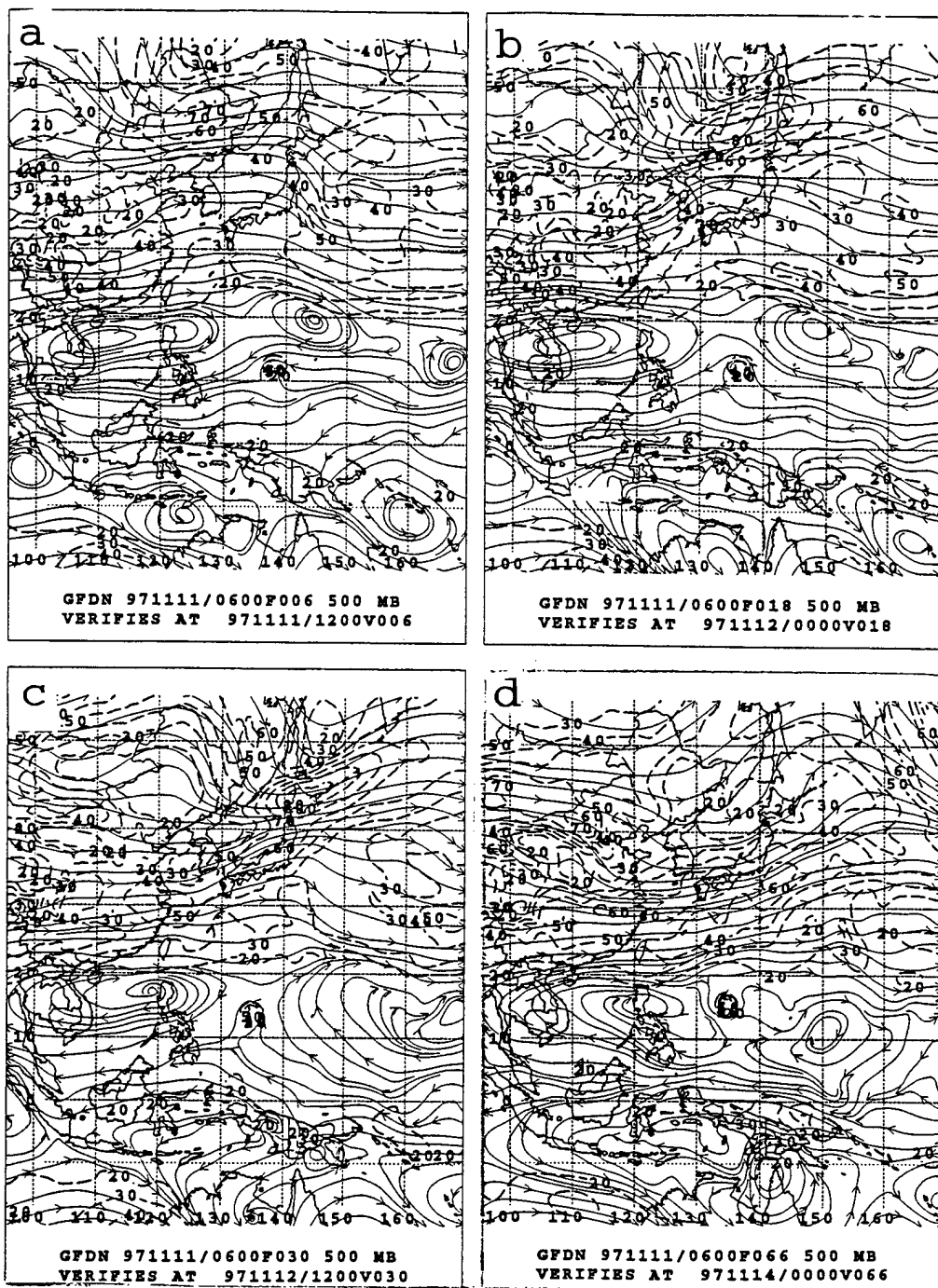


**Figure 7.4.** GFDN 500-mb streamline and isotach predictions as in Fig. 3.6, except forecast for TY Mort initiated at 06 UTC 11 November 1997, and verifies at (a) 12 UTC 11 November, (b) 00 UTC 12 November, (c) 12 UTC 12 November, and (d) 00 UTC 14 November. Notice that GFDN erroneously predicts TY Mort to move through the S/WR pattern/synoptic region.

### **C. STATISTICS**

Of the 27 storms during the 1997 typhoon season in the western North Pacific that were analyzed, only this case of TY Mort was classified under the conceptual model of section A.



## VIII. 1997 STATISTICAL SUMMARY

Each of the six conceptual models that were described in Chapters III through VII has been assigned a number that is listed in Table 8.1. Of the 27 storms during the 1997 typhoon season in the western North Pacific that were analyzed for this study, six were not classified into a conceptual model (Table 8.2). Reasons for not classifying a TC were: (1) lack of model fields; (2) a TC moved over land fairly early in the forecast; or (3) a TC moved out of the western North Pacific before any significant errors were noted. The remaining 21 storms are classified in Table 8.3 into at least one of the six conceptual models. In each case, the TC included a period of large forecast track errors by either NOGAPS or GFDN or both. The numbers associated with each conceptual model in Table 8.1 are used to designate the apparent source of the large forecast error. Notice that individual TCs may have been classified into more than one conceptual model. One reason for classifying a TC under two conceptual models may have been because a large FTE was found to have been caused by two distinct scenarios. For example, TY Marie (6W) was left of the best track due to an apparent wind shift of the forecast TC center and during the same forecast interval it was behind the best track because of a delay through the WR synoptic region. A second reason for classifying a TC under two conceptual models may have been because large FTEs occurred during separate model runs, and each of these large FTEs was attributed to a different scenario. For example, TY Ivan underwent erroneous ITI in an early model run and during a later model run had a retarded transition into the MW synoptic region.

NOGAPS had more situations (23 cases) in which large FTEs could be attributed to

1	FALSE TC INTERACTION a- POSITION-INDUCED b- HORIZONTAL STRUCTURE-RELATED c- FALSE TC/2nd CYCLONIC CIRCULATION
2	RETARDED TRANSITION FROM WR INTO MW a- AHEAD OF BEST TRACK b- BEHIND BEST TRACK
3	ERRONEOUS INDIRECT TC INTERACTION (ITI)
4	TC WIND FIELD SHIFT
5	TOO RAPID S/DR TO P/PO TRANSITION
6	ERRONEOUS TRANSITION THROUGH A THIN SUBTROPICAL RIDGE

**Table 8.1.** List of conceptual models described in Chapters III through VII that account for large NOGAPS or GFDN forecast track errors. The numbers in the left column will be used in Table 8.3 as indicators of the associated conceptual models leading to large track errors during the 1997 season.

TC NUMBER	TC NAME	REASON FOR NON-CLASSIFICATION
16W	TD 16	1
20W	CASS	1
22W	FRITZ	3
23W	ELLA	1
25W	HANK	1
30W	LINDA	2

**Table 8.2.** Storm number/name during 1997 that were not classified into one of the conceptual models in Chapters III through VII. Reasons for non-classification are given in the text.

TC NUMBER	TC NAME	NOGAPS WAS SUSCEPTIBLE	GFDN WAS SUSCEPTIBLE
5W	LEVI	4	
6W	MARIE	2b , 4	
7W	NESTOR	1c , 2b	
8W	OPAL	2b	2b
9W	PETER	1b	5
10W	ROSIE	1b	1b
11W	SCOTT	1b	
12W	TINA	3	3
13W	VICTOR	3	3
14W	WINNIE		1c
15W	YULE	1b , 4	
17W	ZITA	3	3
18W	AMBER	3	3
19W	BING	3	3
21W	DAVID	3	3
24W	GINGER	2b , 5	
26W	TD 26	1b	
27W	IVAN	2b	3
28W	JOAN	3	3
29W	KEITH	2b	2a
31W	MORT		6

**Table 8.3.** Storm number/name during 1997 in which large forecast track errors in NOGAPS or GFDN models could be attributed to the conceptual model numbers as given in Table 8.1 and described in Chapters III through VII.

one of the conceptual models listed in Table 8.1. A frequent error source for NOGAPS (Table 8.3) was an erroneous indirect TC interaction (category 3 in Table 8.1), which occurred seven times. Examples of TY Amber and TY Bing are given in Chapter V for this source. Another frequent error source for NOGAPS was one of the three forms of false direct TC interaction (category 1 in Table 8.1), which also occurred six times. Five of these cases involved a horizontal structure-related source, and TS Scott described in Chapter III is an example. A false TC or second cyclonic circulation was attributed to be the error source in one case, and ST Nestor is an example, as described in Chapter III. The next most frequent NOGAPS error source with three cases was the TC wind field shift (category 4 in Table 8.1). An example of this error source is TY Marie, which was described in Chapter IV. Another error source for NOGAPS was a too rapid S/DR to P/PO transition (category 5 in Table 8.1) which occurred one time. An example of this error source is TY Ginger, which was described in Chapter VI. No cases of an erroneous transition through a thin subtropical ridge were observed for NOGAPS during 1997.

As indicated in Table 8.3, GFDN had less cases (14) in which large FTEs could be attributed to one of the conceptual models listed in Table 8.1. The most frequent error source for GFDN was erroneous TC interaction, which occurred eight times. Examples of TY Zita and TY Amber are given in Chapter V for this type of error source. The next-most frequent error source was a too-fast S/DR to P/PO transition, which occurred one time. An example of this error source is TY Ginger, which was described in Chapter VI. All other situations in which large FTEs could be attributed to one of the conceptual models that is listed in Table 8.1 occurred only one time. ST Keith is an example of an ahead of best track

transition from the WR synoptic region into the MW synoptic region (category 2a in Table 8.1) and is described in Chapter IV. No cases of either a motion-induced shifting of the TC wind field or position-induced false TC interaction were observed for GFDN during 1997. The motion-induced shifting of the TC wind field (Fig. 4.2) is not expected in the GFDN model because of its high horizontal resolution, which allows an intense TC vortex and the wind center and vorticity center will be nearly collocated. Similarly, a situation with a misplaced vortex as in Fig. 3.1 is unlikely in GFDN because the initial condition specification technique (Chapter I.A.2) first removes the existing vortex and replaces it with the new vortex.



## IX. CONCLUSIONS AND RECOMMENDATIONS

### A. CONCLUSIONS

The performance of both the NOGAPS and the GFDN models during the 1997 western North Pacific typhoon season is documented. In the context of the Systematic Approach of Carr and Elsberry (1994) and Carr *et al.* 1997, a knowledge base of six conceptual models is proposed that associates recurring types of TC forecast track errors with various types of TC structure and environmental structure. These six conceptual models are presented as several individual case studies in Chapters III through VII to illustrate recurring scenarios with poor performance in either the NOGAPS model, GFDN model, or both. The frequency of occurrence of each of the six error sources is given in Table 8.3 in Chapter VIII.

The first conceptual model (False TC Interaction) consists of three types described in Chapter III. The first type (Position-Induced False TC Interaction) may occur in the NOGAPS forecast when the TC location in the model first-guess field differs from the location of the synthetic observations or specified vortex. The second type (Horizontal Structure-related False TC Interaction) may be predicted in either model when two or more TCs/cyclonic circulations are in close proximity. Too-large predicted TCs/cyclonic circulations can result in a reduced separation distance between the two circulations and also a merger of the circulations. The third type (False TC/Second Cyclonic Circulation Interaction) may be predicted in a model when another forecast circulation that does not exist in nature is found in close proximity to the TC. When False TC Interaction occurs in the model forecast, a characteristic cyclonic rotation of the two circulations around a center point

often occurs and usually results in a forecast position behind and left of the actual position. This error source was attributed to be the cause of six (two) cases of large errors in the NOGAPS (GFDN) model (Table 8.3).

The second conceptual model (Retarded Transition into the MW synoptic region) may occur in the model forecast when the predicted TC structure is inaccurate. In this conceptual model (Chapter IV), the TC track forecast beginning near the subtropical ridge axis and moving into the MW synoptic region is degraded. In situations when TC intensity is under-forecast by a model, a shallower vertical extent than actual may be predicted. Consequently, the TC is steered from a lower atmospheric layer, which typically results in a slow forecast in the along-track direction. Conversely, the vertical extent of the TC is increased when TC intensity is over-forecast by a model and the steering current for that system occurs over a deeper atmospheric layer. In this situation, the result is often a faster forecast in the along-track direction. The numbers of NOGAPS and GFDN errors attributed to this source are six and two, respectively (Table 8.3).

The third conceptual model (Motion-Induced Shifting of a TC Wind Field Center) may be predicted by NOGAPS when a TC is under-forecast. In this conceptual model (Chapter IV), the addition of the environmental steering flow and the weak TC wind field results in an offset wind center in the vicinity of the TC. Typically, the wind center is shifted to the left of the actual TC location and the predicted motion of the TC is consistently left of track. The number of NOGAPS errors attributed to this source is three (Table 8.3).

The fourth conceptual model (Erroneous Indirect TC Interaction) may occur in the model forecast when an anticyclone between two TCs is predicted to be weakened more than

in nature (Chapter V). The effects of weakening the anticyclone between the two TCs are a decrease in the poleward steering flow of the western TC and a decrease in the equatorward steering flow across the eastern TC. This error source is attributed to seven (eight) cases of large track errors in the NOGAPS (GFDN) model (Table 8.3).

The fifth conceptual model (Too Rapid S/DR to P/PO Transition) may occur in the model forecast when the horizontal extent of a TC in S/DR is over-predicted. When this occurs, an anticyclone to the east-southeast of the TC tends to over-develop and connect to the subtropical anticyclone that is to the north of the TC. As a result, the synoptic pattern is changed too early from the S/DR to the P/PO pattern/region. The predicted steering current is changed too soon to a poleward flow and the forecast motion for the TC has an incorrect northern component. The numbers of NOGAPS and GFDN model errors attributed to this source are two and two, respectively (Table 8.3).

Finally, the sixth conceptual model (Erroneous Recurvature through a Thin Subtropical Ridge) may be predicted in a model forecast when a TC initially located in the S/DR synoptic pattern/region is predicted to be stronger than, or larger in horizontal extent, than actually occurs in nature. As the TC is erroneously forecast to increase in horizontal extent, the model forecast may predict an erroneous movement into and through a thin subtropical ridge, and thus erroneously recurve. This error source did not cause any large errors in NOGAPS and only one case in GFDN (Table 8.3) in this sample of 1997 TCs. However, preliminary analysis suggests that a repeated poleward bias in NOGAPS forecasts of TY Isa (02W) during April 1997 is tentatively attributed to recurvature through a thin ridge.

Use of these conceptual models and their supporting case studies may allow the JTWC forecaster to better understand how the NOGAPS model and GFDN model may perform in specified synoptic environments. It is hoped that the JTWC forecaster can use the information in this study to provide more accurate TC track forecasts by rejecting inappropriate model guidance during future typhoon seasons in the western North Pacific. Additionally, this thesis may provide feedback to model producers as to situations in which large track errors have occurred, in hopes that the model might be improved in the future.

## **B. RECOMMENDATIONS AND FUTURE WORK**

This thesis has studied only the 1997 typhoon season in the western North Pacific basin. The 1997 GFDN fields are currently available for the eastern and central North Pacific basin and a similar study should be accomplished for that region. Additionally, the North Atlantic basin may be studied by using NOGAPS and GFDL forecast fields. The study of these two additional basins will hopefully provide a more statistically firm conclusion. If such a study for all three basins yields consistent error sources, a similar project should be accomplished in future years to gain a better understanding of when the NOGAPS model or the GFDN (GFDL) model guidance should be accepted or rejected in specific environmental scenarios. Another possibility is the extension of this type of study to other dynamical models or other objective aids.

Whereas this is a diagnostic study of known large track error cases, the goal should be to demonstrate that such conceptual models can be applied in real-time. That is, objective criteria or subjective techniques for recognizing potential large track error scenarios need to be developed. This may allow the forecaster to indicate either a high or low confidence level

associated with each forecast scenario, which would be useful information for the customer of these forecasts.

This type of study may be useful when the forecaster is trying to decide the correct model to use for his/her official TC track forecast. When a notable difference in the dynamical model-predicted tracks occurs, a selective consensus for choosing the correct model forecast must be found. The goal of an on-going study of an Expert System (L.E. Carr, personal communication, 1998) is to provide the JTWC forecaster with an automated system, which incorporates the conceptual models of this thesis, to help choose between significantly different model TC tracks. By intelligently selecting the best guidance, and rejecting likely erroneous guidance, the TC track forecasts should be improved, which will allow more time to prepare for these dangerous storms.



## LIST OF REFERENCES

- Carr, L. E., III, and R. L. Elsberry, 1994: Systematic approach to tropical cyclone track forecasting. Part I. Approach overview and description of meteorological basis. Tech. Rep. NPS-MR-94-002, Naval Postgraduate School, Monterey, CA 93943, 273 pp.
- Carr, L. E. III, M. A. Boothe, S. R. White, C. S. Kent, and R. L. Elsberry, 1995: Systematic approach to tropical cyclone track forecasting. Part II. Climatology, reproducibility, and refinement of meteorological knowledge base. Tech. Rep. NPS-MR-95-001, Naval Postgraduate School, Monterey, CA 93943, 96 pp.
- Carr, L. E. III, R. L. Elsberry, and M. A. Boothe, 1998: Condensed and updated version of the systematic approach meteorological knowledge base, western North Pacific. Tech. Rep. NPS-MR-98-002, Naval Postgraduate School, Monterey, CA 93943, 169 pp.
- Goerss, J. S., 1997: NOGAPS 1996 tropical cyclone forecast performance. *Preprints, 22nd Conf. Hurr. Trop. Meteor.*, Ft. Collins, CO, Amer. Meteor. Soc., Boston, MA 02108, 617-618.
- Goerss, J. S., and P. Phoebus, 1992: The Navy's operational atmospheric analysis. *Wea. Forecasting*, **7**, 232-249.
- Goerss, J. S., and R. A. Jeffries, 1994: Assimilation of synthetic tropical cyclone observations into the Navy Operational and Global Atmospheric Prediction System. *Wea. Forecasting*, **9**, 557-576.
- Goerss, J. S., and S. A. Petko, 1995: The impact of synthetic tropical cyclone observations on a global forecast model. *Preprints, 21st Conf. Hurr. Trop. Meteor.*, Miami, FL, Amer. Meteor. Soc., Boston, MA 02108, 149-151.
- Goerss, J. S., L. R. Brody, and R. A. Jeffries, 1991: Assimilation of tropical cyclone observations into the Navy Operational and Global Atmospheric Prediction System. *Preprints, Ninth Conference on Numerical Weather Prediction*, Denver, CO, Amer. Meteor. Soc., Boston, MA 02108, 638-641.
- Kurihara, Y., M. A. Bender, and R. J. Ross, 1993: An initialization scheme of hurricane models by vortex specification. *Mon. Wea. Rev.*, **121**, 2030-2045.
- Kurihara, Y., M. A. Bender, R. E. Tuleya, and R. J. Ross, 1995: Improvements in the GFDL hurricane prediction system. *Mon. Wea. Rev.*, **123**, 2791-2801.
- Kurihara, Y., R. E. Tuleya, and M. A. Bender, 1997: The GFDL hurricane prediction system and its performance in the 1995 hurricane season. *Mon. Wea. Rev.* (in press)

Rennick, M. A., 1997: GFDN performance in NWPAC during 1996. FNMOC Models Dept. Tech. Note 1-97, 23 pp.

## INITIAL DISTRIBUTION LIST

	No. Copies
1. Defense Technical Information Center .....	2
8725 John J. Kingman Rd., STE 0944	
Ft. Belvoir, VA 22060-6218	
2. Dudley Knox Library .....	2
Naval Postgraduate School	
411 Dyer Rd.	
Monterey, CA 93943-5101	
3. Commanding Officer .....	1
Naval Pacific Meteorology and Oceanography Center	
Box 113	
Pearl Harbor, HI 96860-5050	
4. Commanding Officer .....	1
Naval Pacific Meteorology and Oceanography Center West	
PSC 489, Box 12	
FPO AP 96540-0051	
5. Dr. R. L. Elsberry .....	2
Code MR/ES	
Naval Postgraduate School	
589 Dyer Rd.	
Monterey, CA 93943-5114	
6. Dr. L. E. Carr III .....	1
Code MR/Cr	
Naval Postgraduate School	
589 Dyer Rd.	
Monterey, CA 93943-5114	
7. Superintendent .....	1
Naval Research Laboratory	
7 Grace Hopper Avenue, Stop 2	
Monterey, CA 93943	

8. Chairman ..... 1  
Department of Meteorology  
Naval Postgraduate School  
589 Dyer Rd.  
Monterey, CA. 93943-5114
9. LT Robert G. Schnabel ..... 1  
954 North 4th St.  
New Hyde Park, NY 11040